INAUGURAL – DISSERTATION

zur

Erlangung der Doktorwürde

der

Naturwissenschaftlich-Mathematischen Gesamtfakultät

der

Ruprecht-Karls-Universität Heidelberg

vorgelegt von

Diplom-Chemiker Sascha Hausberg

aus Groß-Gerau

Tag der mündlichen Prüfung: 17. Juni 2011

Prediction of Exchange Coupling Constants with

Density Functional Theory and Molecular Mechanics

Acknowledgements – Danksagungen

"Die Rechenautomaten haben etwas von den Zauberern im Märchen.

Sie geben einem wohl, was man sich wünscht,

doch sagen sie einem nicht, was man sich wünschen soll."

Norbert Wiener (1894-1964), amerik. Mathematiker

Contents

Abstract

The aim of this PhD project was to develop a fast and reliable method for the calculation of exchange coupling constants which are used in the description of the coupling of unpaired electrons in di-, tri- and oligonuclear transition metal complexes. In order to achieve both accurate results and low computational costs, a combination of quantum chemistry (QC) and molecular mechanics (MM) calculations has been employed.

The exchange coupling describes the energy gap between the states of ferro- and antiferromagnetically coupled transition metal centers in a molecule and can help to gain insight into the electronic and magnetic properties of a compound. The prediction of exchange coupling constants is vital for virtual screening of magnetic properties as well as to fit experimental results, e. g. electron paramagnetic resonance (EPR) or magnetism measurements. While the exchange coupling between two transition metal centers can be determined by single point calculations based on X-ray structure geometries, geometry optimization is the key element for predictability when no experimental data is available. As the method should be usable to not only reproduce experimental data, but also to predict exchange coupling constants of *in silico*-generated complexes, the computational procedure has to involve a geometry optimization at one point of the process.

A systematic benchmark approach for the deduction of exchange coupling constants from density functional theory (DFT) single point calculations is presented. Based on benchmark calculations of a small dinuclear molecule, a suitable functional and basis set combination for the fast and accurate calculation of coupling constants has been identified and tested on a large series of transition metal compounds, which include Cu^{II}, Fe^{III}, Cr^{III}, V^{IV}, Mn^{II}, Mn^{III}, Mn^{IV}, Ni^{II} and Co^{III} ions. The calculations were based on X-ray structure geometries obtained from literature data and have been compared to exchange coupling constants calculated from DFT-optimized structures. The results based on optimized structures were found to have comparable accuracy which shows, that the optimization of a structure is a viable approach to exchange coupling constant prediction.

A ligand field term has been implemented in a molecular mechanics program, employing the programming language C++. This allows for the calculation of electronic effects with MM methods. Based on reference information from X-ray structures and UV/VIS spectra the ligand field term has been automatically parametrized . Since the prediction of exchange coupling constants based on optimized geometries is possible, molecular mechanics calculations with an additional electronic effect present a computationally efficient way for this step of the process. Parametrizations based on

simple test molecules and one or more X-ray structures with transition metal compounds showing electronic effects like Jahn-Teller distortions are presented and the functional form of the ligand field term implemented into the software is discussed in detail.

A possible improvement of the parametrization process which uses the information of the first and second derivatives of the energy with respect to atomic coordinates is presented. Also, a parametrization based on DFT-optimized structures is discussed. If DFT-optimized structures are used as the reference data for a force field, all calculations for the determination of exchange coupling constants are based on the same potential energy surface (PES). Both geometry optimization and the calculation of the magnetic properties then only involve structures on the DFT hypersurface. This is an advantage from the theoretical chemists' point of view, since the usual procedure for the calculation of exchange coupling constants involves X-ray structure geometries which do not represent a minimum on the DFT hypersurface.

Kurzfassung

Das Ziel der vorliegenden Doktorarbeit war die Entwicklung einer zuverlässigen und schnellen Methode, um Austauschkopplungskonstanten, die die Kopplung von ungepaarten Elektronen in zwei-, drei- oder mehrkernigen Übergangsmetallkomplexen beschreiben, zu berechnen. Um genaue Ergebnisse bei geringem Rechenaufwand zu gewährleisten wurde eine Kombination von quantenchemischennn Rechenmethoden und Kraftfeldmethoden benutzt.

Die Austauschkopplung beschreibt die Energielücke zwischen den antiferro- und ferromagnetisch gekoppelten Spinzuständen der Übergangsmetallzentren eines Moleküls und kann Hinweise auf dessen elektronische und magnetische Eigenschaften geben. Die Vorhersage von Austauschkopplungskonstanten ist entscheidend für "Virtual Screening"-Anwendungen und hilft bei der Interpretation von experimentellen Ergebnissen, die z. B. bei Elektronenspinresonanz (ESR)- und magnetischen Messungen erhalten werden. Während Austauschkopplungskonstanten eines Moleküls durch "Single Point"-Rechnungen auf Basis von Röntgenstrukturdaten berechnet werden können, sind Geometrieoptimierungen der Schlüsselschritt bei der Vorhersage von magnetischen Eigenschaften von bisher nicht synthetisierten Molekülen. Da die Methode sowohl bei der Interpretation von Daten zu bereits experimentell bestimmten Strukturen helfen, als auch Werte für *in silico*-generierte Strukturen bestimmen sollte, wurde der Schritt der Geometrieoptimierung in den Gesamtprozess aufgenommen.

Um Austauschkopplungskonstanten mit Hilfe von Dichtefunktionaltheoriemethoden (DFT-Methoden) zu berechnen, wurde ein systematischer Benchmark-Test durchgeführt. Basierend auf einem dinuklearen Cu^{II}-Komplex wurde eine geeignete Kombination von Funktional und Basissatz für die schnelle und akkurate Berechnung der Kopplungskonstanten identifiziert. Die Methode wurde im Anschluß anhand einer Reihe von Übergangsmetallkomplexen verifiziert, wobei Cu^{II}, Fe^{III}, Cr^{III}, V^{IV}, Mn^{II}, Mn^{III}, Mn^{IV}, Ni^{II} und Co^{III} zu den betrachteten Metallionen zählten. Die Berechnungen stützen sich auf die Röntgenstrukturen der Komplexe, die der Literatur entnommen wurden. Die berechneten Kopplungskonstanten wurden mit Ergebnissen, die auf DFT-optimierten Strukturen basierten, verglichen. Die Ergebnisse beider Berechnungen zeigen ähnlich gute Genauigkeit im Vergleich zu experimentellen Resultaten. Die Berechnung von Austauschkopplungskonstanten auf Basis von DFT-optimierten Strukturen erweist sich somit als geeigneter Ansatz für die Vorhersage bei Strukturen, zu denen noch keine experimentellen Daten vorliegen.

Um den erforderlichen rechnerischen Aufwand für die Geometrieoptimierung zu reduzieren wurde ein Ligandenfeldterm in das Kraftfeldprogramm Momec mit Hilfe der Programmiersprache C++ implementiert. Zusätzlich wurde eine automatische Parametrisierung entwickelt, die sowohl Kraftfeldparameter für klassische Terme als auch für das Ligandenfeld aus Referenzdaten, bestehend aus Röntgenstrukturinformationen und UV/VIS-Spektren, ableiten kann. Durch die Implementierung eines Ligandenfeldterms können die elektronischen Effekte, die einen Einfluß auf die Koordinationsstruktur der Übergangsmetallzentren haben, durch Kraftfeldrechnungen erfaßt werden. Der Prozess der Geometrieoptimierung wird durch den Einsatz von Kraftfeldmethoden erheblich beschleunigt. Auf der Basis von Teststrukturen und Röntgenstrukturen von Übergangsmetallkomplexen mit Jahn-Teller-verzerrten Metallzentren werden Parametrisierungen sowie die funktionelle Form des Ligandenfeldpotentials diskutiert.

Das letzte Kapitel der vorliegenden Arbeit beschäftigt sich mit der weiteren Entwicklung der Methode zur Vorhersage von Austauschkopplungskonstanten. Ein neuer Ansatz zur Parametrisierung von Ligandenfeldkraftfeldern auf der Basis der ersten und zweiten Ableitungen der Energie in Bezug auf die Atomkoordinaten eines Moleküls wird diskutiert. Erste Ergebnisse in Hinblick auf eine Parametrisierung auf Basis von DFT-optimierten Strukturen zeigen außerdem, daß durch Referenzdaten aus DFT-Rechnungen das Problem der verschiedenen Hyperflächen während des Gesamtprozesses der Vorhersage von Austauschkopplungskonstanten vermieden werden kann. Die Berechnung von Austauschkopplungskonstanten wird in der Regel auf Basis von Röntgenstrukturen durchgeführt, die im Allgemeinen nicht ein Minimum auf einer DFT-Hyperfläche darstellen. Durch die Geometrieoptimierung mit Hilfe der DFT bzw. durch die Optimierung durch ein Kraftfeld, welches mit Hilfe von DFT-Strukturen parametrisiert wurde, läßt sich sicherstellen, daß die Austauschkopplungskonstante auf Basis einer Minimumsstruktur der DFT-Hyperfläche berechnet wird.

Objective

Single molecule magnets (SMMs)[1–3] present an interesting class of compounds with multiple possible applications in fields of modern technology, e. g. highly efficient data storage systems, molecular freezers[4,5], switches, quantum computers[6] or contrast agents[7]. Therefore, the interest in the development of new compounds, which exhibit single molecule magnet behavior at room temperature or above is high. While experimentalists have been able to synthesize a large number of SMMs with anisotropy barriers of up to 170 K[8], a systematic approach to find compounds which show SMM behavior is still lacking and new discoveries of SMMs are often by pure chance. As the synthesis and characterization of this class of compounds is tedious and time-consuming, the constantly evolving field of computational chemistry can provide a suitable approach for a more systematic and thorough investigation in this field of research. While improving computer hardware is constantly opening up new possibilities for more and more accurate calculations of medium sized molecules, the systematic screening of hundreds or thousands of compounds is still impossible with high-level quantum chemistry (QC) calculations. The goal of this PhD project therefore was to develop an approach for the calculation of exchange coupling constants of transition metal complexes, which can yield accurate results while the computational costs remains at a reasonable level for large scale calculations.

The exchange coupling describes the energy gap between the different spin states of coupled transition metal centers (see Part II for a detailed description) and can help to gain insight into the low-lying electronic states of a molecule. Together with additional parameters like the zero-field splitting (ZFS) (see Part I) a qualitative and quantitative understanding of the exchange coupling is therefore important for the rational design of new SMMs. While the calculation of the actual constant based on X-ray geometries is feasible with density functional theory (DFT) methods, the geometry optimization necessary for the creation of *in silico*-structures is time consuming when QC calculations are involved. Since geometry optimizations are necessary when no X-ray structure is available, the process of geometry optimization with subsequent exchange coupling constant calculation may be divided, and QC and molecular mechanics (MM) methods have been employed. The underlying theory of QC and MM calculations as well as molecular magnetism is described in detail in the first Part of this thesis.

MM methods can generate very accurate molecular geometries, which are computed within a couple of seconds on modern computer hardware. As the molecules of interest contain transition metal ions, the underlying force fields have to be specifically tailored to this kind of problem and, in order to be able to correctly describe electronic effects caused by the unpaired electrons on the metal ions, may

include an additional electronic term. We have chosen to implement a ligand field term[9,10] into our own molecular mechanics package[11,12], which can correctly reproduce e. g. Jahn-Teller[13] distorted coordination sites and thus can yield accurate molecular geometries when transition metal centers are present in the molecule (see Part III for details). As the parametrization of this ligand field term should be simple, reliable and also possible within an affordable amount of time, the implementation of an automatic parametrization procedure has also been a goal of this PhD project (detailed description in Part IV). Parametrization is necessary when a new class of compounds is investigated or new functional forms for an energy term are developed, e. g. the change of the ligand field potential form presented in Part III of this thesis.

With the combination of a ligand field augmented molecular mechanics calculation for the geometry optimization of a complex and the subsequent determination of magnetic properties, e. g. the exchange coupling constant, by DFT based methods, we have taken a first step towards a systematic computational screening of possible candidates for single molecule magnets. For a more complete description of the single molecular magnet behavior other terms e. g. the ZFS parameters for axial (D) or rhombic (E) splitting are necessary. These can also be computed by QC methods but are usually smaller by an order of magnitude compared to the exchange coupling constant J and are therefore much more difficult to reproduce correctly.

Part I

Theoretical Background

1 Quantum Chemistry

1.1 Hartree-Fock Theory

Quantum chemical methods have become a major field of research in the last century and quantum chemistry calculations are nowadays an important tool to study reaction mechanisms, structural conformations, energy profiles and spectroscopic properties. Calculations are used to explain, but also to support experimental findings. The major difference to force field methods, which will be described in Ch. 2 of this Part, is the treatment of electrons, which are explicitly included in quantum mechanical methods. Therefore, quantum chemistry methods are able to describe electronic effects, e.g. Jahn-Teller[13] distortions in transition metal complexes or excited states, and can in principle describe every property of a given molecule.

1.1.1 The Born-Oppenheimer Approximation

The time-independent Schrödinger equation[14], Eq. 1.1.1, describes the stationary state of a system and can be used to derive the energy levels of a molecule.

$$\mathbf{H}\Psi = E\Psi \tag{1.1.1}$$

where $\mathbf{H}$ is the Hamilton operator, E the energy eigenvalue and Ψ the wave function, which is a function of all electron and nuclei coordinates as well as electron spins. If this equation (or an approximation to it) is solved without empirical parameters, the method is referred to as an *ab-initio* method, which means, it is based on first principles and thus rigorously derived from quantum mechanics.

For an N electron and M nuclei system, the Hamiltonian[15] is given in Eq. 1.1.2:

$$\mathbf{H} = -\sum_{i}^{N}\frac{1}{2}\nabla^2 i - \sum_{A}^{M}\frac{1}{2M_A}\nabla^2 A - \sum_{i}^{N}\sum_{A}^{M}\frac{Z_A}{r_{iA}} + \sum_{i}^{N}\sum_{j>i}^{N}\frac{1}{r_{ij}} + \sum_{A}^{M}\sum_{B>A}^{M}\frac{Z_A Z_B}{R_{AB}} \tag{1.1.2}$$

Here, M_A is the mass of the nucleus A, Z_A its atomic number, r_{iA} the distance between nucleus A

and electron i, r_{ij} the distance between electrons i and j and R_{AB} the distance between nuclei A and B. The first term accounts for the kinetic energy of the electrons while the second term represents the kinetic energy of the nuclei. The third term describes the Coulomb attraction between electrons and nuclei and terms four and five represent the repulsion between electrons and nuclei, respectively.

Since nuclei are much heavier than electrons, they move more slowly. With the Born-Oppenheimer approximation[16,17], one can separate the electronic problem from the motion of the nuclei and treat the electron movement in a field of point charges generated by the nuclei. The electronic Hamiltonian (Eq. 1.1.3) is therefore reduced from Eq. 1.1.2 to only include the terms for the kinetic energy of the electrons, the Coulomb attraction between electrons and nuclei and the Coulomb repulsion between electrons. Since the electrons "feel" the nuclei as point charges, the electronic energy of a system also depends parametrically on the Coulomb repulsion of the nuclei, Eq. 1.1.3:

$$\mathbf{H_{elec}} = -\sum_i^N \frac{1}{2}\nabla^2 i - \sum_i^N \sum_A^M \frac{Z_A}{r_{iA}} + \sum_i^N \sum_{j>i}^N \frac{1}{r_{ij}} + \sum_\mathbf{A}^\mathbf{M} \sum_{\mathbf{B>A}}^\mathbf{M} \frac{\mathbf{Z_A Z_B}}{\mathbf{R_{AB}}} \qquad (1.1.3)$$

Solutions to the Schrödinger equation based on the electronic Hamiltonian are given by the electronic wave function, Eq. 1.1.4:

$$\Psi_{elec} = \Psi_{elec}(r_i, R_A) \qquad (1.1.4)$$

In this form, the electronic Hamilton operator neglects relativistic and other additional effects[18]. If those become important, e. g. for fourth or fifth row elements, or if other Hamiltonians, for example for spin-spin or spin-orbit coupling effects, are needed, the electronic Hamiltonian has to be extended to account for these interactions. This will be the case, when the broken symmetry formalism is introduced and the Hamiltonian is extended by a term which describes the interaction between two transition metal centers (see Pt. II, Ch. 2).

1.1.2 Molecular Orbitals

The electronic Schrödinger equation can only be solved in closed form for one-electron systems like the hydrogen atom. Approximate, iterative solutions for multi-electron systems are based on the variational principle, which states that the expectation value of the Hamiltonian is always equal or higher than the exact energy (Eq. 1.1.5):

$$\langle\Psi|\mathbf{H_{elec}}|\Psi\rangle \geq E_{exact} \qquad (1.1.5)$$

For a correct description of the wave function of a single electron in the nonrelativistic case, two

parts are needed. First, a spatial orbital Ψ_i, which describes the spatial distribution of an electron in dependence of r. The atomic wave functions Ψ_i are defined to be orthonormal, Eq. 1.1.6:

$$\int dr\, \Psi_i^*(r)\Psi_j(r) = \delta_{ij} \tag{1.1.6}$$

where δ_{ij} is the Kronecker-Delta. Second, the electronic spin quantum numbers for an electron with the two possible states $+\frac{1}{2}$ and $-\frac{1}{2}$, which correspond to the spin up and spin down states of parallel or anti-parallel alignment along an external magnetic field have to be introduced *ad hoc*[18]. The spin functions are orthonormal as well, Eq. 1.1.7:

$$\begin{aligned}
\langle\alpha|\alpha\rangle = \langle\beta|\beta\rangle = 1 \\
\langle\alpha|\beta\rangle = \langle\beta|\alpha\rangle = 0
\end{aligned} \tag{1.1.7}$$

The combination of both elements yields the spin orbitals χ, Eq. 1.1.8

$$\chi(x) = \begin{cases} \Psi(r)\alpha(\omega) \\ or \\ \Psi(r)\beta(\omega) \end{cases} \tag{1.1.8}$$

Given non-interacting electrons, the Hamiltonian $\mathbf{H_{elec}}$ is a sum of one-electron Hamiltonians and the corresponding wave function gives rise to the electronic energy E_{elec}, which is a product of one-electron wave functions, the spin orbitals. The product is called the Hartree product (Eq. 1.1.9):

$$\Psi_{Hartree} = \chi_i(x_1)\chi_j(x_2)\ldots\chi_k(x_N) \tag{1.1.9}$$

This represents an uncorrelated ansatz, because the probability of finding electron one at position x_1 is independent of the probability of finding electron two at position x_2. The total probability of finding each electron at each position is thus the product of all one-electron probabilities[15]. Since electrons have to be described as fermions obeying the Pauli principle[19], interchanging the coordinates of two fermions must result in a change of the sign of the wave function. Therefore, the quantum numbers of two electrons cannot be the same, and the wave function has to be antisymmetric with respect to interchanging two electronic coordinates. As the Hartree product does not fulfill this principle, the linear combination of the Hartree product has to be used instead. For two electrons, the simplest correct description is (Eq. 1.1.10):

$$\Psi(x_1, x_2) = \frac{1}{\sqrt{2}}(\chi_i(x_1)\chi_j(x_2) - \chi_j(x_1)\chi_i(x_2)) \tag{1.1.10}$$

where $\frac{1}{\sqrt{2}}$ is a normalization factor and the minus sign ensures the antisymmetry of $\Psi(x_1, x_2)$[15]. This can be written as a determinant, the so-called Slater Determinant[20], given in Eq. 1.1.11 for the N-electron case:

$$\Psi(x_1, x_2, \ldots, x_N) = \frac{1}{\sqrt{N!}} \begin{vmatrix} \chi_i(x_1) & \chi_j(x_1) & \cdots & \chi_k(x_1) \\ \chi_i(x_2) & \chi_j(x_2) & \cdots & \chi_k(x_2) \\ \vdots & \vdots & & \vdots \\ \chi_i(x_N) & \chi_j(x_N) & \cdots & \chi_k(x_N) \end{vmatrix} \tag{1.1.11}$$

In a Slater Determinant, the electronic coordinates are given along the rows, while the columns are made up by single electron wave functions. These are combined to molecular orbitals when the electronic Schrödinger equation is solved for a molecule.

1.1.3 The Fock Operator

As the variational principle states, the energy of the best wave function obtainable with an approximate functional form is equal or higher to the exact energy of the electronic problem. The variation of this problem is induced by the choice of spin orbitals and the aim is to choose the best set of spin orbitals for a given problem. The equation, which describes the best set of spin orbitals, is the Hartree-Fock integro-differential equation[15], given in Eq. 1.1.12 for the case of a single electron denoted as electron-one, which yields the orbital energy ϵ_a of the spin orbital χ_a.

$$\left[h(1) + \sum_{b \neq a} \mathbf{J}_b(1) - \sum_{b \neq a} \mathbf{K}_b(1) \right] \chi_a(1) = \epsilon_a \chi_a(1) \tag{1.1.12}$$

Here, $h(1)$ is the operator for the kinetic energy and the potential energy for the attraction of a single electron to the nuclei. The two sums over $b \neq a$ depend on electron-electron interactions, where the first term is the Coulomb term and the second term is the exchange term. The Coulomb term can be interpreted as a one-electron potential in Hartree-Fock (HF) theory, since the summation over all $b \neq a$ corresponds to an averaged potential of the N - 1 electrons, which act on electron χ_a (Eq. 1.1.13):

$$v_a^{coul}(1) = \sum_{b \neq a} \int dx_2 |\chi_b(2)|^2 r_{12}^{-1} \chi_a(1) \tag{1.1.13}$$

We can therefore define a Coulomb operator, Eq. 1.1.14

$$\mathbf{J}_b(1) = \int dx_2 |\chi_b(2)|^2 r_{12}^{-1} \tag{1.1.14}$$

which defines the average local potential at x_1, arising from an electron in χ_b.

The exchange operator $\mathbf{K}$, Eq. 1.1.15, does not have a classical interpretation as the Coulomb operator, but one can define $\mathbf{K}$ by its effect when it operates on a spin orbital $\chi_a(1)$:

$$\mathbf{K}_b(1)\chi_a(1) = \left[\int dx_2 \chi_b^*(2) r_{12}^{-1} \chi_a(2) \right] \chi_b(1) \tag{1.1.15}$$

The Coulomb operator can be expressed in a similar form, Eq. 1.1.16:

$$\mathbf{J}_b(1)\chi_a(1) = \left[\int dx_2 \chi_b^*(2) r_{12}^{-1} \chi_b(2) \right] \chi_a(1) \tag{1.1.16}$$

The comparison of Eqs. 1.1.15 and 1.1.16 shows, that the Coulomb operator is a local operator, which acts on the same electron ($\chi_b(2)$) whereas the exchange operator is a non-local operator, which acts on two different electrons ($\chi_b(2)$ and $\chi_a(2)$).

With Eq. 1.1.15 and Eq. 1.1.16 it follows, that the difference between Coulomb and exchange operator acting on electron-one in χ_a is zero, Eq. 1.1.17:

$$\left[\mathbf{J}_a(1) - \mathbf{K}_a(1) \right] \chi_a(1) = 0 \tag{1.1.17}$$

This term, when added to Eq. 1.1.12, eliminates the restriction of the sum, which now runs over all spin orbitals b. The HF equation can now be written as (Eq. 1.1.18)

$$f(i)\chi(x_i) = \epsilon\chi(x_i) \tag{1.1.18}$$

with the Fock operator $f(i)$ (Eq. 1.1.19):

$$f(i) = -\frac{1}{2}\nabla^2 i - \sum_i^N \sum_A^M \frac{Z_A}{r_{iA}} + v^{HF}(i) \tag{1.1.19}$$

where $v^{HF}(i)$ represents the combined Coulomb and exchange operator, which reduces the many-electron problem of the original Hamiltonian (the electron-electron interaction terms) to an effective one-electron problem. As the field of electrons used in this one-electron problem depends on the

spin orbitals of the electrons and thus the Fock operator depends on its eigenfunctions, the equation system is nonlinear and must be solved iteratively. This iteration procedure is called the self-consistent field (SCF) method, as the field of electrons has to be varied, until overall self-consistency is achieved. When a set of initial coefficients for the molecular orbitals is chosen, the average field the electrons induce on each other can be calculated and the HF equation (Eq. 1.1.18) can be solved to arrive at a new set of orbitals. The new set of orbitals is then again used to calculate the field, solve the equation, etc., until the orbitals (and thus the determinant) no longer change and self-consistency is achieved. The orbitals with their respective eigenvalues now represent the canonical molecular orbitals (MOs) with orbital energies of the best solution for the ground state of a given molecule.

1.2 Basis Sets

As seen in the preceding Chapter, the objective of an SCF calculation is to find a set of MO coefficients which minimize the energy of the electronic eigenvalue problem. So far, we have only derived the operator acting on the MOs; now, the functional form of the wave function built from the MOs will be discussed. Since the exact functional form of the MOs is unknown, the MOs are expressed as a set of functions of which the functional form is known. For a correct description, an infinite amount of functions would be needed, which is not feasible for a calculation. Therefore, a finite set of functions is used, the so called basis set. Each MO is then expressed by atomic orbitals (AOs) of this basis set in a linear combination (LCAO).

There are two commonly used types of AOs in quantum chemistry methods: Slater type orbitals (STOs)[21] (Eq. 1.1.20) and Gaussian type orbitals (GTOs)[22] (Eq. 1.1.21).

$$\chi_{\zeta,n,l,m}(r,\theta,\phi) = NY_{l,m}(\theta,\phi)r^{n-1}e^{-\zeta r} \tag{1.1.20}$$

$$\chi_{\zeta,n,l,m}(r,\theta,\phi) = NY_{l,m}(\theta,\phi)r^{2n-2-l}e^{-\zeta r^2} \tag{1.1.21}$$

Here, N is a normalization constant, $Y_{l,m}(\theta,\phi)$ represent the spherical harmonic functions and r adds the radial dependence to form the AOs. While STOs are more exact from a chemical point of view, since STOs represent the exact description for the hydrogen atom, GTOs are much easier to calculate, since the product of two GTOs is again a GTO. To achieve STO accuracy with GTOs, roughly three times as many basis functions are needed[18].

The minimum basis set of a given atom consists of the minimum number of AOs to contain all electrons present on the atom. For a hydrogen atom, this would simply be one s-orbital (1s), for a carbon a set of two s- (1s, 2s) and three p-orbitals (p_x, p_y, p_z). To increase the accuracy of the MO-description, one can introduce additional basis functions. A double zeta (DZ) basis set consists

of twice the amount of basis functions needed to form the minimum basis set, i. e. two s-functions for a hydrogen atom, four s- and six p-functions for a carbon atom. The amount of functions can be similarly increased to triple zeta (TZ), quadruple zeta (QZ), quintuple zeta (5Z) or higher order basis set expansions.

Additionally, the description of the electron distribution can be improved by adding polarization functions with a higher angular momentum[1]. Polarizing an s-orbital requires p-functions, polarizing a p-orbital requires d-functions etc. Commonly found are also diffuse functions, which help to describe the tail of an atomic orbital far away from the nucleus.

To reduce the amount of basis functions for a given atom, only the valence shell orbitals can be described by an additional set of basis functions. This produces a split valence basis set and is justified by the fact, that core electrons are rarely involved in chemical bonding and behavior of the chemical environment of an atom.

Another very common approach which goes in the same direction is the basis set contraction. Core orbitals may be represented by a fixed linear combination of basis functions and therefore the number of functions varied during the calculation is reduced. The contracted Gaussian type orbitals (CGTOs) are expressed by a sum of primitive Gaussian type orbitals (PGTOs) (Eq. 1.1.22):

$$\chi(CGTO) = \sum_{i}^{k} a_i \chi_i(PGTO) \tag{1.1.22}$$

Pople style basis sets, for example 6-31G[23], make use of this contraction. The 6-31G basis set is a split valence basis, where the core orbitals are described by a contraction of six, the inner part of the valence shell by three and the outer part of the valence by one PGTO. Another example is the TZV basis set by Ahlrichs and coworkers[24,25], which for example contracts a 11s6p1d basis for a carbon atom to a 5s3p1d pattern[2]. The core orbitals are again described as a contraction of six orbitals, and the degree of contraction decreases when moving towards the valence shell orbitals.

If this approach is taken a step further, effective core potentials (ECPs) can be introduced. Expanding the core orbitals of a third or higher row element needs many basis functions, but the electrons are normally not involved from a chemical point of view. Therefore, ECP basis sets model the core orbitals by a single function and by that reduce the number of required basis functions drastically[27,28]. An example for an ECP basis is the LACV3P[29,30] basis used in Pt. II of this work.

---

[1]   This is extremely important e. g. when describing bonds in transition metal complexes.
[2]   Taken from an Orca 2.6 output file[26]

1.3 Density Functional Theory

Density functional theory (DFT) has become one of the most important tools for the theoretical chemist in the last decades and is nowadays also widely used by experimentalists to support their findings[31,32]. With the ongoing development in computer hard- and software, DFT today allows the treatment of molecules with 100-200 atoms readily and thus can be used to solve many of the challenges which arise in modern computational chemistry.

The fundamentals of DFT go back to Hohenberg and Kohn[33], who proved that the ground-state energy of a system can be completely described by the electron density ρ. The $4N$ variable (three Cartesian coordinates and one spin coordinate for each electron) problem of the wave function approach is reduced to a three coordinate problem for the density, which is independent of the number of electrons. The density is calculated from the square of the wave function, integrated over N - 1 electron coordinates. While this approach simplifies the calculation of a ground-state energy significantly, the following problem arises: Since the electron density is correlated to the ground-state energy, a different density also produces a different energy. The functional[3] which connects these entities is unknown and to find the functional, which correctly describes the relation between electron density and the energy of a molecule, is the main problem of DFT.

As shown in one of the preceding Chapters, the electronic energy can be divided into four parts, and we can adapt this approach from HF theory. The total energy of a molecule in the HF framework consists of the kinetic energy $T[\rho]$, the nuclei-electron attraction $E_{ne}[\rho]$, and the electron-electron repulsion consisting of the Coulomb and Exchange part, $J[\rho]$ and $K[\rho]$. Since we use the Born-Oppenheimer approximation, the nuclear-nuclear repulsion E_{nn} can again be treated as constant (Eqs. 1.1.23 to 1.1.26).

$$T_{TF}[\rho] = \frac{3}{10}(3\pi^2)^{\frac{2}{3}} \int \rho^{\frac{5}{3}}(r)dr \tag{1.1.23}$$

$$E_{ne}[\rho] = \sum_a \int \frac{Z_a\rho(r)}{|R_a - r|}dr \tag{1.1.24}$$

$$J[\rho] = \frac{1}{2} \int \int \frac{\rho(r)\rho(r')}{|r - r'|}drdr' \tag{1.1.25}$$

$$K_D[\rho] = -\frac{3}{4}(\frac{3}{\pi})^{\frac{1}{3}} \int \rho^{\frac{4}{3}}(r)dr \tag{1.1.26}$$

In the Thomas-Fermi[34,35] approach, the electrons are treated as a non-interacting uniform electron

---

[3]   A functional is a function of a function, where the inner function depends on parameters and the outer function depends on this inner function.

gas. The total energy, Eq. 1.1.27,

$$E[\rho] = T_{TF}[\rho] + E_{ne}[\rho] + J[\rho] \tag{1.1.27}$$

is known as the Thomas-Fermi energy[34,35]. Including the exchange part $K_D[\rho]$ yields the Thomas-Fermi-Dirac energy[36,37].

Since the approximation of a non-interacting uniform electron gas is not valid for molecules, the energies calculated in the Thomas-Fermi-Dirac model are unacceptable with respect to chemical accuracy ($\sim$ 1 kcal/mol or 4 kJ/mol). To improve the model, Kohn and Sham introduced the Kohn-Sham (KS) orbitals[38]. Since the kinetic energy is represented poorly in the Thomas-Fermi description, the idea by Kohn and Sham was to split this functional in a part, which can be calculated exactly, and another part, which is a small correction to the exact energy. The KS orbitals are used to calculate the exact part of the kinetic energy for a system of non-interacting electrons, which are described by a single Slater determinant of molecular orbitals, which is re-introduced to the DFT formalism. Calculating the electron density of such a determinant, the kinetic energy, Eq. 1.1.28, is given as

$$T_S = \sum_i^N \left\langle \phi_i \left| -\frac{1}{2}\nabla^2 \right| \phi_i \right\rangle \tag{1.1.28}$$

Even with Eq. 1.1.28, the total kinetic energy of a system cannot be calculated, since the approximation of non-interacting electrons is still used. To get to the exact kinetic energy, an exchange-correlation term has to be included. The total DFT energy is then (Eq. 1.1.29)

$$E_{DFT}[\rho] = T_S[\rho] + E_{ne}[\rho] + J[\rho] + E_{XC}[\rho] \tag{1.1.29}$$

where E_{XC} is defined as (Eq. 1.1.30)[32]

$$E_{XC}[\rho] = (T[\rho] - T_S[\rho]) + (E_{ee}[\rho] - J[\rho]) \tag{1.1.30}$$

The exchange-correlation functional can also be separated into a pure exchange and a pure correlation part, Eq. 1.1.31:

$$E_{XC}[\rho] = E_X[\rho] + E_C[\rho] \tag{1.1.31}$$

The objective is now similar to HF theory, namely one has to find a set of orbitals, which minimize the energy of the system. As the exchange and kinetic parts depend on the density, the orbitals have to be determined iteratively.

With the definition of a KS operator $\mathbf{h}_{KS}$, one can define the KS equations, Eq. 1.1.32

$$\mathbf{h}_{KS}\psi_i(x) = \epsilon_i\psi_i(x)$$
$$\mathbf{h}_{KS} = -\frac{1}{2}\nabla^2 + V_{eff} \tag{1.1.32}$$

which lead to the energy eigenvalues. Here, V_{eff} is defined as (Eq. 1.1.33)

$$V_{eff}(r) = V_{ne}(r) + \int \frac{\rho(r')}{|r - r'|}dr' + V_{XC}(r) \tag{1.1.33}$$

and V_{XC}, the exchange-correlation potential, is the derivative of the exchange-correlation energy with respect to the density (Eq. 1.1.34):

$$V_{XC}(r) = \frac{\partial E_{XC}[\rho]}{\partial \rho(r)} \tag{1.1.34}$$

The orbitals can again be expressed in a set of basis functions, comparable to the HF method. It should be noted however, that the energy of the orbitals will be different compared to the HF result.

Deriving the basics of DFT, it becomes clear, that the theory is quite similar to HF theory. The major difference is, that DFT includes correlation consistently, including the Coulomb correlation, which describes the electron-electron interaction of two electrons with the same spin, while HF theory does not. So in principle, if the exact functional would be known, the exact energy of a system within the given model chemistry could be calculated.

1.3.1 Local Density Methods (LDA)

One approach to define the exchange functional are the local density approximation (LDA) methods. Here, it is assumed, that the density can locally be treated as a uniform electron gas. The exchange energy is then given by the Dirac formula (Eq. 1.1.35)

$$E_X^{LDA}[\rho] = -\frac{3}{4}(\frac{3}{\pi})^{\frac{1}{3}} \int \rho^{\frac{3}{4}}(r)dr \tag{1.1.35}$$

Popular examples of LDA methods are the $X\alpha$ method by Slater[39], the VWN functional by Vosko, Wilk and Nusair[40] or the PW91 functional by Perdew and Wang[41]. Common to the LDA functionals is a general underestimation of the exchange energy and an overestimation of the electron correlation energy. Therefore, bonds are normally too strong ("over-binding") when this approach is used, but the overall accuracy is often comparable to HF methods[18].

1.3.2 Gradient Corrected Methods (GGA)

Gradient corrected methods (or generalized gradient approximation (GGA)) extend LDA methods to a non-uniform treatment of the electron gas. Gradients of the electron density are used to improve exchange and correlation energies. As GGAs still only take the density of a given point into account, GGAs are also local methods[18].

Members of the family of GGA methods include the PW86 functional by Perdew and Wang[42] and the B88 correction proposed by Becke[43], both modifying the LDA approach exchange functional. For the correlation energy, Lee, Yang and Parr[44] proposed their LYP functional and Perdew[45,46] published the P86 functional, which was later modified by Perdew and Wang[47] to PW91.

1.3.3 Hybrid Methods

Hybrid methods include a fraction of exact exchange calculated by HF methods into the total exchange-correlation energy. Given the two extremes of non-interacting electrons, where the correlation energy is zero, and fully interacting electrons, where the energy is described by correlation and exchange, the true system can be described by an average between those points, Eq. 1.1.36:

$$E_{XC} \simeq \frac{1}{2} \langle \Psi_0 \left| V_{XC}(0) \right| \Psi_0 \rangle + \frac{1}{2} \langle \Psi_1 \left| V_{XC}(1) \right| \Psi_1 \rangle \tag{1.1.36}$$

The exchange energy at point zero can be described exactly by HF methods, if the KS orbitals are identical to the HF orbitals[4]. The total exchange-correlation energy of this "half-and-half" functional (Eq. 1.1.37), proposed by Becke[48], then relates to

$$E_{XC}^{H+H} = \frac{1}{2} E_X^{HF} + \frac{1}{2} (E_X^{LDA} + E_C^{LDA}) \tag{1.1.37}$$

Another very popular example of a hybrid method is the B3LYP functional, which consists of the Becke three-parameter functional and the Lee, Yang, Parr description of the correlation energy[49–51]. Here, the exchange-correlation energy is calculated by a combination of exact HF exchange energy, LDA exchange energy, an additional correction to the exchange energy and a LDA and GGA part for the correlation energy (Eq. 1.1.38):

$$E_{XC}^{B3} = (1-a)E_X^{LDA} + aE_X^{HF} + b\Delta E_x^{B88} + E_C^{LDA} + c\Delta E_C^{GGA} \tag{1.1.38}$$

---

[4]   This is generally not the case, but nevertheless represents a good approximation to the problem

The coefficients a, b and c are determined empirically. In the original B3LYP functional $a = 0.20$, $b = 0.72$ and $c = 0.81$, so 20% of the total exchange-correlation energy is given by the exact HF exchange. The amount of exact HF exchange can be increased, which has been done in functionals like B1LYP[52] (25% of exact HF exchange), or decreased, e. g. in B3LYP*[53,54] (15% of exact HF exchange).

2 Force Field Methods

Force field methods represent one of the more simplistic but nevertheless very popular and powerful approaches in computational chemistry. Opposed to quantum chemistry calculations, force fields do not handle electrons explicitly, but are parametrized to include electronic effects implicitly. Force fields are generally more applicable to problems related to relative energies of conformers or isomers, cavity sizes, conformational searches and molecular dynamics, all of which are mostly governed by steric effects, and can be used for large scale calculations, as the computational cost is significantly lower compared to QC methods.

Force field methods handle molecules as an ensemble of atoms connected by bonds with a given connectivity. Forces between atoms can either occur along a bond, e. g. bond stretching or valence angle bending, or through space, e. g. van der Waals interactions and electrostatics. Through bond interactions are usually described by a classical mechanics "balls and springs" model. Therefore, force field methods are also referred to as molecular mechanics methods[18].

The steric (or strain) energy E_{steric} in a force field is calculated by the deviation of the individual interactions from their reference values. Reference values for bond distances, valence bond angles, torsion angles etc. are usually gathered empirically from crystal structures, spectroscopic data or quantum mechanical calculations. The complete steric energy of a molecule can be described as a sum over all these individual contributions (Eq. 1.2.1):

$$E_{steric} = \sum E_{stretch} + \sum E_{bend} + \sum E_{torsion} + \sum E_{vdW} + \sum E_{electrostatic} \qquad (1.2.1)$$

Additional cross terms, e. g. out of plane interactions or a stretch-bend term, can also be included in the force field. As Saunders and Jarret have shown[55], interactions for bond and torsion angles can also be replaced by distances in a central force field approach.

In the force field used by Momec[11,12,56–61], the individual contributions from Eq. 1.2.1 are calculated as follows, Eqs. 1.2.2 to 1.2.6:

$$E_{stretch}(r - r_0) = \frac{1}{2}k(r - r_0)^2 \qquad (1.2.2)$$

$$E_{bend}(\theta - \theta_0) = \frac{1}{2}k(\theta - \theta_0)^2 \qquad (1.2.3)$$

$$E_{torsion}(\omega) = \sum_{n=1} V_n cos(n\omega) \qquad (1.2.4)$$

$$E_{vdW}(r) = Ae^{-Br} - \frac{C}{r^6} \qquad (1.2.5)$$

$$E_{elec.}(r) = \frac{Q^A Q^B}{\epsilon r} \qquad (1.2.6)$$

The *stretch energy* $E_{stretch}$ (Eq. 1.2.2) is treated by Hook's Law and described by a Taylor series around an equilibrium bond length, which in the simplest fashion gives a harmonic oscillator. k is the force constant and r_0 the equilibrium bond length, both of which are parameters of the force field. The harmonic approximation fails to reproduce the correct dissociation behavior for a bond, as the energy tends to infinity with larger bond lengths. For a correct description, a Morse potential, Eq. 1.2.7, or a Taylor expansion around the equilibrium bond length has to be used instead:

$$E_{Morse}(r - r_0) = D[1 - e^{\alpha(r-r_0)}]^2 \qquad (1.2.7)$$

D is the dissociation energy and α the curvature, which is related to the force constant by Eq. 1.2.8:

$$\alpha = \sqrt{\frac{k}{2D}} \qquad (1.2.8)$$

However, for small deviations from the equilibrium bond length, a harmonic description of the stretch interaction is sufficient.

The *bending energy* E_{bend} (Eq. 1.2.3) is treated similarly to the stretch energy by Hook's law and a Taylor expansion around the equilibrium angle, usually terminated at second order. Again, k is the force constant and θ_0 the equilibrium bond angle parametrized in the force field.

The *torsional energy* $E_{torsion}$ (Eq. 1.2.4) for a torsion around a bond B-C in a sequence of four bonded atoms A-B-C-D has to account for the periodicity of the torsion. Therefore, the energy is given as a Fourier series where n describes the periodicity of the torsion and V_n gives the appropriate rotation barrier around B-C.

The *van der Waals energy* E_{vdW} (Eq. 1.2.5) describes the repulsion at very short, attraction at medium and no interaction at very large distances of non-bonded atoms. The "Buckingham" or "Hill" potential[62] is one approach to describe van der Waals interactions where A, B and C are interaction specific constants parametrized in the force field. The Lennard-Jones potential[63], Eq. 1.2.9, is also commonly used:

$$V(r) = 4D\left\{ \left(\frac{\sigma}{r}\right)^{12} - \left(\frac{\sigma}{r}\right)^6 \right\} \qquad (1.2.9)$$

where D is the depth of the potential well and σ the equilibrium distance.

The *electrostatic energy* $E_{elec.}$ (Eq. 1.2.6) describes the interaction between charged atoms. The classical interaction between point charges is given by the Coulomb potential where Q^A and Q^B are the atomic charges of atoms A and B and ϵ is the vacuum permittivity, which is defined as (Eq. 1.2.10):

$$\epsilon = \frac{1}{\mu_0 c_0^2} \qquad (1.2.10)$$

where μ_0 is the vacuum permeability and c_0 the speed of light.

In addition to the functional form of a force field, which has just been described, one also has to define a suitable set of parameters. To account for different bonding situations, e.g. of a carbon atom, atom types are introduced. In the Momec97[56–61] force field (see Appendix C for details) currently 14 different carbon atom types are defined, which range from a general tetrahedral sp^3 hybridization (Atom type CT) to very specific bonding situations like a carbon atom in an imine bound to a Cu^I center (Atom type CI). Atom types are based on the general assumption that a molecule is built from functional units and that the general behavior of these units is transferable between molecules. As an example, a bond between two carbon sp^3 atoms has a bond length of about 1.54 Å in every molecule and thus can be parametrized with an equilibrium bond length around that value.

In contrast to the definition of multiple atom types per element, Rappé et al. proposed a universal force field (UFF) approach[64–66], where the force field parameters are automatically calculated for every atom type of the periodic table. The parameters are derived from literature values, e. g. atom-type specific single bond order radii.

Force field methods are inexpensive when it comes to computational cost. Geometry optimizations can normally be performed within a few seconds, even with large molecules like proteins. Given a well parametrized force field, molecular mechanics methods can make accurate predictions of geometries and relative energies for a large number of compounds quickly and are often the only method to investigate the full potential energy surface (PES) of a molecule.

3 Molecular Magnetism

Molecular magnetism represents one of the emerging fields in modern chemistry. First transition metal complexes which exhibit cooperative magnetic properties of magnetic centers were discovered as early as in the 1950s[67], while interest in the field heightened just at the end of the last century[68–70]. Following shortly was the discovery of a new class of compounds, the so called single molecule magnets (SMMs)[1–3]. SMMs contain unpaired electron spins, usually in form of transition metal centers, and show a slow relaxation of the magnetization at low temperatures. They therefore retain their magnetic information, which makes these compounds attractive e. g. for highly efficient data storage systems, molecular freezers[4,5], switches and quantum computers[6].

To understand the theory behind SMMs, some fundamental aspects of magnetism have to be introduced. When a material enters a magnetic field, the field lines are distorted. One can distinguish between diamagnetic materials, where the magnetic field inside the material is smaller than the outer field, or paramagnetic materials, where unpaired electrons align along the outer field and thus generate a larger total field inside the compound. The difference between inner and outer field is the magnetization M, Eq. 1.3.1:

$$M = (B - H_0)/4\pi \tag{1.3.1}$$

Here, B is the inner field and H_0 the outer field.

If multiple magnetic centers, e. g. atoms or molecules, interact with each other, three different situations may occur: ferromagnetic, anti-ferromagnetic or ferrimagnetic behavior. One can observe these properties for example in the well-known Weiss domains[71]. Parallel alignment of all spins in one domain induces ferromagnetism, anti-parallel alignment induces anti-ferromagnetism. Ferrimagnetism is similar to anti-ferromagnetism, but in this case the number of spins pointing in opposite directions differ, which leads to an overall reduced magnetization.

Given the derivative of the magnetization M with respect to the outer field H, one can define a new quantity, the molar magnetic susceptibility[72], Eq. 1.3.2

$$\chi = \frac{\partial M}{\partial H} \tag{1.3.2}$$

which is defined as a molar quantity. It is important to note, that the cgsemu unit system is often used in the field of molecular magnetism, since important constants, like the permeability in vacuum, which is equal to one, are easier to handle in this system. Therefore, the magnetization M is often given in units of Gauss.

If only a weak magnetic field is present, the magnetization M is linearly dependent on the outer field H and Eq. 1.3.2 simplifies to Eq. 1.3.3

$$M = \chi H \tag{1.3.3}$$

The susceptibility consists of a negative diamagnetic (χ^D) and a positive paramagnetic (χ^P) part. If χ^D is much larger than χ^P, the material shows diamagnetic behavior, whereas the compound shows paramagnetic behavior, if χ^P is larger than χ^D.

Since χ^D is independent of the outer field and the temperature, it can be approximated by a simple formula, Eq. 1.3.4:

$$\chi^D = k\mathbf{M} \times 10^{-6} mol^{-1} \tag{1.3.4}$$

where k is a molecule-specific constant between 0.4 and 0.5 and $\mathbf{M}$ is the molecular weight of the molecule. Pascal[73] also introduced an additive method to estimate the diamagnetic susceptibility.

With the definition of the molar magnetic susceptibility as the interaction between the outer field and the total spin of the molecule, this relation can be transferred to classical mechanics, where the magnetization depends on the change in energy E of the system with respect to the outer magnetic field H (Eq. 1.3.5):

$$M = -\frac{\partial E}{\partial H} \tag{1.3.5}$$

Quantum mechanics introduces the description of the total energy of a molecule by discrete energy levels E_n. Thus, the microscopic magnetization μ_n is defined as the change of these energy levels with respect to the change of the outer field (Eq. 1.3.6):

$$\mu_n = -\frac{\partial E_n}{\partial H} \tag{1.3.6}$$

If the Boltzmann distribution is used over all energy levels and a summation is done over all possible states n, one can define the macroscopic magnetization M (Eq. 1.3.7) as:

$$M = N \frac{\sum_n -\frac{\partial E_n}{\partial H} exp(-\frac{E_n}{kT})}{\sum_n exp(-\frac{E_n}{kT})} \tag{1.3.7}$$

Eq. 1.3.7 is the "fundamental expression in molecular magnetism"[72], since the formula relies solely on constants and observables and does not contain any approximations.

3.1 The van Vleck Equation

While Eq. 1.3.7, derived in the previous section, is able to describe the exact magnetization of a given molecule, this would only be possible if all states E_n which depend on the applied magnetic field are known. Since this is not the case, van Vleck proposed an approximation in 1932[74], based on a few simplifications.

He stated, that the energy of one of the microscopic states, E_n, can be expressed as a Taylor series expansion of the outer field H given in Eq. 1.3.8

$$E_n = E_n^{(0)} + E_n^{(1)} H + E_n^{(2)} H^2 + \dots \tag{1.3.8}$$

where $E_n^{(0)}$ stands for the energy of the system in zero field and $E_n^{(1)}$, $E_n^{(2)}$, ... represent the Zeeman coefficients of first, second and higher order. This expansion can be used together with the definition of the microscopic magnetization (Eq. 1.3.6) and the following expression can be derived (Eq. 1.3.9):

$$\mu_n = -E_n^{(1)} - 2E_n^{(2)} H + \dots \tag{1.3.9}$$

In addition, van Vleck assumed, that the ratio H/kT is small compared to unity, if the outer field is small compared to the temperature. This approximation is used together with the series expansion in Eq. 1.3.7 and the magnetization M can be expressed as (Eq. 1.3.10)

$$M = N \frac{\sum_n (-E_n^{(1)} - 2E_n^{(2)} H)(1 - E_n^{(1)} \frac{H}{kT}) exp(-\frac{E_n^{(0)}}{kT})}{\sum_n (1 - E_n^{(1)} \frac{H}{kT}) exp(-\frac{E_n^{(0)}}{kT})} \tag{1.3.10}$$

Since the magnetization vanishes in zero field, it follows that (Eq. 1.3.11):

$$\sum_n E_n^{(1)} exp(-\frac{E_n^{(0)}}{kT}) = 0 \tag{1.3.11}$$

If Eq. 1.3.11 is used in conjunction with Eq. 1.3.10 and only terms linear in H are retained, the magnetization is then defined as given in Eq. 1.3.12

$$M = N \frac{H \sum_n (\frac{E_n^{(1)2}}{kT} - 2E_n^{(2)}) exp(-\frac{E_n^{(0)}}{kT})}{\sum_n exp(-\frac{E_n^{(0)}}{kT})} \tag{1.3.12}$$

and the magnetic susceptibility as

$$\chi = N \frac{\sum_n (\frac{E_n^{(1)2}}{kT} - 2E_n^{(2)}) exp(-\frac{E_n^{(0)}}{kT})}{\sum_n exp(-\frac{E_n^{(0)}}{kT})} \tag{1.3.13}$$

Eq. 1.3.13 is called the van Vleck-formula, which allows to calculate the susceptibility from the energies $E_n^{(0)}$, $E_n^{(1)}$ and $E_n^{(2)}$. If $E_n^{(0)}$ and the eigenfunctions $|n\rangle$ of the Hamilton operator in zero field are know, $E_n^{(1)}$ and $E_n^{(2)}$ can be determined by perturbation theory (Eq. 1.3.14 and 1.3.14):

$$E_n^{(1)} = \langle n |\mathbf{H}_{ZE}| n \rangle \tag{1.3.14}$$

$$E_n^{(2)} = \sum_{E_m^{(0)} \neq E_n^{(0)}} \frac{\langle n |\mathbf{H}_{ZE}| n \rangle^2}{(E_n^{(0)} - E_m^{(0)})} \tag{1.3.15}$$

$\mathbf{H}_{ZE}$ is the Zeeman operator which describes the interaction between the magnetic field and the electronic angular momenta (Eq. 1.3.16)

$$\mathbf{H}_{ZE} = \beta \sum_i (\mathbf{I}_i + g_e \mathbf{s}_i) \cdot H \tag{1.3.16}$$

$\mathbf{I}_i$ stands for the orbital momentum and $\mathbf{s}_i$ for the spin momentum of electron i. g_e is the gyromagnetic factor of the free electron (2.0023) and β is the Bohr magneton ($4.669 \cdot 10^{-5} cm^{-1} G^{-1}$).

3.2 Curie's Law

In its simplest form, molecular magnetism is represented by a single magnetic center, e. g. a transition metal with unpaired electrons. If the electronic ground-state does not have an angular momentum, i. e. the total spin is not larger than $\frac{1}{2}$, and the excited energy levels are much higher in energy, the spin states are degenerate in zero magnetic field.

When the external field is applied, the energy levels are split into the Zeeman levels, Eq. 1.3.17:

$$E_n = M_S g \beta H \tag{1.3.17}$$

where M_s varies from $-S$ to $+S$ and g represents the isotropic gyromagnetic factor. This splitting can be assumed, since the excited states are much higher in energy and thus cannot couple with the ground state.

With the approximations of van Vleck (Eq. 1.3.13), the energy terms of zeroth (Eq. 1.3.18) and first order (Eq. 1.3.19) are

$$E_n^{(0)} = 0 \tag{1.3.18}$$

$$E_n^{(1)} = M_S g \beta \tag{1.3.19}$$

The magnetic susceptibility then equals to (Eq. 1.3.20)

$$\chi = \frac{Ng^2\beta^2}{3kT} \sum_{M_S=-S}^{+S} \frac{M_S^2}{(2S+1)} \tag{1.3.20}$$

which can be expressed as

$$\chi = \frac{Ng^2\beta^2}{3kT}S(S+1) \tag{1.3.21}$$

As all factors other than the temperature are constants, the molar magnetic susceptibility can also be expressed as $\chi = C/T$, where C is the Curie constant which depends on the total spin of the ground state. Eq. 1.3.21 is known as Curies law, postulated in 1895 by Pierre Curie[75].

3.3 Zero-Field Splitting

When introducing Curie's law, we assumed, that only a single electron with spin $\frac{1}{2}$ is present on the magnetic center of interest. If the number of spins is larger, e.g. in transition metal centers with multiple unpaired electrons and thus a multiplicity larger than 2, a splitting of the Zeeman levels in zero field due to spin-orbit coupling is observed. The so called zero-field splitting (ZFS) leads to magnetic anisotropy even without an external magnetic field.
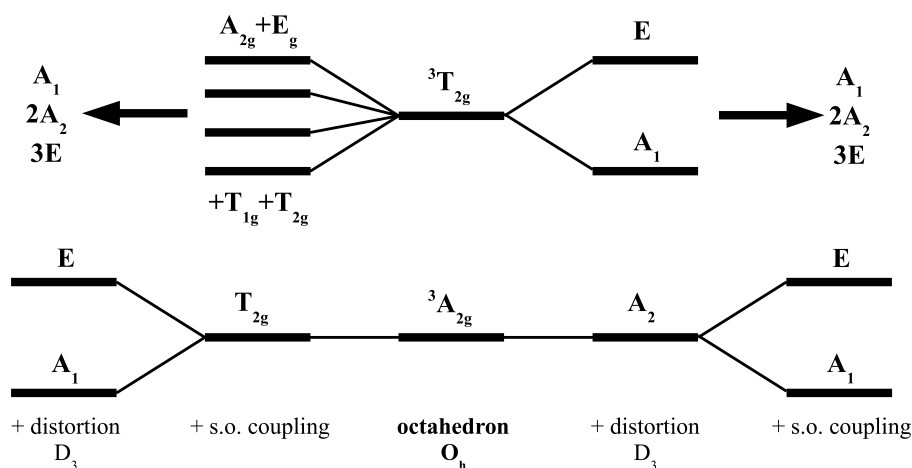
Figure 1.3.1: ZFS in a Ni^{II} ion in a trigonally distorted octahedral coordination geometry[72]

Given a Ni^{II} ion in octahedral symmetry (O$_h$ point group) one can explain the ZFS in a qualitative way[1] (see also Fig. 1.3.1). Ni^{II} has a t$_2^6$e^2 ground-state with a ^{3}A$_{2g}$ term and a t$_2^5$e^3 excited state with a ^{3}T$_{1g}$ and a ^{3}T$_{2g}$ term. Since the ^{3}T$_{2g}$ term is lower in energy, we will use it during the following illustration. Splitting of the energetic levels may be achieved by two effects: symmetry reduction and spin-orbit coupling. Lowering of the symmetry from O$_h$ to e. g. D$_3$ splits the ^{3}T$_{2g}$ term of the excited state into an ^{3}A$_1$ term and a doubly degenerate ^{3}E term while the ground-state term ^{3}A$_2$ is retained. Applying spin-orbit coupling leaves the molecular symmetry unchanged, but applies a T$_{1g}$ operation to both ground and excited states. The direct product of T$_{1g}\times$T$_{2g}$ is A$_{2g}$+E+T$_{1g}$+T$_{2g}$, splitting the excited state into a singly, doubly and two triply degenerate terms. For the ground state, T$_{1g}\times$A$_{2g}$ is T$_{2g}$, so the ground state retains its degeneracy. Applying both distortions, the degeneracy of the ground state is lifted. If spin-orbit coupling is applied first, the following reduction of the symmetry to D$_3$ splits the T$_{2g}$ ground state into A$_1$ and E. If the symmetry is reduced first, the spin-orbit operation transforms as A$_2$ and E and thus also splitting the ground state into A$_1$ and E. The ZFS is usually characterized by two constants, the axial ZFS parameter D and the rhombic ZFS parameter E. Given a low symmetry, degeneracies may not be lifted totally. States which retain their double degeneracy are called Kramers doublets and may occur in systems with even spin multiplicity.

3.4 Single Molecule Magnets

When a magnetic field is applied to a magnetic material until the maximum magnetization has been reached, the relaxation of the magnetization after switching off the field can be measured. The relaxation time τ defines the rate at which the magnetization decays. Assuming an exponential behavior of the relaxation, Eq. 1.3.22 can be formulated[76]

---

[1]   For a detailed introduction to the term symbols used here see Pt. III Ch. 1

$$M(t) = M_{eq}(H) + \delta M_0 exp(-t/\tau) \tag{1.3.22}$$

Here, $M_{eq}(H)$ is the equilibrium magnetization and τ the relaxation time. If τ is measured in dependence of the temperature T, an Arrhenius correlation can be derived, Eq. 1.3.23

$$\tau = \tau_0 exp(T/T_0) \tag{1.3.23}$$

where T_0 is the calculated maximum energy barrier in Kelvin at which the magnetization is retained (see below). At very low temperatures however, the Arrhenius law is not observed in measurements of SMMs such as $Mn_{12}ac$[2] ($[Mn_{12}O_{12}(CH_3COO)_{16}(H_2O)_4]$). The magnetization is retained, even when the magnetic field is switched off. This behavior can be explained if a potential barrier U which separates the $-S$ from the $+S$ states (Fig. 1.3.2) is assumed, where S is the total spin of the molecule.
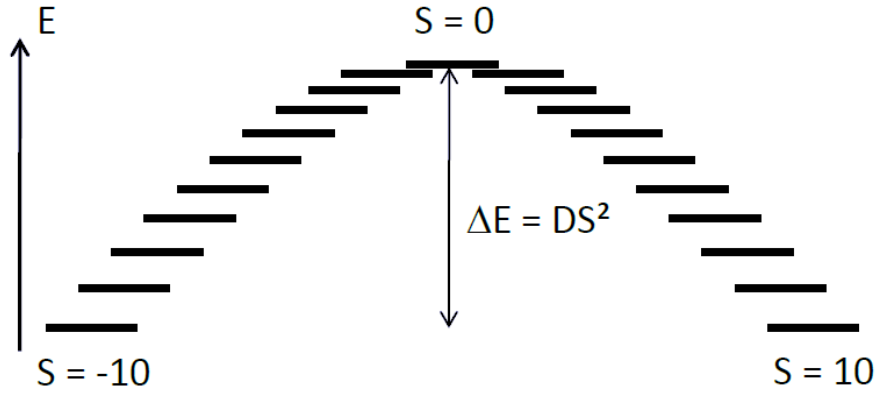
Figure 1.3.2: Potential barrier between the S=-10 and S=10 states in $Mn_{12}ac$.

The barrier between the two states of maximum magnetization is described by the Hamiltonian given in Eq. 1.3.24

$$\mathbf{H} = DS_z^2 \tag{1.3.24}$$

where D is the axial ZFS and S_z the total spin of the system along the magnetization axis. The sign of D has to be negative in order for the states with maximum S to be the low lying states. Relaxation of the magnetization can occur via thermal relaxation or quantum tunneling between the lowest lying or excited states. The potential barrier U and thus the effectiveness of an SMM directly depends on D and S. For integer spin systems, the barrier is calculated by Eq. 1.3.25 (a) whereas for half-integer systems the barrier is given by Eq. 1.3.25 (b)

$$\begin{array}{ll} (a) & U = |DS^2| \\ (b) & U = |D(S^2 - 1/4)| \end{array} \tag{1.3.25}$$

Part II

DFT Benchmarks for the Calculation of Exchange Coupling Constants

1 Introduction

As explained in greater detail in the general introduction of this thesis, a thorough understanding of the electronic structure of transition metal centers and the quantitative estimate of the exchange coupling are of great interest in the field of molecular magnetism. In order to be able to design and prepare new efficient SMMs, an accurate prediction of the exchange coupling constant is of importance, as the exchange coupling can give insights about the low-lying electronic states of transition metal complexes[77]. After initial calculations based on the $X\alpha$ method[78], the broken symmetry approach[79] was developed, which will be described in greater detail in the following Chapter. More involved quantum-chemical calculations such as complete active space SCF (CASSCF)[18] or configuration interaction (CI)[18] methods have been applied to calculate exchange interactions[80], but are to date only rarely used because of the computational demands. Semi-empirical methods have been used for a qualitative description of magnetic interactions, but DFT methods have been established as the method of choice for quantitative calculations[81].

As a systematic benchmark for different DFT functionals, basis sets and software packages was not available in the literature, a simple dinuclear complex was chosen and used to benchmark the broken symmetry method. The well-characterized bisphenolato-bridged dicopper(II) complex[82,83] (Fig. 2.1.1) with two antiferromagnetically coupled Cu^{II} centers shows an exchange coupling constant[1] of J = -298 cm^{-1}. Since the system is relatively small, it is attractive for a systematic study, because the computational cost for calculations is low and an efficient and thorough testing of different methods and software packages is possible.

---

[1]   Based on Eq. 2.2.1; the derivation of the exchange coupling constant and the Heisenberg-Dirac-van-Vleck Hamiltonian will be presented in detail in Ch. 2 of this Part.
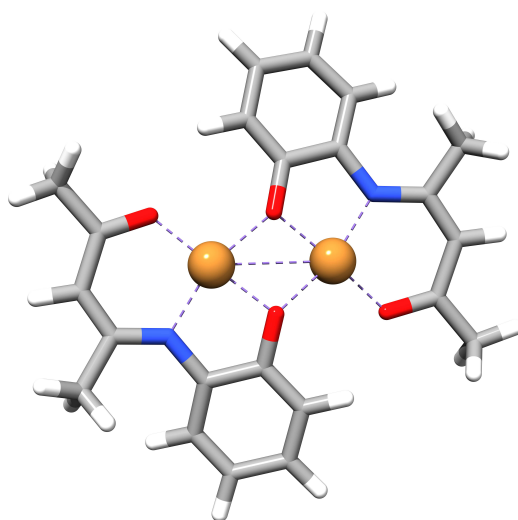
Figure 2.1.1: Bisphenolato-bridged dicopper(II) complex

The information obtained from the benchmark procedure was then used to calculate the exchange coupling constant for a wide range of oligonuclear compounds which contained Cu^{II}, Fe^{III}, Cr^{III}, V^{IV}, Mn^{II}, Mn^{III}, Mn^{IV}, Ni^{II} and Co^{III} transition metal ions.

Since the aim of this project was to predict exchange coupling constants, geometry optimizations have also been done where possible and the exchange coupling constants have been calculated from the optimized structures. The geometry optimization of a structure represents the only way to obtain magnetic properties for novel complexes, where X-ray structure data is not available as a starting geometry for the calculation.

2 The Broken Symmetry Approach

If unpaired electrons are present on the metal centers of an oligonuclear transition metal complex, the spins of these electrons can couple either ferro- or antiferromagnetically, Figs. 2.2.1 and 2.2.2:
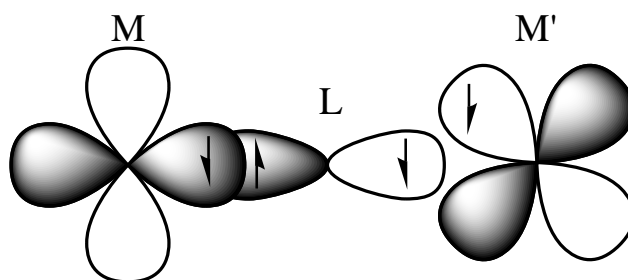
Figure 2.2.1: Ferromagnetic coupling of two metal centers via σ-bonding
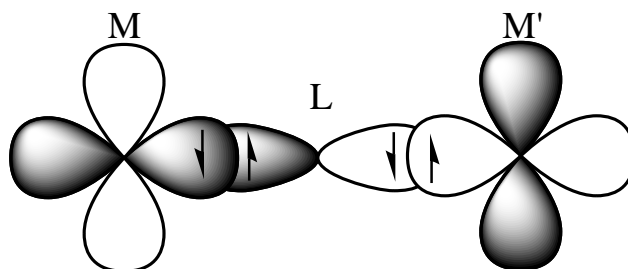
Figure 2.2.2: Anti-ferromagnetic coupling of two metal centers via σ-bonding

Given the interaction between the two centers, atomic spin quantum numbers are no longer valid to describe the coupled spin system. A total spin quantum number S, which in the simplest case of one unpaired electron at each of the metal centers (e. g. Cu^{II}_2) is either S = 0 for the antiferromagnetically coupled or S = 1 for the ferromagnetically coupled state, is used for a proper description of the system. The energy difference between the two states is described by the exchange coupling constant J. A negative value of J denotes an anti-ferromagnetic ground state while a positive J indicates a ferromagnetic ground state[72]. The energy and the magnetic properties of dinuclear transition metal systems can be described by the Heisenberg-Dirac-van Vleck Hamiltonian[74,84–86]:

$$\hat{H}_{HDVV} = -2J_{12}\hat{S}_1\hat{S}_2 \tag{2.2.1}$$

Here, J_{12} is the exchange coupling constant between the two metal centers, and $\hat{S}_1$ and $\hat{S}_2$ are the spin operators for the magnetic centers. At this point it is important to note, that several definitions of the

Heisenberg-Dirac-van Vleck Hamiltonian are used in the literature[81]. While results in this thesis are consistently based on Eq. 2.2.1 if not noted otherwise, one may encounter the following definitions elsewhere (Eqs. 2.2.2 to 2.2.4):

$$\hat{H}_{HDVV_2} = 2J_{12}\hat{S}_1\hat{S}_2 \tag{2.2.2}$$

$$\hat{H}_{HDVV_3} = J_{12}\hat{S}_1\hat{S}_2 \tag{2.2.3}$$

$$\hat{H}_{HDVV_4} = -J_{12}\hat{S}_1\hat{S}_2 \tag{2.2.4}$$

The calculation of the exchange coupling constant J causes a problem with the underlying DFT theory. While the high spin state for a dinuclear system ($\uparrow\uparrow$) is easily described in the density functional theory framework, the low spin state ($\uparrow\downarrow - \downarrow\uparrow$) can only be described by multiple determinants, which is not possible in DFT[31].

An approach for this problem is the so called broken symmetry method which was first proposed by Noodleman[79]. Starting from a single determinant wave function ($\uparrow\downarrow$ or $\downarrow\uparrow$) as a guess for the true low spin state, the variational principle to re-optimize the orbitals is applied[87]. The relaxed wave function then represents the broken symmetry solution to the problem. As an artifact of this method, the result will yield the correct charge density of the molecule, but an incorrect spin density. The true spin density of the low spin state should be zero throughout the whole molecule, which is not the case for the broken symmetry solution (see Fig. 2.2.3).
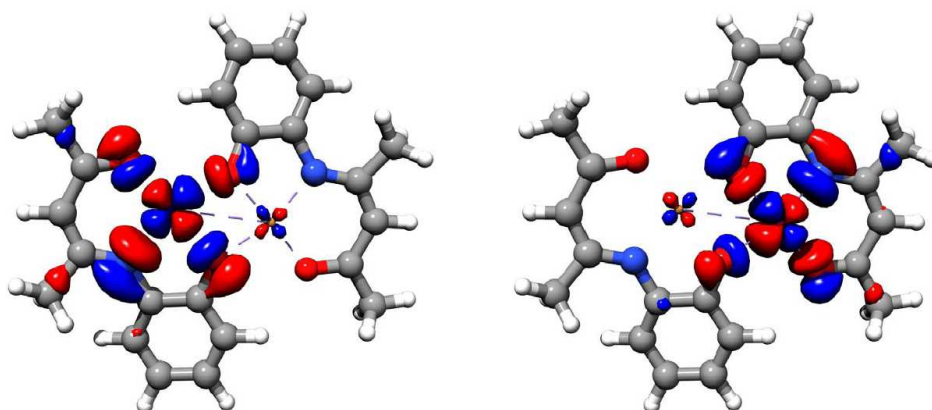
Figure 2.2.3: Spin densities of the broken symmetry solution for the Cu^{II}_2 benchmark system. Clearly visible are the two uncoupled spins in the $d_{x^2-y^2}$ orbitals of the two metal centers. Some spin density is also delocalized over the bridging atoms.

With the spin Hamiltonian (Eq. 2.2.1) and the correct charge density and thus the correct energy of the high- and low-spin state of the dinuclear complex one now can compute the exchange coupling constant between metal centers 1 and 2. Given the relation in Eq. 2.2.5, where $\hat{S}$ is the total spin

operator and $\hat{S}_1$, $\hat{S}_2$ are the spin operators for the individual magnetic centers,

$$\hat{S}^2 = \hat{S}_1^2 + \hat{S}_2^2 + 2\hat{S}_1\hat{S}_2 \tag{2.2.5}$$

the Heisenberg-Dirac-van Vleck Hamiltonian (Eq. 2.2.6) becomes

$$\hat{H}_{HDVV(spin)} = -J(\hat{S}^2 - \hat{S}_1^2 - \hat{S}_2^2) \tag{2.2.6}$$

If one assumes, that the wave functions of the high- and low-spin states are eigenfunctions of $\hat{S}_1^2$ and $\hat{S}_2^2$, the expectation values are, Eqs. 2.2.7 and 2.2.8

$$E_{HS} = -J(\langle \hat{S}^2 \rangle_{HS} - S_1(S_1+1) - S_2(S_2+1)) \tag{2.2.7}$$

$$E_{BS} = -J(\langle \hat{S}^2 \rangle_{BS} - S_1(S_1+1) - S_2(S_2+1)) \tag{2.2.8}$$

where $\langle \hat{S}^2 \rangle_{HS}$ and $\langle \hat{S}^2 \rangle_{BS}$ are the spin expectation values of the high- and low-spin state, respectively. When Eq. 2.2.7 and Eq. 2.2.8 are subtracted from each other and the result is solved for J, Eq. 2.2.9 can be derived:

$$J = -\frac{E_{HS} - E_{BS}}{\langle \hat{S}^2 \rangle_{HS} - \langle \hat{S}^2 \rangle_{BS}} \tag{2.2.9}$$

Eq. 2.2.9 has been proposed by Yamaguchi et al.[88,89] and represents an "interpolative"[77] broken symmetry solution. In the extreme cases of an uncoupled system or a "true" coupled low-spin configuration, Eq. 2.2.9 reduces to the so called spin-projected equation (Eq. 2.2.10) for the former, or spin-unprojected equation (Eq. 2.2.11) for the latter case:

$$J = -\frac{E_{HS} - E_{BS}}{S_{max}^2} \tag{2.2.10}$$

$$J = -\frac{E_{HS} - E_{BS}}{S_{max}(S_{max} + 1)} \tag{2.2.11}$$

The spin-projected formalism is directly implied by Noodlemans[79] treatment of the broken symmetry problem while the spin-unprojected approach was developed by Ruiz et al.[90]

3 Computational Methods

In order to benchmark available DFT methods, corresponding basis sets and software packages, a large number of calculations on the bisphenolato-bridged dicopper(II) complex were performed (Fig. 2.1.1 and Table 2.4.1). Gaussian 03 (G03)[91], Jaguar 6.5[92] and Orca 2.6.04[26] were chosen as software packages, since the majority of all calculations in this field of research are done with one of these packages. As DFT functionals, a number of hybrid (B3LYP[49–51], B3P86[45], B3PW91[93]), GGA (BLYP[43,44,94], BP86[43–45,94], BPW91[93], PBE[95]) and LDA (SVWN[33,40]) functionals were compared. For the basis sets, the small basis 3-21G[96–101] was compared to the triple zeta basis TZV[24,25], the polarized triple zeta TZVP[24,25] and basis set combinations of TZVP for metal atoms and DZP[102–104] for the remaining atoms as well as TZVP for metal atoms plus first coordination sphere and 6-31G*[23,105–113] for the remaining atoms (see Fig. 2.3.1)[1].
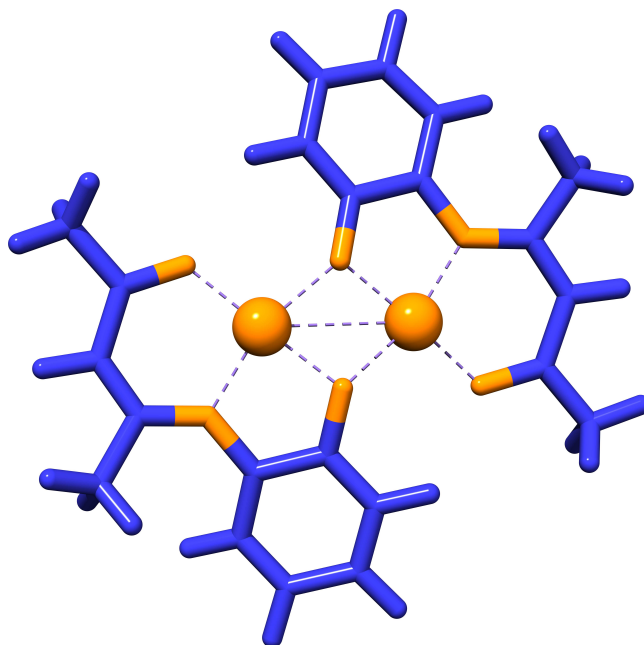
Figure 2.3.1: Split basis set approach shown on the Cu[II] benchmark system; orange atoms are described by a high basis (TZVP or LACV3P++**) while blue atoms are described with the 6-31G* basis set.

As the goal for this benchmark was to identify an accurate, fast and reliable method for the calculation of exchange coupling constants, a performance criterion was also the amount of time needed to obtain the result as well as accuracy compared to experimental results.

---

[1]   For technical reasons concerning calculations on more than one processor, TZVP was substituted by the qualitatively similar basis set LACV3P++**[29,30] in parallel calculations done with the Jaguar program.

Initial guesses for the electronic structure of the high-spin state are trivial to get in all three software packages, and Jaguar was used to get the broken symmetry initial guess for G03[2]. While the generation of broken symmetry states was already possible with a combination of Gaussview and G03 (but included a tedious identification of the magnetic orbitals), the fragment approach of the new release Gaussian 09 (G09)[114] introduced a similar functionality to Jaguars' atomic section and thus makes the generation of the initial guess with Jaguar obsolete. For Orca, the "BrokenSym" keyword of the %scf section has been used.

All calculations were converged to a threshold of 10^{-6} hartree (= $2.625 \cdot 10^{-3}$ kJ/mol) for the change in energy and a root mean square deviation in the density of 10^{-8}. For geometry optimizations, the high-spin state was used as a reference for the multiplicity and default options were used for Jaguar as well as for Orca[3]. Geometries were checked for PES minima by frequency calculations and single points were calculated to yield the exchange coupling constants.

Since calculated values are compared to experimental values, the root mean square deviation (RMSD) was calculated according to the following formula:

$$RMSD(J) = \sqrt{\frac{\sum\limits_{n=1}^{N} (J_{n(calc)} - J_{n(ref)})^2}{N}} \qquad (2.3.1)$$

---

2   keyword ip160 = 4
3   The iascf=4 flag was set in Jaguar to achieve faster convergence.

4 Results and Discussion

In order to establish a reliable and fast method to compute exchange coupling constants, the first step was to benchmark the software packages, functionals and basis sets mentioned in the preceding Chapter on the dinuclear copper(II) system (see Fig. 2.1.1). The results of these benchmark calculations are given in Table 2.4.1.

Table 2.4.1: Exchange coupling constant J calculated for the benchmark complex
(Fig. 2.1.1, J_{exp} = -298 cm^{-1}) with different basis sets, software packages and functionals.

method	J_{G03} [cm^{-1}][a]	J_{Orca} [cm^{-1}]	J_{Jaguar} [cm^{-1}]	CPU time$_{Jaguar}$ [h]
B3LYP/TZV	-229	-231	-231	4.60
B3P86/TZV	-238	-227	-241	3.71
B3PW91/TZV	-228	-230	-227	3.44
BLYP/TZV	-838	-838	-854	4.00
BP86/TZV	-861	-834	-880	4.26
BPW91/TZV	-831	-832	-848	4.20
PBE/TZV	-841	-841	-854	4.31
SVWN/TZV	-1156	-1178	-1181	5.07
B3LYP/3-21G	-103	-99	-114	0.56
B3LYP/TZVP	-215	-214	-231	4.60
B3LYP/DZP/TZVP[b]		-218	-246	4.12
B3LYP/6-31G*/TZVP[c]	-237	-216	-239	2.38

[a] Initial guess obtained with Jaguar 6.5, see Pt. II Ch. 3
[b] TZVP for Cu^{II}, DZP for the remaining atoms
[c] TZVP for Cu^{II} and the donor atoms, 6-31G* for the remaining atoms

As not only the accuracy but also the time needed to get to a result was of interest, Figure 2.4.1 shows a comparison of speed and accuracy of the Jaguar calculations.
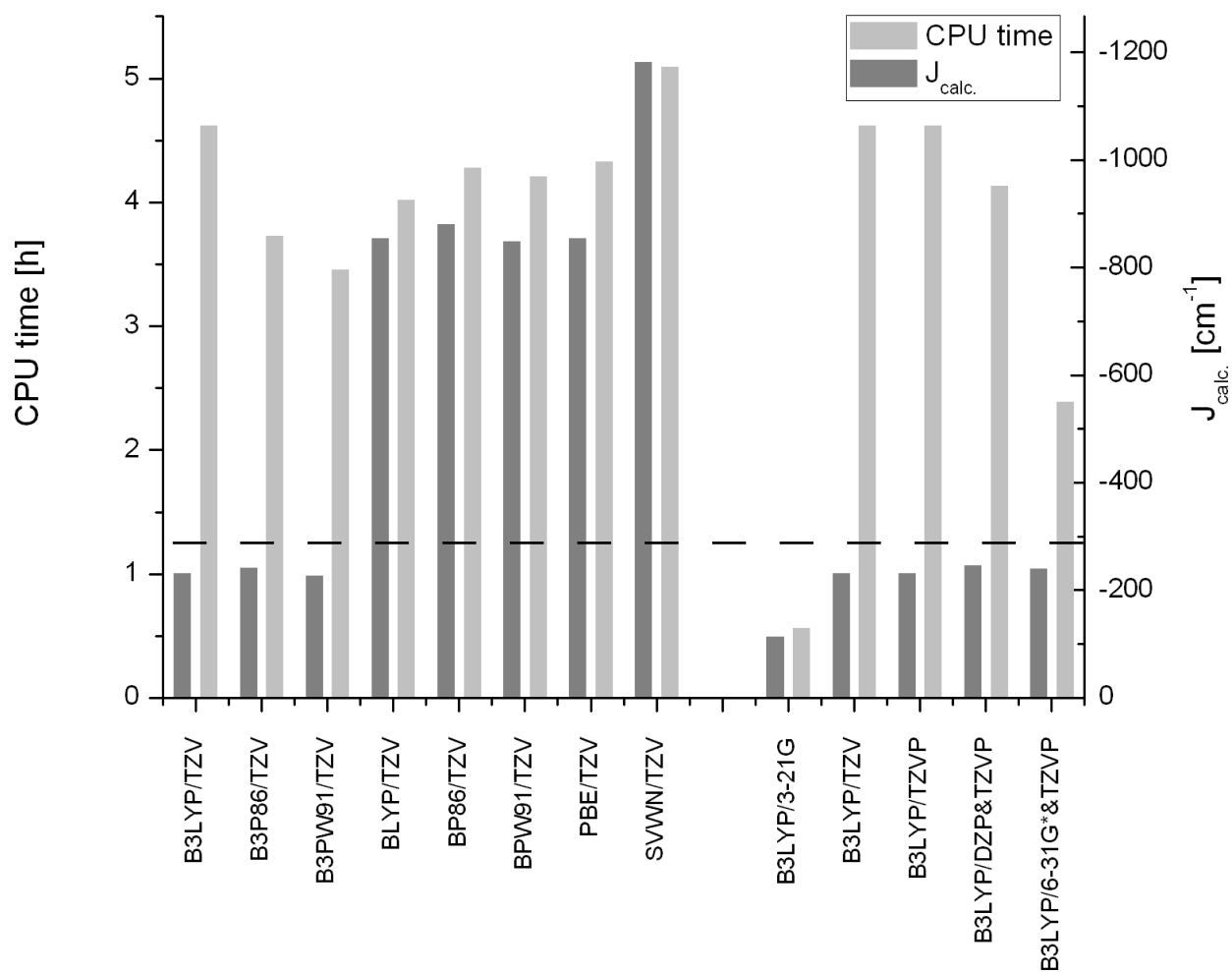
Figure 2.4.1: CPU time required for the computation of J [Quad-Core Q9450 (one processor), 8GB RAM; light
gray] and accuracy compared with the experimental value of J (dashed line, J = -298 cm^{-1}) of the
bisphenolato-bridged dicopper(II) complex shown in Fig. 2.1.1, as a function of the method used
(see Table 2.4.1; calculations performed with Jaguar).

From a qualitative point of view, the three software packages used in the benchmark study perform
equally well. There are differences in the amount of time needed to prepare the input files and to
perform the actual calculation, but no significant advantage has been found for one of the software
packages and therefore only Jaguar timings are presented here. Having a closer look at the func-
tionals, the hybrid functionals are superior to the GGA and LDA functionals, which supports earlier
findings[115]. The reason is the poor description of the broken symmetry state in case of the functionals
BLYP, BP86, BPW91, PBE and SVWN which leads to an overestimation of the exchange coupling
constant J. Adjusting the amount of exact HF exchange in the hybrid functionals did not lead to an
improvement in the accuracy compared to experimental results (values not shown here).

As expected, very small basis sets like 3-21G are not sufficient to describe the energy difference
between the high- and low-spin state. Employing basis sets larger than DZP for the whole molecule
however does not further improve the results. To account for this observation, a combination of the
TZVP basis on the metal centers and the DZP basis on the remaining ligand has been widely used in

the literature[116,117]. Based on these findings we decided to not only describe the metal centers but also the first coordination sphere with a large basis, to improve the quality of the calculations (see Figs. 2.3.1 and 2.4.1). To save computer time, the remaining atoms were described by the smaller 6-31G* basis set. As seen in Table 2.4.1 and Fig. 2.4.1, the cost in computational time could be cut in half while the accuracy was practically unaffected. This split basis method was therefore used in the successive studies. By this approach, it was possible to study larger spin clusters in a reasonable amount of time.

Table 2.4.2: Comparison of experimental and computed exchange coupling constants J of a series of transition metal complexes with Cr^{III}, Mn^{II}, Mn^{III}, Fe^{III} and Cu^{II} centers (J_{calc} is obtained with Eq. 2.2.9 and is derived from the experimental structure (Jaguar, 6-31G*/LACV3P++**); see Appendix A for structures of the complexes)

compound	J_{calc} [cm^{-1}]	J_{exp} [cm^{-1}]	note[a]	Figure	references
TPP[HO-Cr(cyclam)-NC-Cr(CN)$_5$][b]	-33.1^c	-29.8	Cr – Cr	6.2.1a	118
Na[HO-Cr(cyclam)-NC-Cr(CN)$_5$][b]	-41.4^c	-35.5	Cr – Cr	6.2.1b	119
trans-Cr[MnL^1]$_2$Cl[d]	-12.5^c	-12.8	Mn – Cr	6.2.1c	120
	5.0^c	0.9	Mn – Mn		
trans-Fe[MnL^1]$_2$Cl[b,d]	9.6^c	8.0	Mn – Fe	6.2.1d	120
	-7.7^c	-0.5	Mn – Mn		
trans-Fe[MnL^1]$_2$PF$_6$[b,d]	6.8^c	4.2	Mn – Fe	6.2.1e	120
	-8.3^c	-0.3	Mn – Mn		
[Tp$_2$(Me$_3$tacn)$_3$Cu$_3$Fe$_2$(CN)$_6$]$^{4+}$	9.1	8.5	Cu – Fe[e]	6.2.1f	121
	-8.8	-	Cu – Cu[e]		
	9.9	-	Fe – Fe[e]		

ª Denotes the pairs of magnetic centers for which the exchange coupling constant has been calculated

ᵇ Counterions are given for reference and have not been included in the calculations. However, the slight distortions in crystal packing induced by the counterions have a measurable effect on the exchange coupling constant, which can be seen from the calculated values.

ᶜ The spin-unprojected formula $J = \frac{E_{BS}-E_{HS}}{2S_1S_2+S_2}$ has been used to calculate the exchange coupling constant of this complex for better agreement with experimental results.

ᵈ L^1 = 3-methyl-9-oxo-2,4-di-(2-pyridyl)-7-(2-pyridylmethyl)-3,7-diazabicyclo[3.3.1]-nonane-1,5-dicarboxylic acid dimethylester

ᵉ In this pentanuclear complex (trigonal bipyramidal, see Appendix A; single-molecular magnetic material) three of the five paramagnetic centers were substituted by diamagnetic Zn^{2+} ions for an efficient calculation of the coupling constant between the remaining two paramagnetic ions. Experimental values for the exchange coupling constants between Cu-Cu and Fe-Fe are not available, because the coupling was neglected in the original publication[121].

Table 2.4.2 shows some results for the calculation of J for larger spin clusters. The overall agreement with experiment is very good, since not only the sign of the exchange coupling constant but also the magnitude is correctly predicted from the calculation. Of special interest in this series of compounds is the pentanuclear complex [Tp$_2$(Me$_3$tacn)$_3$Cu$_3$Fe$_2$(CN)$_6$]$^{4+}$ (see Appendix A, Fig. 6.2.1f). The experimental data has been fitted only with the Cu-Fe coupling while the Cu-Cu and Fe-Fe interactions

have been neglected[121]. Our calculations show that there is a significant exchange interaction between all three different pairs of metal centers. To obtain this result, we have substituted three of the five transition metal centers by diamagnetic Zn^{II} ions to reduce the overall number of possible interactions. To explicitly consider all possible coupling pathways, 11 spin states which lead to 10 different J values would have to be considered. Table 2.4.2 shows, that the Cu^{II}/Cu^{II} pairs are coupled antiferromagnetically while the Cu^{II}/Fe^{III} and Fe^{III}/Fe^{III} pairs are coupled ferromagnetically. The total magnetic behavior measured experimentally may then be observed as ferromagnetic.

In addition to the oligonuclear complexes shown in Table 2.4.2 a series of dinuclear complexes which contain various transition metals have been calculated. Table 2.4.4 shows the comparison of the calculated values generated with Jaguar and Orca with the experimental values. Also shown is the effect of the basis set reduction from TZVP or LACV3P++** for all atoms to the split basis method described in the preceding Chapter. As can be seen from the data in the table, the overall RMSD(J) and thus the overall accuracy compared to experiment is almost unaffected by the basis set reduction.

Table 2.4.3 compares calculated and experimental values with values obtained after optimizing the structures for the same series of compounds. As discussed, optimizing a structure is of critical importance for the design of new SMMs. Optimizing a molecule to a potential minimum of the corresponding method gives the "right" answer considering the energy, but may induce large structural changes. As the exchange coupling constant is very sensitive to the structure around the metal centers[120,138–142], this may lead to significant discrepancies compared to the experimental values.

As the values in Table 2.4.3 show, the overall agreement to experiment gets slightly better when pre-optimizing the structures. However, the sign of the J value is calculated incorrect in three of the 25 cases. In two complexes, $[Cu_2(\mu\text{-}OH)_2(bipym)_2]^{2+}$ and $[HB(pz)_3VO(OH)_2]_2$, this may be due to a wrong starting geometry, whereas in the third case, $[(VO(Hsabhea))_2]$, the absolute value of J is very small and certainly below the accuracy of the method. One generally has to assume that agreement with the experiment is by pure chance in cases with very small J values.

So far we have studied molecules in the "gas phase" and crystal packing effects have not been included in the calculations. To efficiently model exchange coupling of new SMMs one would have to include these effects. In the series of compounds studied here, crystal packing distortions seem to be of minor importance or structures are enforced in specific conformations even during the optimization step.

Using a geometry optimization to generate a structure for the calculation of the exchange coupling between two transition metal centers seems to be a viable approach for compounds which have not yet been synthesized. However, since the optimization step with DFT involves much computational effort, reducing the time for the initial optimization is only possible by using MM methods. The procedure towards a MM approach will be described in the following Parts of this work.

Table 2.4.3: Comparison of B3LYP-calculated and experimental J values of a series of dinuclear complexes (J_{calc} and J_{opt} are obtained with Eq. 2.2.9, J_{calc} is derived from the experimental structure (Jaguar, 6-31G*/LACV3P++**) and J_{opt} from the DFT-refined structure (high-spin state, Orca, 6-31G*/TZVP); see Appendix A for structures of the complexes, the numbers in parentheses in the table refer to the corresponding Figures)

compound	J_{calc} [cm^{-1}]	J_{opt} [cm^{-1}]	J_{exp} [cm^{-1}]	Figure	references
[Cu$_2$(MeC(OH)(PO$_3$)$_2$)$_2$]$^{4-}$	−103.0	−118.2	−30.9	6.2.2a	77, 122
[(Et$_5$dien)$_2$Cu$_2$(μ-C$_2$O$_4$)]$^{2+}$	−99.0	−112.2	−37.4	6.2.2b	77, 123
[Mn(Me$_6$-[14]ane-N$_4$)Cu(oxpn)]$^{2+}$	−40.8	−37.0	−15.7	6.2.2c	77, 124
[(μ-OCH$_3$)VO(maltolato)]$_2$	−84.3	−83.4	−107.0	6.2.2d	77, 125
[Fe$_2$OCl$_6$]$^{2-}$	−148.0	−109.5	−112.0	6.2.2e	77, 126
[MnMn(μ-O)$_2$(μ-OAc)DTNE]$^{2+}$	−156.3	−117.9	−110.0	6.2.2f	77, 116
[Cu$_2$(μ-OH)$_2$(bipym)$_2$]$^{2+}$	95.8	−98.5	57.0	6.2.2g	77, 127
[(Dopn)Cu(OH$_2$)Cr(OCH$_3$)Me$_3$tacn]$^{2+}$	12.8	31.5	18.5	6.2.2h	77, 128
[(Dopn)Cu(μ-CH$_3$COO)Mn(Me$_3$tacn)]$^{2+}$	54.2	54.9	54.4	6.2.2i	77, 128
[V$_2$O$_2$(μ-OH)$_2$([9]aneN$_3$)$_2$]$^{2+}$	−241.8	−52.5	−177.0	6.2.2j	129, 130
[Et$_3$NH]$_2$[(VO)$_2$(BBAC)$_2$]	−160.9	−81.6	−167.9	6.2.2k	129, 131
[HB(pz)$_3$VO(OH)$_2$]$_2$	14.3	29.2	−38.8	6.2.2l	129, 132
[(VO)$_2$(cit)(Hcit)]$^{3-}$	−267.8	−29.0	−212.0	6.2.2m	129, 133
[V$_2$O$_2$(μ-OH)(tpen)]$^{2+}$	−461.7	−19.1	−150.0	6.2.2n	129, 134
[(VO)$_2$L(μ-SO$_4$)]	−132.6	−121.9	−128.0	6.2.2o[a]	129, 135
[V$_2$O$_2$(OH)(C$_4$O$_4$)$_2$(H$_2$O)$_3$]$^-$	−245.7	−211.2	−117.0	6.2.2p	129, 136
[(VO(Hsabhea))$_2$]	8.9	−2.5	1.5	6.2.2q	129, 137
[(VO(Hsabhea))(VO(acac)(HOMe))(μ_2-OMe)]	18.6	15.4	5.3	6.2.2r	129, 137
[Cu$_2$(tren)$_2$CN](ClO$_4$)$_3$[b]	−98.6	−98.3	−79.0	6.2.2s	138
[Cu$_2$(tren)$_2$CN][BF$_4$)$_3$[b]	−119.1	−71.9	−80.0	6.2.2t	138
[Cu$_2$(tren)$_2$CN](ClO$_4$)(PF$_6$)$_2$[b]	−77.0	−79.2	−91.5	6.2.2u	138
[Cu$_2$(tmpa)$_2$CN](ClO$_4$)$_3$[b]	−70.1	−57.8	−52.0	6.2.2v	138
[Cu$_2$(tmpa)$_2$CN][BF$_4$)$_3$[b]	−69.8	−57.9	−50.0	6.2.2w	138
[Cu$_2$(tmpa)$_2$CN][BF$_4$)$_3$·(CH$_3$CN)$_2$[b]	−76.9	−57.9	−49.5	6.2.2x	138
[Ni$_2$(tetren)$_2$CN][Cr(CN)$_6$]	−15.4	−9.3	−12.5	6.2.2y	138
RMSD(J) (see Eq. 2.3.1)	75.6	71.2			

[a] see ref.[135] and references therein for detailed structural information
[b] Counterions are given for reference and have not been included in the calculations.

Part II   DFT Benchmarks for the Calculation of Exchange Coupling Constants

Table 2.4.4: Comparison of B3LYP-calculated and experimental J values of a series of oligonuclear complexes using different software packages and basis sets for the calculation of the exchange coupling constant.

compound	J_{J65} [cm^{-1}][a]	J_{J65} [cm^{-1}][b]	J_{J65} [cm^{-1}][c]	J_{J65} [cm^{-1}][d]	J_{Orca} [cm^{-1}][e]	J_{Orca} [cm^{-1}][f]	J_{exp} [cm^{-1}]
	[a] 6-31G*/TZVP	[b] TZVP	[c] 6-31G*/LACV3P++**	[d] LACV3P++**	[e] 6-31G*/TZVP	[f] TZVP	
$[Cu_2(MeC(OH)(PO_3)_2)_2]^{4+}$	−131.9	−91.6	−103.0	−143.4	−120.1	−109.4	−30.9
$[(Et_3dien)_2Cu_2(\mu\text{-}C_2O_4)]^{2+}$	−100.8	−29.7	−99.0	−108.4	−102.3	−103.4	−37.4
$[Mn(Me_6\text{-}[14]ane\text{-}N_4)Cu(oxpn)]^{2+}$	−44.6	−57.7	−40.8	−40.0	−43.7	−42.7	−15.7
$[(\mu\text{-}OCH_3)VO(maltolato)]_2$	−85.5	−87.9	−84.3	−79.4	−101.1	−101.0	−107.0
$[Fe_2OCl_6]^{2-}$	−158.2	−158.2	−148.0	−148.0	−159.4	−159.4	−112.0
$[MnMn(\mu\text{-}O)_2(\mu\text{-}OAc)DTNE]^{2+}$	−166.8	−163.8	−156.3	−157.7	−168.3	−168.2	−110.0
$[Cu_2(\mu\text{-}OH)_2(bipym)_2]^{2+}$	67.0	71.9	56.8	85.0	88.7	81.8	57.0
$[(Dopn)Cu(OH_2)Cr(OCH_3)Me_3tacn]^{2+}$	15.2	12.4	12.8	12.4	11.9	10.5	18.5
$[(Dopn)Cu(\mu\text{-}CH_3COO)Mn(Me_3tacn)]^{2+}$	83.9	46.6	54.2	43.2	49.1	48.1	54.4
$[V_2O_2(\mu\text{-}OH)_2([9]aneN_3)_2]^{2+}$	−263.8	−262.1	−241.8	−241.7	−278.9	−270.0	−177.0
$[Et_3NH]_2[(VO)_2(BBAC)_2]$	−172.3	−145.0	−160.9	−159.2	−186.9	−185.3	−167.9
$[HB(pz)_3VO(OH)]_2$	10.5	9.6	14.3	33.0	8.4	9.4	−38.8
$[(VO)_2(cit)(Hcit)]^{3-}$	−286.3	−294.4	−267.8	−260.5	−298.3	−303.5	−212.0
$[V_2O_2(\mu\text{-}OH)(tpen)]^{2+}$	−493.7	−498.7	−461.7	−459.9	−529.7	−525.8	−150.0
$[(VO)_2L(\mu\text{-}SO_4)]$	−135.9	−146.2	−132.6	−134.9	−140.7	−149.7	−128.0
$[V_2O_2(OH)(C_4O_4)_2(H_2O)_3]^-$	−255.6	−257.6	−245.7	−242.0	−261.5	−259.1	−117.0
$[(VO(Hsabhea))_2]$	−0.1	−3.8	8.9	15.2	7.2	6.2	1.5
$[(VO(Hsabhea))(VO(acac)(HOMe))(\mu_2\text{-}OMe)]$	13.1	16.4	18.6	19.6	14.6	15.1	5.3
$[Cu_2(tren)_2CN](ClO_4)_3$	−101.8	−100.3	−98.6	−108.1	−103.0	−104.0	−79.0
$[Cu_2(tren)_2CN](BF_4)_3$	−120.7	−130.2	−119.1	−129.3	−119.5	−120.7	−80.0
$[Cu_2(tren)_2CN](ClO_4)(PF_6)_2$	−80.1	−83.5	−77.0	−88.8	−85.6	−86.7	−91.5
$[Cu_2(tmpa)_2CN](ClO_4)_3$	−71.3	−71.4	−70.1	−70.1	−63.1	−72.3	−52.0
$[Cu_2(tmpa)_2CN](BF_4)_3$	−70.0	−66.8	−69.8	−56.9	−69.7	−68.7	−50.0
$[Cu_2(tmpa)_2CN](BF_4)_3\cdot(CH_3CN)_2$	−78.7	−65.7	−76.9	−72.1	−77.1	−78.5	−49.5
$[Ni_2(tetren)_2CN][Cr(CN)_6]$	−16.5	−15.5	−15.4	−15.5	−16.8	−17.0	−12.5
RMSD(J) (see Eq. 2.3.1)	84.6	82.7	75.6	77.9	91.4	90.2	

Part III

Development of a Molecular Mechanics Force Field with a Ligand Field Term

1 Introduction to Ligand Field Theory

1.1 Crystal Field Theory

ligand field theory (LFT) represents a theoretical approach to describe the d-orbital splitting of transition metal compounds and can be used to interpret electronic and magnetic properties, like UV/VIS, circular dichroism (CD) or magnetic circular dichroism (MCD) spectra or the zero-field splitting (ZFS). Based on a symmetry treatment, LFT can predict the number, range and intensity of transitions and can quantify parameters in Hamiltonians which describe these interactions. Since the coordination geometry and its underlying symmetry is mainly responsible for the splitting of the d-orbitals in a transition metal ion, LFT allows for a semi-quantitative approach to describe the energetics involved in these splittings.

The origins of LFT go back to Bethe[143] and van Vleck[144], who derived the underlying crystal field theory (CFT). Treating ions in a crystal lattice as point charges, they described the potential acting on the central ion, e. g. a Fe^{3+}, by the sum of all individual potentials generated by the surrounding ions, e. g. Cl^-. They explained the coordination geometry solely by the interaction of these point charges, that is, a pure electrostatic treatment of the metal to ligand interaction. Since Bethe's research was based on lattices, which in his assumption could only occur in a crystal, he referred to the theory as CFT[145]. The expansion of this idea to a more general form of a central ion in a field of the surrounding ligands (treating not only their electrostatic contribution and not necessarily assuming alignment in a crystal lattice) lead to the concept of LFT[146]. CFT can be seen as a special case of LFT, where the influence of the ligands on the central ion is of purely electrostatic nature, that is, the electrons of the ligands do not mix with the electrons of the central metal ion[145]. LFT introduces covalency and treats cases, where the interaction between the ligand and the metal electrons is not zero.

LFT is mainly concerned with the elements of the three d-transition series. Here, the ligand field effects are stronger than the other effects responsible for perturbation of the d-orbital energies, e. g. spin-orbit coupling. As mentioned above, the coordination geometry is mainly responsible for the splitting of the d-orbitals, and LFT connects the positions of the ligands with the energetics of the d-orbitals and thus with the physical properties seen in the spectra of the molecule[145].

With the underlying aspects of CFT, the general splitting of the d-orbitals e. g. in an octahedral field

can be deduced. As the central metal ion enters the field of the ligands, the energy of the degenerate set of orbitals is raised, as the interaction between the spherical field of point charges leads to a general destabilization of the d-orbitals. Since the real ligand field is not of spherical symmetry, the five-fold degenerate set is split into two sets of orbitals. The t_{2g} set consist of the d_{xy}, d_{xz} and d_{yz} orbitals, which have their lobes pointing between the ligands, and the e_g set consists of the $d_{x^2-y^2}$ and d_{z^2} orbitals pointing directly at the ligands. The coordinate system for the description of the molecule is chosen to match these assumptions. The t_{2g} set is thus stabilized, the e_g set destabilized compared to the five-fold degenerate set of orbitals in the spherical field of ligands. The energy difference between the two sets is 10 Dq or Δ_{oct} (see Figure 3.1.1). In a tetrahedral coordination geometry, the order of the sets is reversed and the splitting is only $\frac{4}{9}\Delta_{oct}$.
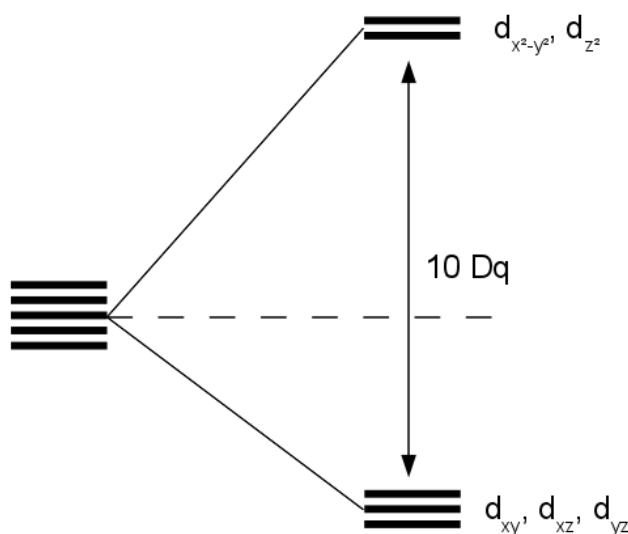
Figure 3.1.1: d-Orbital splitting in an octahedral crystal field.

1.2 The Inter-Electronic Repulsion

While CFT is sufficient to explain e. g. the transition around 20,000 cm^{-1} in the one-electron system Ti^{3+}, which can be associated with the transition of the single electron from the set of orbitals corresponding to a t_{2g} term to the e_g term orbital set, it fails to interpret more complex spectra, e. g. that of the d^2 system V^{3+}. The two transitions at 17,800 and 25,700 cm^{-1} cannot be assigned to a single and double excitation from the lower lying t_{2g} term to the orbitals corresponding to a e_g term. Even if the first transition could be assigned to the single excitation, the double excitation should appear at much higher energies.

In order to be able to describe the spectra of the d^2 system correctly, the simple term picture is not sufficient, but a more complex approach has to be used instead. Terms describe a group of energy equivalent multi-electron wave functions and are characterized by the term symbols, consisting of the total spin angular momentum S and the total orbital angular momentum L. The spin quantum

number M_S, the multiplicity, runs from -S to +S in half-integer steps, the quantum number M_L runs from -L to +L in integer steps. The total degeneracy of the term is thus $(2S+1)(2L+1)$. The term symbol is labeled $^{(2S+1)}X$, where X stands for a capital letter, which represents the total orbital angular momentum. X equals to S for L = 0, P for L = 1, D for L = 2, F for L = 3 and continues alphabetically afterwards.

Given the electron configuration of d^2, the corresponding terms can be derived as follows: Arranging two electrons with either spin up or spin down in five d-orbitals gives rise to 45 different possibilities, called micro-states. The different micro-states can be grouped according to their M_L and M_S values. This leads to 2 micro-states with $M_L = \pm 4$, 8 micro-states with $M_L = \pm 3$, 10 micro-states with $M_L = \pm 2$, 16 micro-states with $M_L = \pm 1$ and 9 micro-states with $M_L = 0$. The micro-states can also be grouped according to their multiplicity, which then gives 20 micro-states with $M_S = \pm 1$ and 25 micro-states with $M_S = 0$.

To arrive at the terms for the d^2 configuration, the table of micro-states has to be reduced systematically, starting with the highest orbital angular momentum number $M_L = 4$. $M_L = 4$ equals to a G term and since two electrons cannot have the same spin in the same orbital (Pauli principle[19]), the term has to be a singlet ^1G term. Subtracting a ^1G term from the list of micro-states results in a maximum $M_L = 3$, which corresponds to an F-term. The reduction of the micro-states is done systematically, until all micro-states are assigned to terms. The final result is, that the d^2 configuration splits into a ^1G, ^3F, ^1D, ^3P and a ^1S term.

Given Hund's rules[147–149], which describe how electrons tend to minimize the repulsion with each other, we can define the energetic order of the terms as ^3F, ^1D, ^3P, ^1G and ^1S (from lowest to highest energy).

1.3 The Ligand Field Splitting

In the last section, the terms for a free transition metal ion have been derived. If the ion is brought into a field of ligands, the terms split according to group theory. The angular momentum of a term acts analogously to one-electron wave functions. The ^3F-term, which is the ground state of the d^2 configuration, is seven-fold degenerate. In an octahedral field, the term splits into $^3A_{2g}$, $^3T_{1g}$ and $^3T_{2g}$ terms, where the $^3T_{1g}$ term represents the new ground state.

When both the inter-electronic repulsion and the ligand field treatment are taken into account, the two bands visible in the V^{3+} spectrum can now be explained. The two bands belong to the transitions between the T_{1g} ground term and the two terms T_{2g} and A_{2g}, which are higher in energy. If the symmetry of the coordination sphere is lowered a further ligand field splitting can be induced. Correlation tables, from which this splitting can be derived, are found in the literature[145].

So far, we have used the "weak field" approach to describe the splitting of the energy levels in transition metal complexes, assuming, that the magnitude of the inter-electronic repulsion is larger than the ligand field. In the "weak field" approach, the free ion terms are deduced first and the ligand field acts as a perturbation on these terms. If the ligand field is of larger magnitude than the inter-electronic repulsion, the "strong field" approach has to be used for the description of the orbital splitting.

In the strong field approach, the energy levels are solely described by electron configurations, which are then again split into terms by the inter-electronic repulsion which acts as a perturbation. The configurations for the d^2 case would include a $t_{2g}{}^2 e_g{}^{*0}$ ground state, i. e. two electrons would be in the t_{2g} set, a first excited state $t_{2g}{}^1 e_g{}^{*1}$ with one electron in each of the orbital sets and a second excited state $t_{2g}{}^0 e_g{}^{*2}$. To arrive at the according terms, the direct product of the terms which describe the two electrons has to be taken. For the ground state, the direct product is (Eq. 3.1.1):

$$T_{2g} \times T_{2g} = T_{1g} + T_{2g} + E_g + A_{1g} \qquad (3.1.1)$$

If the direct product for the first and second excited configurations is calculated, the derived terms are the same as the ones, which have been derived with the weak field approach, but the energetic order is different. The qualitative correlation between the two approaches can be visualized with correlation diagrams[145] whereas a quantitative visualization has been proposed by Tanabe and Sugano[150–152].

2 The Angular Overlap Model

In the preceding Chapter, the splitting of the d-orbitals has been described by perturbations of the inter-electronic repulsion and the field generated by the ligands surrounding the central metal ion. Another approach for the description of the energetic levels of the d-orbitals is the angular overlap model (AOM)[153], which is based on a simple MO approach and describes the metal to ligand bonds in terms of covalent σ, π and δ interactions[145]. The AOM is a parametrized model, where the parameters directly correlate with experimental findings. Since the parameters do not refer to a certain complex geometry or coordination but to a single metal-ligand pair, the parameters are not transferable among different structures[154–157]. However, calculations have shown[154,158], that parameters can be used approximatively for a wider range of complexes with the same structural motif.

In order to derive the parameters for a specific metal-ligand interaction, the AOM makes use of basic quantum mechanics. As seen in Pt. I Ch. 1, the energy E_i of a molecular orbital ϕ_i is obtained by the Schrödinger equation, Eq. 3.2.1

$$\mathbf{H}\phi_i = E_i\phi_i \tag{3.2.1}$$

If the multi-orbital problem is simplified to the case of one metal d-orbital and one ligand orbital, the wave function ϕ_i becomes (Eq. 3.2.2)

$$\phi_i = c_{iM}\phi_M + c_{iL}\phi_L \tag{3.2.2}$$

with the orbital coefficients c_i for the atomic orbitals ϕ_M and ϕ_L. The energies of the metal and ligand orbital can be derived from the secular determinant, Eq. 3.2.3

$$\begin{vmatrix} H_M - E & H_{ML} - S_{ML}E \\ H_{ML} - S_{ML}E & H_L - E \end{vmatrix} = 0 \tag{3.2.3}$$

where H_M and H_L are the orbital energies of the metal and ligand, respectively, H_{ML} is the exchange integral and S_{ML} is the overlap integral between metal and ligand orbitals. Since the d-orbitals are higher in energy than the ligand orbitals, H_M is large compared to H_L. If the overlap integral is assumed to be small, the energies E_a which destabilize the resulting anti-bonding MO relative to the

level of the d-orbitals, and E_b which stabilize the bonding MO relative to the ligand orbital level are (Eq. 3.2.4):

$$E_a = H_M + \frac{(H_{ML} - H_M S_{ML})}{H_M - H_L}$$
$$E_b = H_M - \frac{(H_{ML} - H_L S_{ML})}{H_M - H_L}$$

(3.2.4)

H_M and H_L are known as the valence state ionization energies of the metal and ligand orbitals and the overlap integral S_{ML} can be calculated numerically[145]. With the Wolfsberg-Helmholtz approximation[159], the exchange integral H_{ML} can be expressed as (Eq. 3.2.5)

$$H_{ML} \simeq S_{ML} \frac{(H_M + H_L)}{2}$$

(3.2.5)

With this approximation, Eq. 3.2.4 then becomes (Eq. 3.2.6)

$$E_a \simeq H_M + \frac{H_L^2 S_{ML}^2}{H_M - H_L}$$
$$E_b \simeq H_M - \frac{H_M^2 S_{ML}^2}{H_M - H_L}$$

(3.2.6)

The energy raise of the anti-bonding MO E_a, and thus the perturbation of the metal d-orbitals when the metal is coordinated by the ligands, can be further approximated as seen in Eq. 3.2.7, since the energy E_a is mainly defined by the metal orbital energy H_M:

$$e \approx K S_{ML}^2$$
$$K \approx \frac{H_L^2}{H_M - H_L}$$

(3.2.7)

The newly introduced parameter e, which describes the energy raise of the anti-bonding MO, is proportional to the square of the overlap integral and the factor K can be directly calculated from the valence state ionization energies of the metal and ligand. Ligands normally bind either via σ- or π-bonding, so three e-parameters are needed for a complete description of the shift in orbital energy of the anti-bonding MO. e_σ describes the σ-interaction and because of its anti-bonding nature with respect to the metal d-orbitals, e_σ usually has a positive value. The $e_{\pi x}$ and $e_{\pi y}$ parameters (x and y denoting the cartesian axes orthonormal to the z (ligand metal) bond axis) can be positive or negative, depending on a destabilizing (donor) or stabilizing (acceptor) effect of the π-bonding to the metal d-orbital, respectively. An additional parameter, e_{ds}, which accounts for the d-s-mixing between the d_{z^2} and the $4s$ orbital and effectively lowers the energy of the d_{z^2} orbital, can also be assigned to a metal-ligand pair. A good approximation is to assume a value of about 1/4 of e_σ for e_{ds}[160].

As stated above, the overlap integral S_{ML} can be calculated numerically. Since the local coordinate system around the ligand defines the e_σ, $e_{\pi x}$ and $e_{\pi y}$ parameters, the global coordinate system, which is centered on the metal, is used to express the position of the ligands in space in polar coordinates. If $\mathbf{d}$ is the vector between the metal and the ligand, θ defines the angle between the global z-axis z_M and $\mathbf{d}$ while ϕ is the angle between the projection of $\mathbf{d}$ onto the global x_My_M plane (the vector $\mathbf{d}'$) and the global x_M axis. The ligands z_L-axis is always treated as being collinear to $\mathbf{d}$, while a third angle ψ defines the final rotation of the ligands' x_L- and y_L-axis along the z_L-axis (see Figure 3.2.1, the insert shows the view along the ligand metal axis).
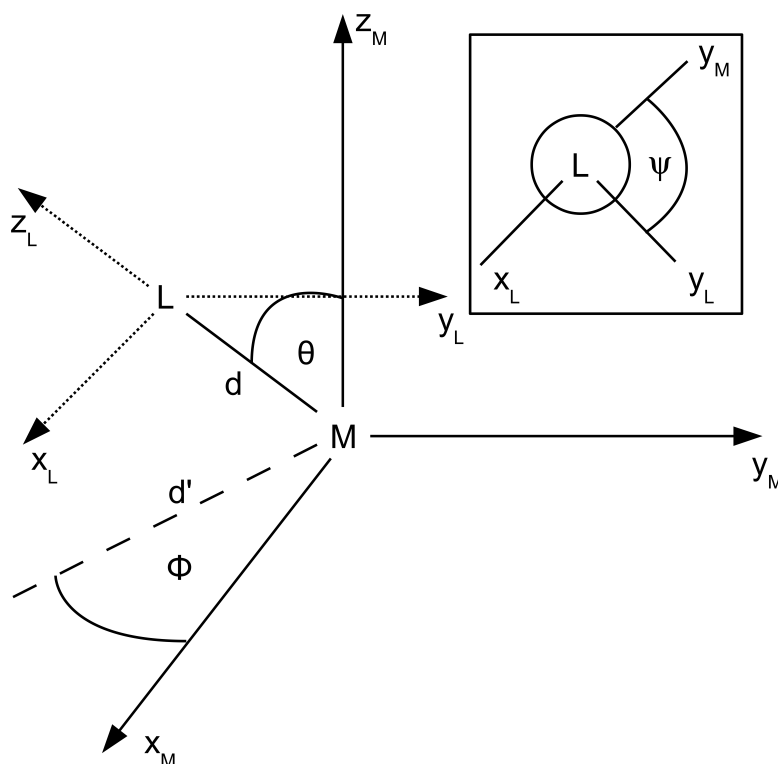
Figure 3.2.1: Ligand coordinate system (x_L,y_L,z_L) in the global metal coordinate system (x_M,y_M,z_M)[145]

With these polar coordinates, the angular overlap factors which define the overlap integral between a metal d-orbital and a ligand orbital can be derived as given in Table 3.2.1[153,161]:

Table 3.2.1: Angular overlap factors for σ and π interactions between metal d-orbitals and ligand orbitals proposed by Schäffer and Jørgensen[153,161].

	$F_\sigma[d, L(\theta, \psi, \phi)]$	$F_{\pi x}[d, L(\theta, \psi, \phi)]$	$F_{\pi y}[d, L(\theta, \psi, \phi)]$
$d_{x^2-y^2}$	$(\sqrt{3}/4)\cos 2\phi(1 - \cos 2\phi)$	$-\sin 2\phi \sin \theta \sin \psi + \frac{1}{2}\cos 2\phi \sin 2\theta \cos \psi$	$-\sin 2\phi \sin \theta \cos \psi - \frac{1}{2}\cos 2\phi \sin 2\theta \sin \psi$
d_{z^2}	$(1 + 3\cos 2\theta)/4$	$(-\sqrt{3}/2)\sin 2\theta \cos \psi$	$(\sqrt{3}/2)\sin 2\theta \sin \psi$
d_{xy}	$(\sqrt{3}/4)\sin 2\phi(1 - \cos 2\phi)$	$\cos 2\phi \sin \theta \sin \psi + \frac{1}{2}\sin 2\phi \sin 2\theta \cos \psi$	$\cos 2\phi \sin \theta \cos \psi - \frac{1}{2}\sin 2\phi \sin 2\theta \sin \psi$
d_{xz}	$(\sqrt{3}/2)\cos \phi \sin 2\theta$	$-\sin \phi \cos \theta \sin \psi + \cos \phi \cos 2\theta \cos \psi$	$-\sin \phi \cos \theta \cos \psi - \cos \phi \cos 2\theta \sin \psi$
d_{yz}	$(\sqrt{3}/2)\sin \phi \sin 2\theta$	$\cos \phi \cos \theta \sin \psi + \sin \phi \cos 2\theta \cos \psi$	$\cos \phi \cos \theta \cos \psi - \sin \phi \cos 2\theta \sin \psi$

The perturbation from the ligands acting on the metal d-orbitals can be summed up over all individual metal-ligand contributions. The matrix elements of the ligand field matrix are given in Eq. 3.2.8[162]

$$\langle d_i \,|V_{LF}|\, d_j \rangle = \sum_{\lambda\omega} \sum_{n=1}^{N} e_{\lambda\omega} F(d_i, L_n) F(d_j, L_n) \tag{3.2.8}$$

Here, d_i is the respective d-orbital, $\lambda\omega$ the interaction type (σ or π interaction) and $F(d_i, L_n)$ the overlap integral given in Table 3.2.1. Given the matrix elements, the symmetrical 5×5 ligand field matrix can be formed. The eigenvectors of the matrix correspond to the wave function which describes the d-orbitals. Their respective orbital energies are given by the eigenvalues. Since the off-diagonal elements of the ligand field matrix are generally not zero, the AOM wave function is a mixture of the five d-functions[145]. Given the trigonometric basis of the AOM overlap integrals, the following sum rule can be derived[153,162], Eq. 3.2.9

$$\sum_{n}^{N} \sum_{i}^{5} F(d_i, L_n)^2 = N \tag{3.2.9}$$

stating that the sum over all angular overlap factors is equal to the number of coordinating ligands N.

3 Implementation of a Ligand Field Term in Momec

3.1 Ligand Field Molecular Mechanics

The eigenvalues of the 5×5 ligand field matrix derived in Chapter 2 of Part III can be used to calculate the total ligand field stabilization energy (LFSE)[9,156,163,164] (Eq. 3.3.1):

$$E_{LFSE} = \sum_a n_a e_a \tag{3.3.1}$$

Here, n_a is the occupation number of the respective d-orbital (0, 1 or 2, which corresponds to the number of electrons in the orbital) and e_a is the d-orbital energy, given by the eigenvalues of the ligand field matrix.

As the LFSE implicitly depends on the coordination geometry and coordination number of a transition metal in a molecule, it can be used to include electronic effects e. g. Jahn-Teller distortions[13] or the spin-orbit coupling in a standard MM force field. This method has been proposed by Deeth and coworkers[9,10,165,166] and has been termed ligand field molecular mechanics (LFMM). It has been used with great success to calculate structures of various transition metal complexes[167,168], different spin states of a transition metal[169] and dinuclear compounds[170].

The LFSE can be included in a classical force field as an additional term to the total strain energy, Eq. 3.3.2:

$$E_{steric} = \sum E_{stretch} + \sum E_{bend} + \sum E_{torsion} + \sum E_{vdW} + \sum E_{electrostatic} + \sum E_{LFSE} \tag{3.3.2}$$

Because the d-orbital energies calculated from the symmetrical 5×5 ligand field matrix are barycentered to zero, the energy added by the E_{LFSE} term is intrinsically negative and thus always stabilizes the calculated structure. Since the original implementation of the ligand field potential by Deeth et al. (see below) is monotonically decreasing with increasing bond lengths, the interaction has to be bal-

anced with an additional classical bond stretch term which then adds up to the correct bond distances when compared to experimental results. Deeth et al. use a Morse fuction (see Pt. I Ch. 2) to describe the classical part of the total metal ligand stretch. The L-M-L bend energy implicitly contained in the LFSE is balanced with additional ligand-ligand repulsion terms, which are of the van der Waals type.

As the overlap integrals between metal d-orbitals and the ligand orbitals are calculated by trigonometric functions, the only parameters which have to be parametrized in the force field are the ligand $e_{\lambda\omega}$-parameters (see Pt. III Ch. 2, Eqs. 3.2.5 to 3.2.7). In the first approaches to LFMM, Deeth et al. parametrized a single e_λ parameter with a linear dependence of the metal-ligand bond length r and used numerical first derivatives to calculate displacements during geometry optimizations[9]. In more recent publications, a series expansion around the bond length r is used for the parametrization of the AOM parameters[171], Eq. 3.3.3, which allows for a greater flexibility of the force field.

$$e_{\lambda\omega} = a_0 + a_1 r + a_2 r^{-2} + a_3 r^{-3} + a_4 r^{-4} + a_5 r^{-5} + a_6 r^{-6} \qquad (3.3.3)$$

a_n are parameters of the force field and $e_{\lambda\omega}$ are the resulting AOM parameters. Terms for π-interactions and d-s-mixing as well as analytical first derivatives have also been implemented[172].

The first LFMM code was implemented in the program package DOMMINO[9], and has later become a part of the Molecular Operating Environment (MOE) software package[173] under the name of DommiMOE as a plug-in written in C and controlled by MOE's internal Scientific Vector Language (SVL).

Other implementations of an additional LFSE term to the total energy have been done by Woodley et al. in the GULP program[174] and Giessner-Prettre et al. in SIBFA[175]. A different approach to the modeling of the transition metal coordination geometry has been used by Comba and Ströhle[176], who implemented an additional harmonic sine function, which acts as an electronic perturbation. The sine function has minima at 90 and 180° and the electronic effect of the interaction between the d-orbitals of the metal and the ligand orbitals is therefore modelled by this additional potential. The drawback of this method comes with the introduction of the additional parameters in the force field. The force constants of the since function are only valid for specific coordination geometries whereas the ligand field parameters used in the LFMM approach by Deeth can model several geometries with a single set of parameters.

3.2 Comparison between DommiMOE and Momec

The original code was donated to us by R. Deeth to whom we extend our gratitude at this point. In order to implement the ligand field code in the software package Momec, of which a new version is currently in development[12,177], it has been adopted and rewritten in C++ to make it compatible to the Momec source code. In contrast to the original implementation in MOE, the ligand field code is

not added to Momec as an external plug-in, but has become an integral part of the program, which has some significant advantages shown below. In order to maintain the functionality of the code, high priority was set on the correct output and verification of calculated values during the implementation process. Several tests including sample ligand field calculations with different types of ligands were implemented and the results of the calculated eigenvectors and eigenvalues as well as the first derivatives were carefully checked against results generated with MOE.

Here, we encountered several problems regarding numerical stability. Due to the origin of the code, which is based on a FORTRAN source, its first application was on 32-bit machines where the data type "double" represented the 32-bit floating point precision, which corresponds to seven significant digits. Therefore, this data type was used throughout the code to assure the maximum accuracy possible at that time. However today, modern computers have a 64-bit architecture and therefore the type "double" has an increased accuracy of at least 15 significant digits. Since the calculation of the AOM overlap integrals is very sensitive to precision, this induced some numerical instabilities and lead to a slight change in the energetic order of the d-orbitals and eigenvectors calculated from the 5×5 ligand field matrix compared to the original implementation. In some cases we have observed degenerate orbitals, which has not been the case in the original implementation of the code because of the differences in precision. However, since the formulae have all been verified, the increased precision is a wanted effect and the data type has even been expanded to "long double" (at least 31 bits precision). No efforts have therefore been made to exactly reproduce the original eigenvalues and vectors and their respective order by arbitrarily lowering the precision of the calculated values.

For comparison of the original implementation in MOE with the current implementation in Momec, the work flow during a single point or geometry optimization for both implementations is shown in Fig. 3.3.1.

In both programs the usage of a graphical user interface (GUI) to either draw or import a molecular structure is straightforward. Common to both implementations is also the atom type assignment done during the import procedure. Here additions had to be made to the force fields present in MOE, since support for transition metals is missing in the force fields originally build into the program (e. g. the MMFF94 force field[178–184]). Additional typing rules for coordinating ligands such as saturated amines are also needed, since standard type rules are not aware of ligand to metal coordination[171]. In Momec, which contains a force field tailored explicitly to transition metals and their coordination chemistry, such atom types and type rules are implemented by default[177,185]. Setting up the calculation is again very similar in both implementations. Setting up the force field and executing the actual calculation, however, is quite different in both programs.
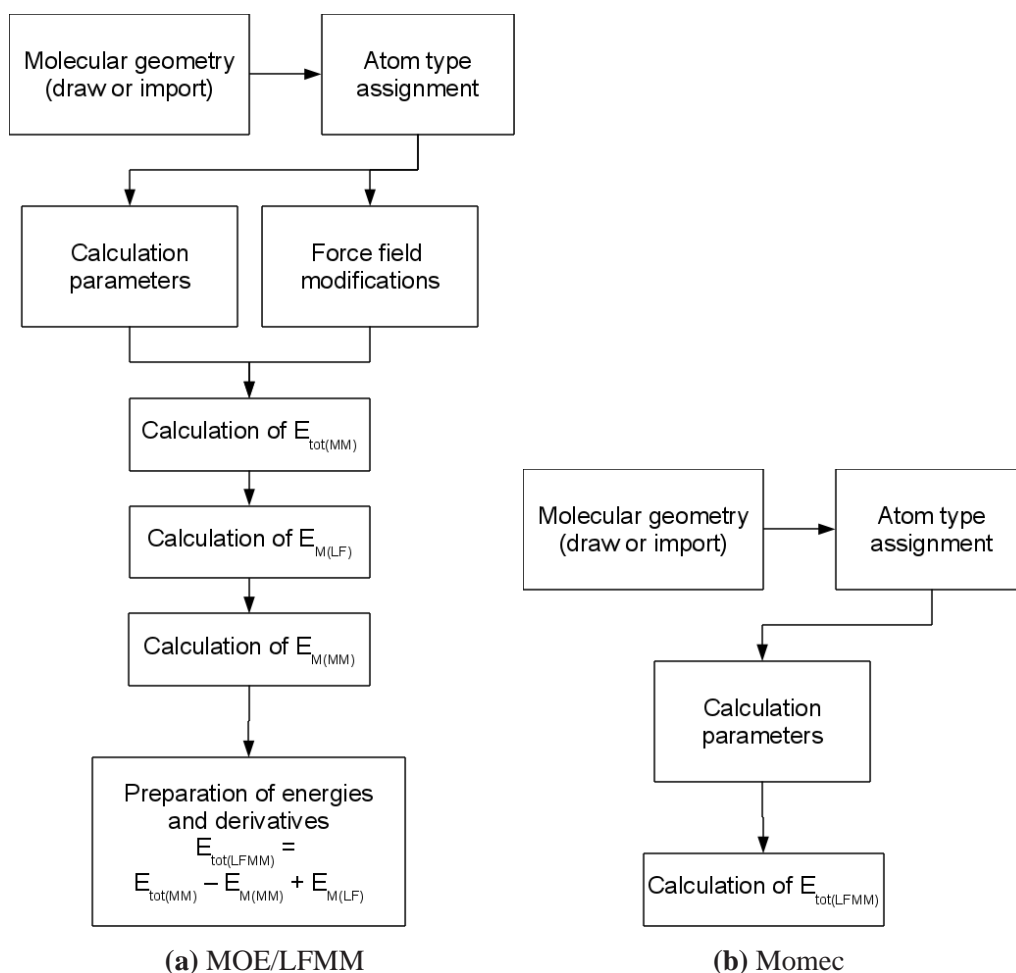
Figure 3.3.1: Work flow during a MOE/LFMM calculation compared to a Momec calculation

In the MOE/LFMM scheme, the molecule is divided into two parts in a QM/MM-like approach. The ligand field code only treats the metal center and the surrounding ligand atoms, whereas the standard force field present in MOE computes the steric energy of the remaining atoms. The ligand field part contains a metal-ligand bond length component, which has to be counterbalanced with a Morse stretch, and a ligand-metal-ligand angle bend component, which has to be balanced with a van der Waals interaction. The part treated by the standard force field contains all steric energy contributions from the remaining atoms as well as angle bends and torsion angles connecting the coordination region, namely the metal and the surrounding ligand atoms, and the ligand region, which is the rest of the molecule. To calculate only the coordination region, the respective atoms are identified by SVL routines and passed to the external ligand field code. The calculated energies and derivatives are then again passed back to the main program via SVL code. At this point, one of the drawbacks of the MOE/LFMM implementation becomes clear. Since the calculation in the main MOE program is done on the entire molecule, the interactions treated exclusively by the ligand field code, that is the M-L bond stretches and L-M-L bend angles, have to be zeroed. On the other hand, any solvation effects which act on the coordination region have to be retained, since they are not treated by the ligand field calculation. Since MOE automatically assigns missing parameters in the force field, simple deleting the metal ligand interactions is not possible. Additionally, the SVL code does not allow to delete

specific interactions from the calculation[171]. Therefore, the additional contribution to the total strain energy by the coordination region has to be calculated separately and subtracted from the final result. This has to be done both for the energy and for the derivatives and involves an additional calculation. Eqs. 3.3.4 to 3.3.6 summarize the process:

$$E_{tot(MM)} = E_{M(MM)} + E_{L(MM)} + E_{ML(MM)} + E_{solv} \tag{3.3.4}$$

$$E_{tot(LF)} = E_{M(LF)} \tag{3.3.5}$$

$$\begin{aligned} E_{tot(LFMM)} &= E_{M(LF)} + E_{L(MM)} + E_{ML(MM)} + E_{solv} \\ &= E_{tot(MM)} - E_{L(MM)} + E_{M(LF)} \end{aligned} \tag{3.3.6}$$

Eq. 3.3.4 gives the total energy $E_{tot(MM)}$ calculated with the conventional force field in MOE, which consist of the coordination region $E_{M(MM)}$, the ligand region $E_{L(MM)}$, the cross terms connecting the two regions $E_{ML(MM)}$ and the solvation energy for the whole molecule E_{solv}. The total ligand field energy given in Eq. 3.3.5 is calculated by the ligand field code and consists of the LFSE, the Morse contributions for the M-L bond stretches and the ligand-ligand van der Waals interactions, all of which are parts of the total ligand field energy for the coordination region $E_{M(LF)}$. Eq. 3.3.6 then gives the total energy consisting of the ligand field energy for the coordination part, the conventional energy for the cross-terms and the remaining ligand and the solvation energy.

Compared to this tedious approach in the MOE/LFMM implementation, the implementation in Momec is straightforward. Since the ligand field code is an integral part of the whole Momec program, the treatment of the ligand field between the metal center and the surrounding ligands is just an additional interaction, which has to be accounted for during a calculation. Since Momec uses a harmonic description for a bond stretch by default, switching to a Morse description is still required, but can be done without additional effort. As Momec uses a points on a sphere model for the L-M-L interactions by default, no additional interactions have to be modified to treat the bending terms involving the metal center correctly.

To summarize, the ligand field implementation in Momec is just a matter of adding an additional interaction to the total list of interactions accounted for during a calculation, where with MOE/LFMM it involves multiple calculations. Additionally, the implementation in C++ allows for transferability to other molecular mechanics packages, since the code no longer depends on the MOE SVL architecture.

3.3 Implementation in Momec

Since the source code of Momec and thus of the ligand field code is open source, no detailed description will be given here and the reader is referred to the Momec website[177]. However, an overview of the routines involved in the ligand field calculation will be given with a short description. As mentioned before, the code was adopted to C++ but the overall functionality has not been changed to retain maximum compatibility and consistency with respect to the resulting values. Apart from the different programming language, the routines are very similar to the implementation of the plug-in to MOE.

The actual ligand field calculation starts with the identification of the transition metal centers and their coordination regions. If a metal is found, the charge and multiplicity given in the input file are used to calculate the number of electrons and the spin state on the metal. With the help of a connection table, the ligand atoms connected to the metal as well as the atoms connected to the ligand atoms are identified. This is necessary in order to define the local ligand coordinate system with respect to the πx and πy AOM parameters. Since the ligand field part only treats a part of the molecule, the information about the relevant atoms is copied to a format which is different from the remaining Momec program[1]. In order to be able to add the ligand field derivatives to the respective atoms later, atom numbers between Momec and the ligand field code are mapped. In addition to the relevant atoms, the ligand field parameters given in the force field are also passed to the ligand field code. This process is done for every transition metal center and every centers' ligand field is calculated separately. Deeth et al. have shown, that this is a valid approach and interactions between the individual centers can be neglected in specific cases[170] in a first order approximation.

When the atoms relevant to the ligand field calculation and the parameters in the force field are identified, the actual $e_{\lambda\omega}$ values along with their first derivatives are generated according to Eq. 3.3.3. This is followed by the calculation of the overlap integrals in the Schäffer-Jørgensen formalism (see Pt. III Ch. 2 Table 3.2.1) and the calculation of the 5×5 ligand field matrix elements. The matrix is then diagonalized. After the matrix is solved, the LFSE is calculated according to Eq. 3.3.1 and the first and second derivatives are prepared. Here, the first derivatives are calculated analytically[172] whereas the second derivatives are computed numerically. The second derivatives are not used in the DommiMOE implementation and therefore no reference values were available. However, in Momec the numerical second derivatives are used in the geometry optimization[2].

When the LFSE, the d-orbital energies and the first and second derivatives have been calculated, the results are passed back into the main Momec calculation routine. The energy is treated as a part of the total strain energy, the d-orbital energies are plotted to the output file and the derivatives are added to the respective atoms in the Jacobian and Hessian during a geometry optimization.

---

[1]   This is due to the implementation process, since formats have been kept untouched where possible

[2]   Future plans include a complete overhaul of this part of the program as well as the implementation of analytical second derivatives.

3.4 Input File Structure

As mentioned, the ligand field code calculates the number of unpaired electrons present on a transition metal center with the charge and the multiplicity of the atom given in the input file. Since the input file format used in the 1997 version of Momec[185], the Hyperchem input file[186], only supports the declaration of a charge of an atom, a new and more flexible file format was needed for the new Momec release and the ligand field code. The decision was taken to use the SD file format[187] in the current version 3. The most important features of this format will be presented here.

The SD file consist of two blocks, where the first block is in fixed format and describes the atom coordinates, while the second block is in free format and contains user-defined tags which can be created without restrictions. An example for the fixed format block is shown in listing 3.3.1:

```
    DUSJAC01


    0   0   0       0   0                   999  V3000
M   V30  BEGIN  CTAB
M   V30  COUNTS  49  54  0  0  0
M   V30  BEGIN  ATOM
M   V30      1    Cu   3.2295   3.0724  −0.0405  0
M   V30      2    N    1.7115   1.3752   0.2577  0
M   V30      .
M   V30      .
M   V30      .
M   V30     49    H    4.5678   6.4336  −1.3823  0
M   V30  END  ATOM
M   V30  BEGIN  BOND
M   V30      1   1      1       2
M   V30      2   1      1       3
M   V30      .
M   V30      .
M   V30      .
M   V30     54   1     19      49
M   V30  END  BOND
M   V30  END  CTAB
M   END
  $$$$
```

Listing 3.3.1: Fixed format block of a version 3 SD file used in Momec

The fixed format block begins with a single line which usually contains the name of the molecule.

The following line can contain some information about the user, the name of the program etc.[187], but can also be replaced by a blank line. The third line contains comments whereas the fourth line is fixed format as written in Listing 3.3.1. Line six includes the number of atoms, followed by the number of bonds and some additional information about the chirality[187]. "BEGIN ATOM" marks the beginning of the atom coordinates whereas "BEGIN BOND" starts the section about the bond information. Here, the number following the index specifies the bond order (1 = single, 2 = double, 3 = triple, 4 = aromatic) whereas numbers three and four give the bond partners. The fixed block ends with four dollar signs. Note that each line of the connection table ("BEGIN CTAB") starts with an "M" followed by two spaces, "V30" for the version and another space.

An example for the free format block adopted during the implementation of the ligand field code[3] in Momec is given in listing 3.3.2.

The free format block in the SD file consists of different sections, where each section starts with a tag in the format "> <Description>". Everything except the angle brackets which define the beginning of a tag is free format. For Momec, we decided to implement tags which contain a version number in the tag itself for easier future versioning. Since the SD files are either parsed by Perl scripts or by C++ routines, including the version in the tags assures that older file formats can still be parsed correctly, even if the tag format changes. The tags used in Momec can be divided into three categories: reference tags, calculation tags and general tags. Reference tags contain information about reference structures used in the parametrization of a force field[4], e.g. stretches, bends and torsions of the reference geometry or spectroscopic data like UV/VIS transitions. Calculation tags contain information generated during a calculation done in Momec, e.g. stretches, bends and torsions of the optimized structure, calculated charges etc. General tags are connected to the molecule or to the file format and include information about the atom types used by the force field, the units used in the SD file[5] and the charge and multiplicity used by the ligand field code. The free format supported by the SD tags also allows an implementation of a hierarchy in the information given in the file. In the example above, the calculated energies of the molecule consist of a bond deformation energy, a non-bonded interaction energy etc. and this can be directly imported into a tree-like data structure in the program and depicts this structure in the output files.

---

[3]   The design of the ligand field tags of the free format block as well as numerous sets of test molecules have been prepared together with Tobias Lauterbach during his research internship.

[4]   see Pt. IV for a detailed description of the parametrization process

[5]   Future plans include the implementation of a unit system in Momec to support the input of e.g. energies in multiple units and the automatic conversion to another unit in the program.

```
>  <MOMEC_ATOM_TYPES_V1>
   1  CU2
   .
   .
   .
   49  H
>  <MOMEC_REF_STRETCHES_V2>
   1  R[U1]=2.29646@1.0  C=1,2
   .
   .
   .
   54  R[U1]=0.90522@0.0  C=19,49
>  <MOMEC_REF_COMMENTS_V1>
  Refcode: DUSJAC01
>  <MOMEC_MULTIPLICITY_V1>
   1  2
>  <MOMEC_CHARGES_V1>
   1  2
>  <MOMEC_UNITS_V1>
   U1  Angstrom
   U4  kJ/mol
>  <MOMEC_CALC_RESULTS_V1>
   Status=not converged
   Steps=1
  RMS=0.00000
  Energies[U4]=>Bond deformation energy=433.42326
              >Non-bonded interaction energy=34.83976
              >Valence angle deformation energy=29.55635
              >Torsion angle deformation energy=35.96001
              >Electrostatic interaction energy=0.00000
              >Out of plane deformation energy=0.00000
              >Hydrogen bond interaction energy=0.00000
              >Twist angle energy=0.00000
              >Ligand field interaction=0.00000
              >Total strain energy=533.77939
```

Listing 3.3.2: Free format block of a SD file version 3 used in Momec

3.5 Changes to the Functional Form of the Ligand Field Term

The functional form of the ligand field term has been investigated and modified in order to enable automatic parametrization. In the original implementation by Deeth et al., the AOM parameters $e_{\lambda\omega}$ are derived from a series expansion around the metal-ligand bond length r, Eq. 3.3.7:

$$e_{\lambda\omega} = a_0 + a_1 r + a_2 r^{-2} + a_3 r^{-3} + a_4 r^{-4} + a_5 r^{-5} + a_6 r^{-6} \tag{3.3.7}$$

The energy of a metal-ligand bond which results from the calculation of the LFSE with the AOM parameters based on this equation can be plotted vs. the bond length. Figure 3.3.2 shows the energy plot for different values of a_5 which corresponds to an r^{-5} dependence of the overlap integral on the metal-ligand bond length. This can be assumed for a simple octahedral case[188,189].
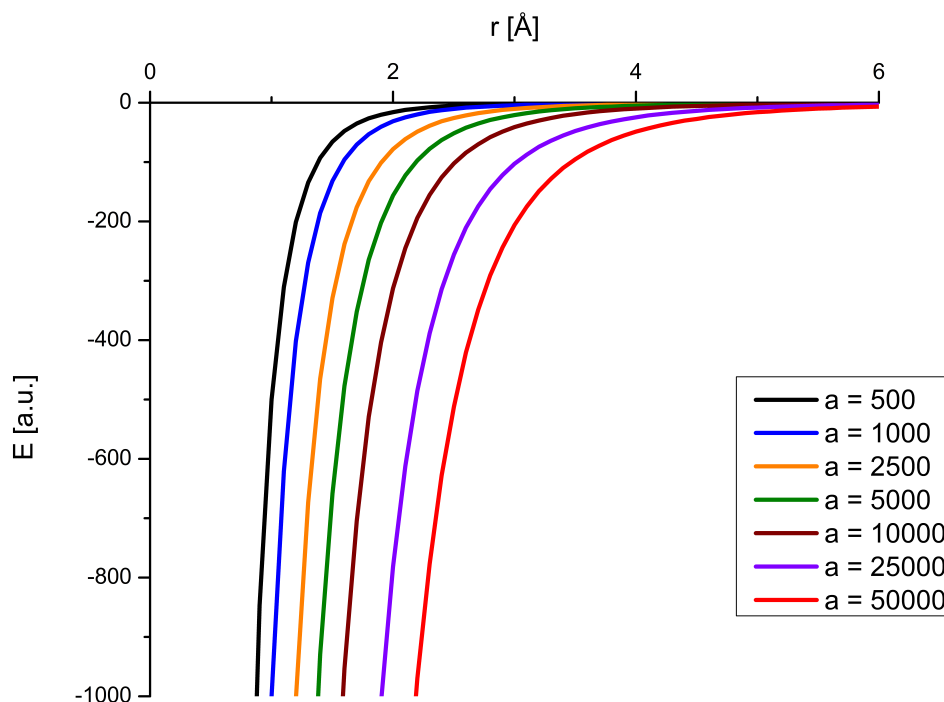
Figure 3.3.2: Metal-ligand bond energy in dependence of r for the original implementation (r^{-5} dependence only) of the ligand field potential

As already mentioned in Pt. III Ch. 3, the negative contribution to the total strain energy of the LFSE has to be balanced with the positive contribution of an additional Morse stretch term in order to generate reasonable bond lengths. As can be seen in Fig. 3.3.2, depending on the choice of a, the ligand field potential is very steep in the region of interest between 1.5 and 3.5 Ångstroms, and the complexity of the form of the function is increased further when additional terms (e. g. r^{-4} or r^{-6} dependence) or interactions (π-bonding and d-s-mixing) are included. Balancing both ligand field and Morse terms during an automatic parametrization is complicated, since multiple parameters

have a drastic effect on only one interaction, namely the total metal-ligand bond stretch energy and its derivatives with respect to r. The problems that arise from two unbalanced potentials are shown graphically in Fig. 3.3.3:
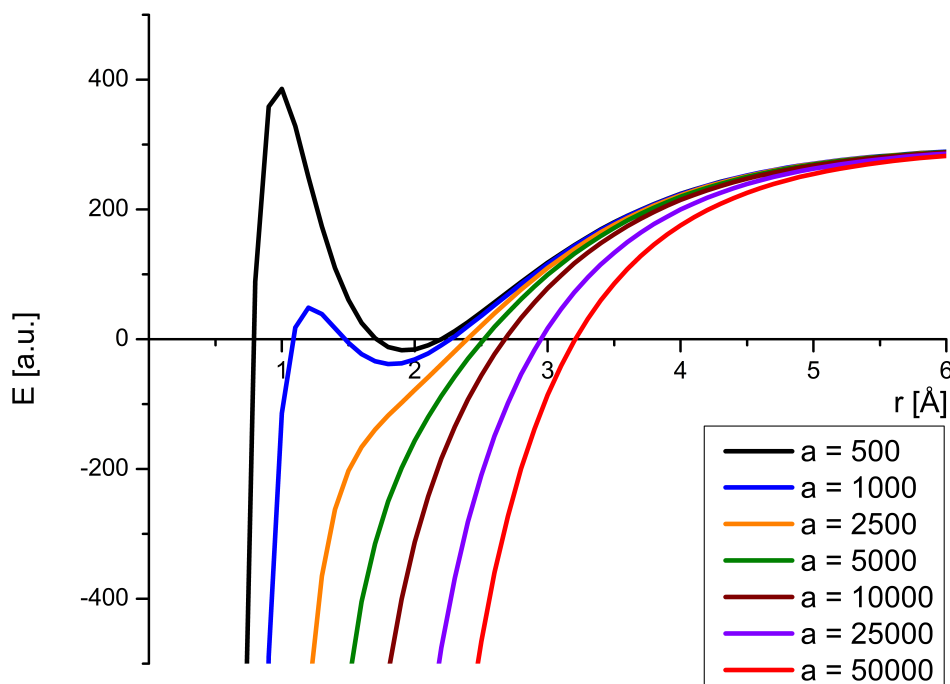
Figure 3.3.3: Summation of the bond energies calculated for the "classical" Morse potential ($D = 300$, $a = 1$, $r_0 = 2.0$) and the original description of the ligand field potential (parameters are given in the plot)

The summation of the ligand field part and the Morse potential should result in a shifted Morse potential, which still has a defined local minimum. Depending on the overlap integral calculated in the ligand field part of the code, the minimum will be shifted to longer or shorter bond lengths, which reflects a destabilization or stabilization, respectively. However, such a minimum on the PES is only achieved in a number of cases, where the two potentials are balanced (black and blue lines). Unbalanced potentials will either result in no significant ligand field effects ($E_{Morse} \gg E_{LF}$), not shown in Fig. 3.3.3, or a strong stabilization of the bond ($E_{Morse} \ll E_{LF}$). In addition, the limiting behavior of the total potential in the case of very short bonds is non-physical. Even if this issue is not encountered in the parametrizations, since bond lengths involving transition metals are normally not found to be within this range, a Monte Carlo parameter optimization trial step can in principle generate parameters which reflect this situation.

To avoid the difficulties in the summation presented here during the automatic parametrization, the functional form of the ligand field parameters has been changed. As the original ligand field potential does not have a defined minimum, which in turn is a difficult problem for the parametrization algorithm, the potential has been replaced by potentials which do have such a defined minimum. While the actual results will be presented in Pt. IV Ch. 3, the theory will be discussed in the following.

As stated above, the ligand field effect can be seen as a perturbation to a classical Morse bond stretch, which shifts the minimum to either longer or shorter bond lengths. As the superposition of two Morse functions gives again a Morse function, our first approach was to mimic the ligand field potential by an additional Morse function of the following form, Eq. 3.3.8:

$$e_{\lambda\omega} = -D(1 - e^{-a(r-r_0)})^2 + D \qquad (3.3.8)$$

where D is the depth of the potential, a the curvature and r_0 the equilibrium bond length. The negative sign of the first D and the addition of the second D result in a maximum of $e_{\lambda\omega}$ at r_0. Figure 3.3.4 shows the energy plot with respect to r of the Morse ligand field function.
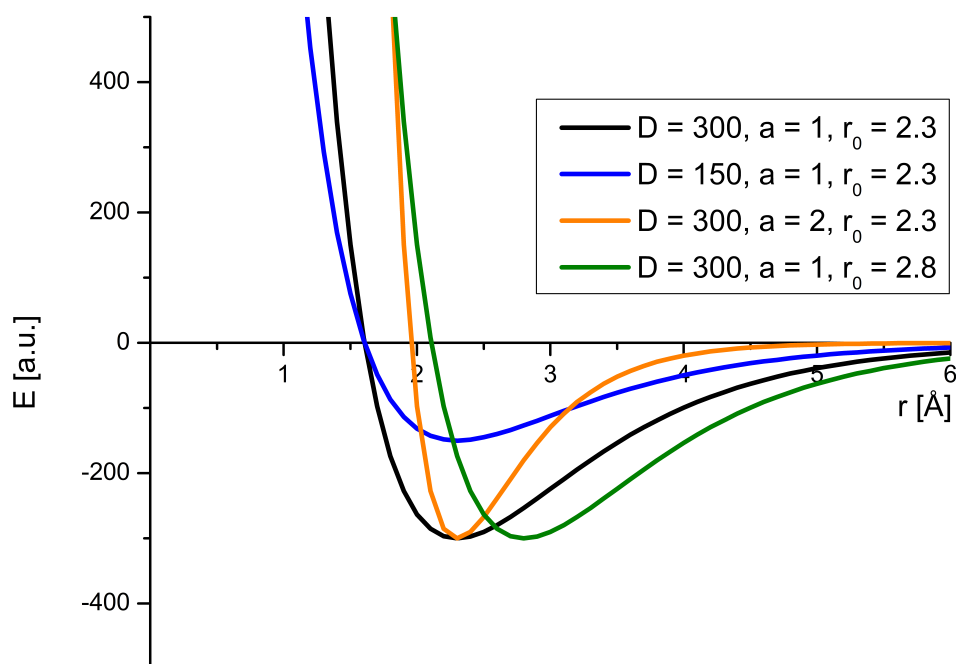
Figure 3.3.4: Metal-ligand bond energy in dependence of r for the Morse implementation of the ligand field potential

As can be seen from Fig. 3.3.5, when a second Morse interaction which describes the "classical" part of the bond stretch is added, the minimum of the potential is retained. Compared to the equilibrium value of 2.0 Ångstroms for the "classical" Morse potential, the equilibrium bond length is shifted to higher values by the addition of the ligand field potential.
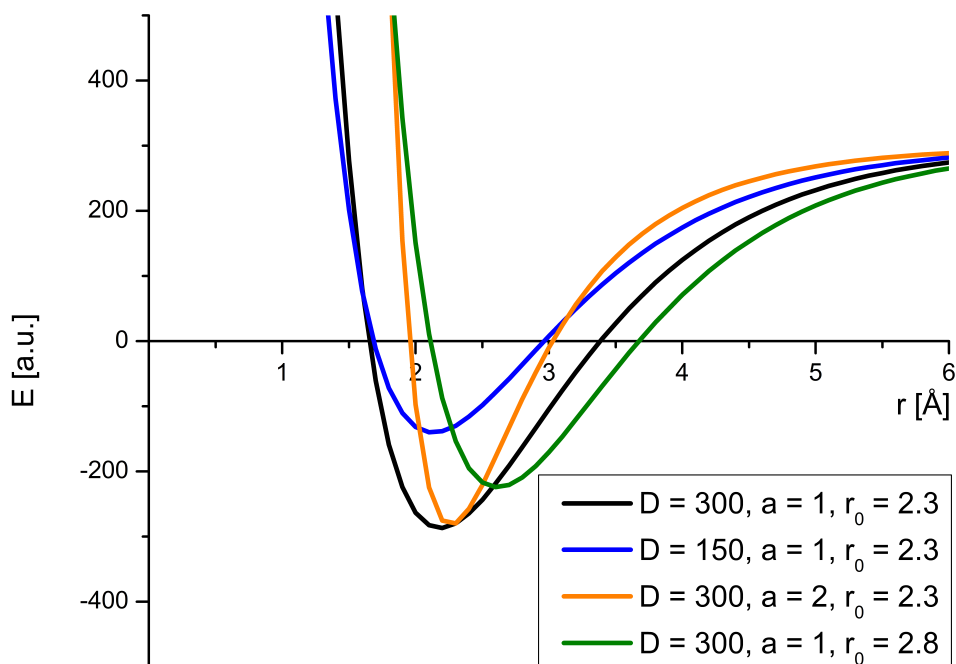
Figure 3.3.5: Summation of the bond energies calculated for the "classical" Morse potential ($D = 300$, $a = 1$, $r_0 = 2.0$) and the Morse description of the ligand field potential (parameters given in the plot)

While this Morse function does have a local minimum and simplifies the overall complexity of the problem (parameter reduction from potentially 7 parameters in the original potential to 3 parameters in the Morse potential), the r^{-5} dependence of the LFSE with respect to the bond length known from experiments and theory is no longer present in this approach. Also, the limiting behavior is only correct in the case of very long bonds, whereas very short bonds are still stabilized by the ligand field and, depending on the parameters chosen by the parametrization algorithm, will dominate the Morse potential for the "classical" part of the metal-ligand bond stretch.

For a more realistic description of the ligand field interaction, a potential featuring an inverse quadratic and sixth degree function has been used, Eq. 3.3.9 and Fig. 3.3.6, which resembles an asymmetric Gauss distribution:

$$e_{\lambda\omega} = \frac{D}{a^2((r-b)^2 + (r-c)^6) + 1} \tag{3.3.9}$$

where D, a, b and c are parameters of the force field and r is the bond length.
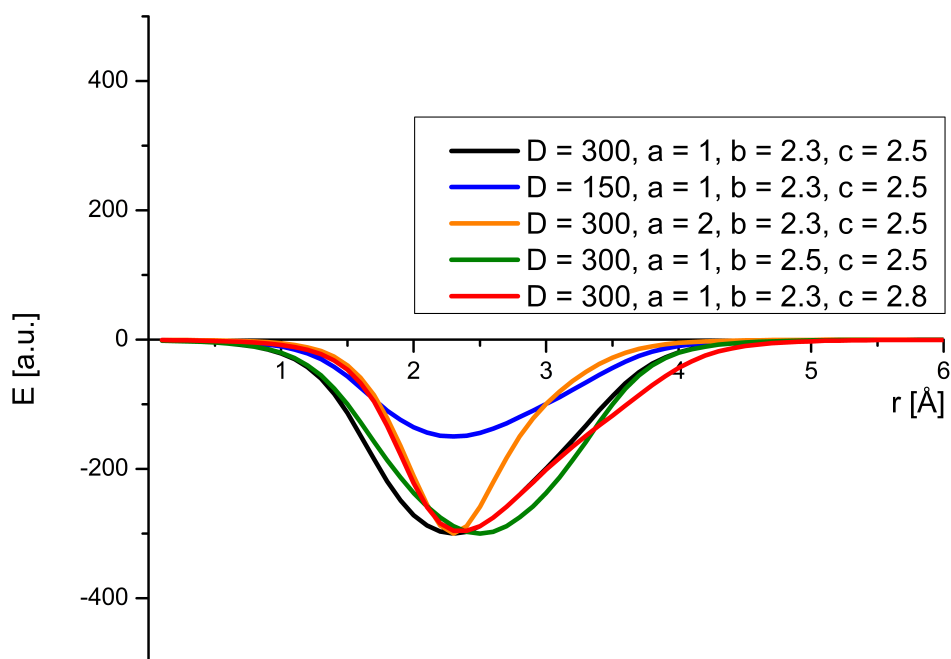
Figure 3.3.6: Metal-ligand bond energy in dependence of r for the "Gauss-type" implementation of the ligand field potential

When this potential form for the ligand field effect is used, the energy for both very short and very longs bonds is zero, and the additional Morse stretch will dominate the total effect on the stretch. Also, the choice of a quadratic and sixth degree polynomial with different equilibrium bond lengths b and c ensures an asymmetry in the potential form and adds more flexibility to describe the PES around the equilibrium bond length. As in the Morse description of the ligand field, this potential also has a local minimum, which improves convergence during the automatic parametrization process.

The summation of the "Gauss-type" potential for the ligand field and a Morse potential for the "classical" bond stretch results in a shifted Morse potential for the full description of a bond stretch, which includes the ligand field perturbation (as shown in Fig. 3.3.7).
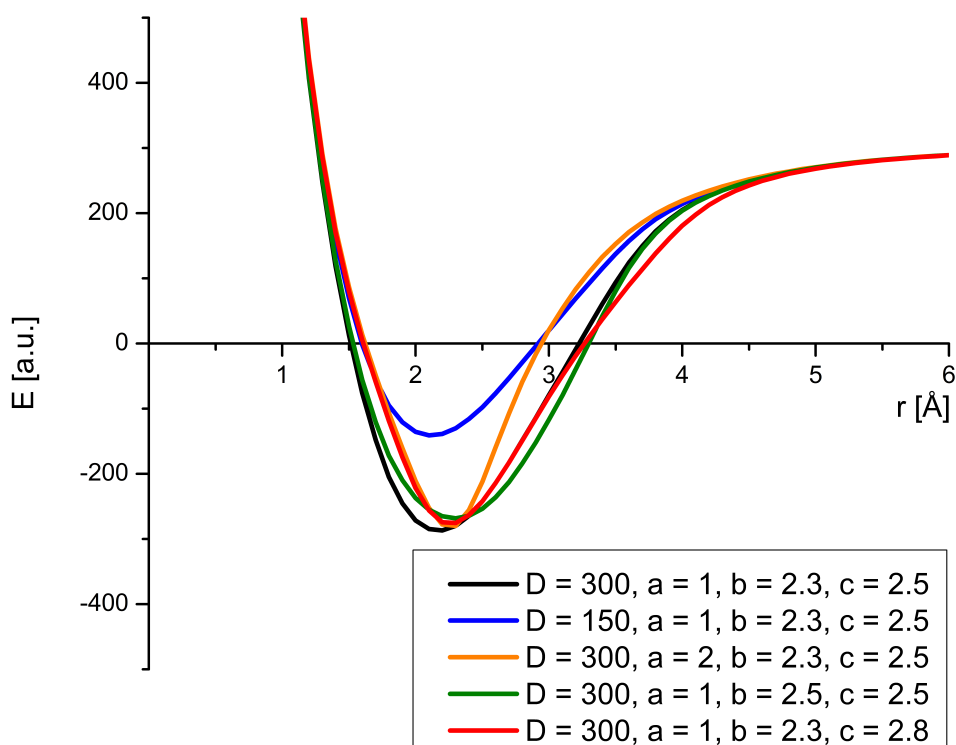
Figure 3.3.7: Summation of the bond energies calculated for the "classical" Morse potential ($D = 300$, $a = 1$, $r_0 = 2.0$) and the "Gauss-type" description of the ligand field potential (parameters given in the plot)

The problem of balancing the "classical" contribution to the stretch interaction with the ligand field contribution results in a shifted Morse description for the combined potential. Our third attempt to solve this problem was to include the classical contribution in the ligand field contribution and therefore describe the whole interaction with just one potential. Since the contribution of every bond to the ligand field matrix is unique, because the overlap integral between the metal and each ligand is different, the combined effect of classical and ligand field energy can be represented with one potential which describes the AOM parameters $e_{\lambda\omega}$ and such, the LFSE. We have implemented this approach both with the Morse and the "Gauss-type" description given above (Eqs. 3.3.8 and 3.3.9). The drawback of this approach is, that properties correlated to one of the potentials (either "classical" or ligand field) can no longer be directly derived from the combined potential, e. g. the UV/VIS transitions obtainable from the ligand field code are no longer connected to the ligand field parameters used in the parametrization. However, since the primary goal of this work was to generate meaningful molecular structures with a ligand field molecular mechanics approach, this drawback has been tolerated at this point.

Part IV

Automatic Parametrization

1 Introduction to Parametrization Methods

As discussed previously in Pt. I Ch. 2, a molecular force field consists of a set of functions, predefined atom types and parameters. The accuracy of a force field is therefore directly correlated to the quality of the parameters and thus, the parametrization of a force field is of crucial importance. The parametrization process includes: a) selection of reference data, on which the force field parameters are based, b) the definition of a parametrization method, which derives the force field parameters from the reference data and c) the optimization and validation of the force field. The data considered for the parametrization process should be adopted to the problem at hand, e.g. a general force field should include a wide selection of reference structures which cover a large chemical variety of a certain interaction. On the other hand, a force field tailored to a specific problem may be parametrized with a small but representative number of reference structures. The selection of the parametrization method mostly influences the performance of the parametrization process and should, in principle, not affect the resulting force field. However, certain algorithms are better suited for specific parametrization problems than others. The optimization and validation of a force field includes leave-one-out tests, where parts of the training set are left out for the parametrization and the resulting force field is then used to calculate the geometry or a molecular property from the left out data. If the force field is stable, the removal of one structure from the training set should still produce a valid force field. With this procedure structures, which are critical for the parametrization, can be identified and additional data exhibiting a comparable geometry can be added to the training set in order to make the force field more robust.

1.1 Selection of Reference Data

Reference data can include a variety of molecular properties, namely structural information, relative energies of conformers, spectroscopic data or information about atomic charges. Structural data is included in most force field parametrizations[190], since molecular properties almost always depend on the molecular structure. Sources for structural information are geometries measured by X-ray crystallography or calculated by QC methods or a mixture of both[191,192]. Since crystals will often contain some sort of crystal lattice effects, flexible interactions like torsions will easily be distorted

with respect to their equilibrium value, whereas stretches and bends are more robust with regard to these distortions, as these interactions contain more energy. Therefore, individual interactions should be compared against the reference set opposed to an all-atom overlay[190]. If interactions are compared in a pairwise fashion, individual weighting and extraction of relevant data from the entire structure is possible , e. g. the interactions involving hydrogen atoms can be omitted, since they are often not resolved accurately in X-ray structures. An approximation commonly made during force field parametrizations is to neglect condensed phase effects, which are assumed to average out, if the data set taken for the parametrization is large enough[193].

Apart from structural information, energies, spectroscopic data and charges can also be used to parametrize a molecular force field. Relative energies of conformers or rotational energy profiles can be derived from QC calculations, which has been used e. g. in the OPLS all-atom force field[194]. Reference data concerning atomic charges are also derived from QC calculations and rarely from experiments, since atomic charges are no observables and thus can only be indirectly obtained from experimental results[190]. An example for a charge parametrization is the implementation of a fluctuating charge model, which allows to study polarization effects in proteins in a liquid solution, in the CHARMM[195] force field. The reference charges are based on DFT calculations of small molecules in the vicinity of a small dipolar probe, which mimics a water molecule[196]. Rappé[197] proposed a charge equilibration method (QEq) which can predict the charge distribution in a molecule and can be used e. g. in molecular dynamics simulations. The model is based on experimental atomic ionization potentials, electron affinities and atomic radii. Spectroscopic data such as IR or Raman vibrations can be included in a parametrization to estimate force constants. Since assignment of experimental results to specific interactions becomes non-trivial with larger structures, vibrational frequencies are often generated by QC methods and the data is directly derived from first and second derivatives of the energy with respect to atomic coordinates[178,190,198]. A detailed description of this approach will be given below.

The definition of the reference data is an important step in the force field development, as the reference data will determine the final accuracy and performance of the force field. In principle, any data from experiments or QC calculations can be used, but should be carefully validated, as errors in the reference data set will directly influence the obtained force field parameters.

1.2 Parametrization Algorithms

After the definition of a reference data set, on which the force field is based, the actual parametrization algorithm has to be selected. The general parametrization concept involves a set of starting parameters, which are used to generate the molecular structure or property. The calculated values are then compared to the data contained in the reference set and an error function, such as the weighted root mean square deviation (RMSD) (Eq. 4.1.1), is used to calculate the quality of the parameter set with respect to the reference data.

$$RMSD = \sqrt{\frac{1}{N}\sum_{n=1}^{N}w_n(v_{n(calc)} - v_{n(ref)})^2} \qquad (4.1.1)$$

Here, w_n is the weighting factor for interaction n, and $v_{n(ref)}$ and $v_{n(calc)}$ are the reference and calculated values of the interaction, respectively. The force field parameters are then varied in an iterative scheme, until the optimum set of parameters is found and the error between reference and calculated data is minimized. The parametrization procedure therefore is a minimization problem and can also be seen as a constrained minimization, if some of the force field parameters are restricted to minimum and/or maximum values. For problems which involve a very limited number of interactions, this parametrization procedure can be done by hand. However, when the number of interactions, atom types and reference structures involved in the problem becomes larger, automatic algorithms based on the simple general scheme outlined above may be preferable.

The general approach to automatic parameter estimation can be divided into techniques with or without the usage of first and second derivatives of the error function with respect to the individual parameters[190]. Methods, which do not use gradient information, include systematic searches, Monte Carlo approaches, the downhill simplex method[199,200] and genetic algorithms[201–204].

The systematic search over all individual parameters is only applicable to problems which involve a limited number of parametrization variables. Also, if the parameter surface is very diverse, the step size between individual points (i. e. points on the parameter surface) has to be small, which makes systematic searches computationally expensive. However, the method is intrinsically parallelizable and thus can benefit from modern computer architectures and supercomputers.

Monte Carlo methods involve random variations of parameters and can be used to scan large parameter surfaces. Hæffner et al.[205] have applied a Monte Carlo parametrization scheme to derive Cu^I parameters for the AMBER[206] force field. Monte Carlo methods can also be used to gain insights on the parameter surface and restrict a second parametrization scheme to a certain area of interest.

The downhill simplex method[199,200] constructs a N+1 polyhedron of points on the surface of the error function, where N is the number of parameters varied during the parametrization. The minimum of the error function is found by systematically eliminating the highest point of the simplex, until all points are within a predefined convergence range. The simplex method is very robust and converges fast for a limited number of variables, but shows slow convergence when the dimension of N is increased. Norrby et al. showed, that the overall convergence can be improved by including the error function in the simplex algorithm[193].

Genetic algorithms[201–204] represent another approach, which does not take any information about the first and second derivatives of the error function into account. Huttner et al.[207,208] used this technique on a set of tripodal metal complexes and defined a binary string based on the parameters and their respective variation range and resolution. The result of the error function was used in conjunction

with the binary strings to generate a starting population. Parts of the binary string were then varied by "single bit"- or "crossing over"-mutation to spawn a generation of offspring. During this process, binary strings with a low error function value had an increased effect on the next generation and were preferred during mutations. The process was repeated, until convergence was achieved. Tafipolsky and Schmid also used genetic algorithms to parametrize Metal-Organic Frameworks (MOFs) from a set of QC reference calculations[209] and Strassner et al.[210,211] presented an automated tool for the generation of MM3 force fields, which uses genetic algorithms for the parametrization process. Cukrowski and Marques[212] used artificial neural networks to derive a set of force field parameters for modelling metalloporphyrins of Mn^{II}, Mn^{III}, Mn^{IV}, Mn^V, Con^I, Co^{II}, Co^{III}, Ni^{II} and Cu^{II}. Artificial neural networks consists of interconnected neurons and based on the information, that comes in and out of the network, the structure and information flow is changed and optimized in the course of the parametrization.

Algorithms which involve gradient information make use of the first (and possibly second) derivatives of the error function with respect to the parameters. With the vector information of the gradient, the optimal direction for the next set of parameters can be identified and so even parametrizations which involve many parameters can be converged. As the curvature around a minimum of the parameter surface tends to zero, gradient based methods generally converge slowly when close to the minimum[190]. Examples for gradient based methods are the Broyden-Fletcher-Goldfarb-Shanno (BFGS)[213–216] and the Fletcher-Reeves-Polak-Ribiere (FRPR)[217,218] algorithm. The BFGS method belongs to the family of Quasi-Newton methods and makes use of first derivatives and an approximation to the Hessian matrix of second derivatives. The FRPR algorithm only uses gradient information and is a representative of the Conjugate Gradient methods.

The information present in the Jacobian and Hessian matrices of QC calculations can also be used to parametrize force fields. The Jacobian (Eq. 4.1.2) is the gradient of the energy with respect to the atomic coordinates whereas the Hessian (Eq. 4.1.3) is a matrix of all second derivatives of the energy.

$$J_E = \begin{pmatrix} \frac{\partial E}{\partial x_1} & \frac{\partial E}{\partial x_2} & \cdots & \frac{\partial E}{\partial x_n} \\ \frac{\partial E}{\partial y_1} & \frac{\partial E}{\partial y_2} & \cdots & \frac{\partial E}{\partial y_n} \\ \frac{\partial E}{\partial z_1} & \frac{\partial E}{\partial z_2} & \cdots & \frac{\partial E}{\partial z_n} \end{pmatrix} \quad (4.1.2)$$

$$H_E = \begin{pmatrix} \frac{\partial^2 E}{\partial x_1 x_1} & \frac{\partial^2 E}{\partial x_1 y_1} & \cdots & \frac{\partial^2 E}{\partial x_1 z_n} \\ \frac{\partial^2 E}{\partial y_1 x_1} & \frac{\partial^2 E}{\partial y_1 y_1} & \cdots & \frac{\partial^2 E}{\partial y_1 z_n} \\ \vdots & & & \vdots \\ \frac{\partial^2 E}{\partial z_n x_1} & \frac{\partial^2 E}{\partial z_n y_1} & \cdots & \frac{\partial^2 E}{\partial z_n z_n} \end{pmatrix} \quad (4.1.3)$$

The potential energy surface described by the Hessian matrix is used as the reference data set and a functional form, namely the force field, is used to reproduce this surface. Maple et al.[219] used this approach and probed the surface of the formiate ion by slightly distorting the molecule from its

equilibrium configuration. The changes in first and second derivatives were weighted and summed in an error function, which then was minimized with respect to the force field parameters, Eq. 4.1.4:

$$S = w_k \sum_{\alpha,i} (g_{\alpha,i} - g_{\alpha,i}^0)^2 + w_H \sum_{\alpha,ij} (H_{\alpha,ij} - H_{\alpha,ij}^0)^2 \qquad (4.1.4)$$

Here, w_k and w_H are the weighting factors and $g_{\alpha,i}$ and $H_{\alpha,ij}$ the first and second derivatives, respectively, where the superscript 0 denotes the reference values obtained from QC calculations. Similar approaches have been used by Palmö et al.[220], Leonard and Ashman[221], Hagler and coworkers[198], Seminario[222], Dasgupta[223–225] and Norrby et al.[193]. We have implemented a strategy which involves a maximum force field, where the resulting Jacobian and Hessian matrices are used as the reference data set for a parametrization. This approach will be discussed in detail in Pt. V Ch. 2.

As the simplex and BFGS methods were used extensively in this study, the methods will be explained in more detail at this point. In the simplex method, among the N+1 points spanning the polyhedron on the surface of the error function, the one with the highest error is identified and reflected through the barycenter of all points (excluding the one with the highest error). If the reflected point does not yield a lower error function value, the simplex is contracted, expanded or the parameter function of the lowest point is mixed with all the other points to generate a new simplex matrix. Fig. 4.1.1 depicts the possible simplex steps. The N+1 dimensional simplex "crawls" along the parameter surface, until the difference between the matrix elements of the simplex is below a certain threshold.
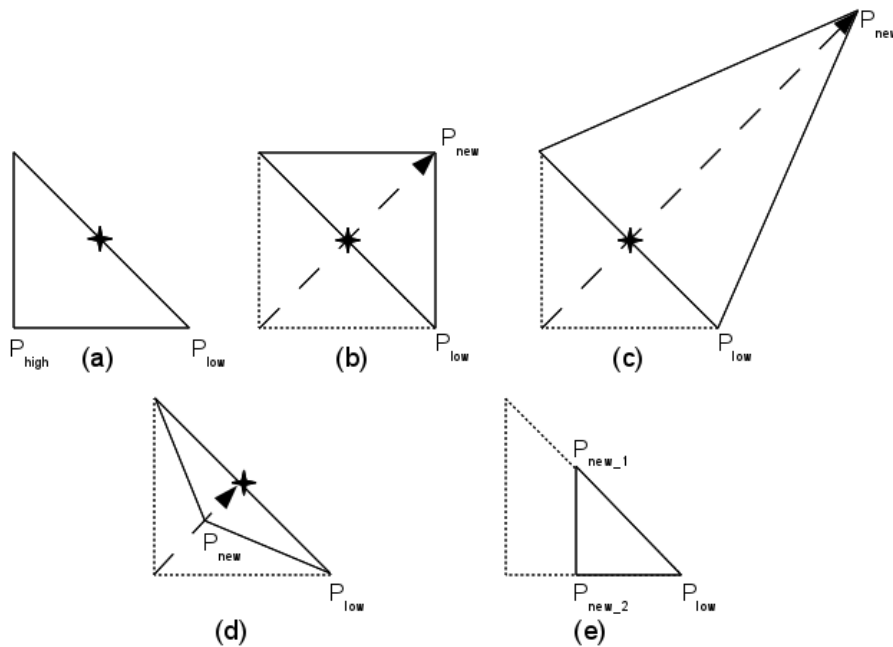
Figure 4.1.1: Possible simplex operations on the N+1 polyhedron on the parameter surface: **(a)** original simplex **(b)** reflection of P_{high} **(c)** reflection and expansion of P_{high} **(d)** contraction of P_{high} **(e)** contraction of all points except P_{low}. (P_{high} denotes the point with the highest value of the error function, P_{low} the lowest point and P_{new} the new point of the simplex. The star represents the barycenter of the simplex)

In the BFGS algorithm, the search direction is evaluated by Eq. 4.1.5:

$$B_k p_k = -\nabla f(x_k) \tag{4.1.5}$$

where B_k is the Hessian matrix approximated from gradient information, p_k is the search direction and $f(x_k)$ is the value of the error function at point x. After the search direction has been found, a line search is done along the vector p_k to identify the step size α_k and set a new point for the next BFGS iteration (Eq. 4.1.6), which starts with the calculation of the new gradient and updates the approximated Hessian matrix.

$$x_{k+1} = x_k + \alpha_k p_k \tag{4.1.6}$$

A graphical representation of the BFGS algorithm is shown schematically in Fig. 4.1.2. Here the perpendicular orientation of the gradient of one step to the next can be seen.
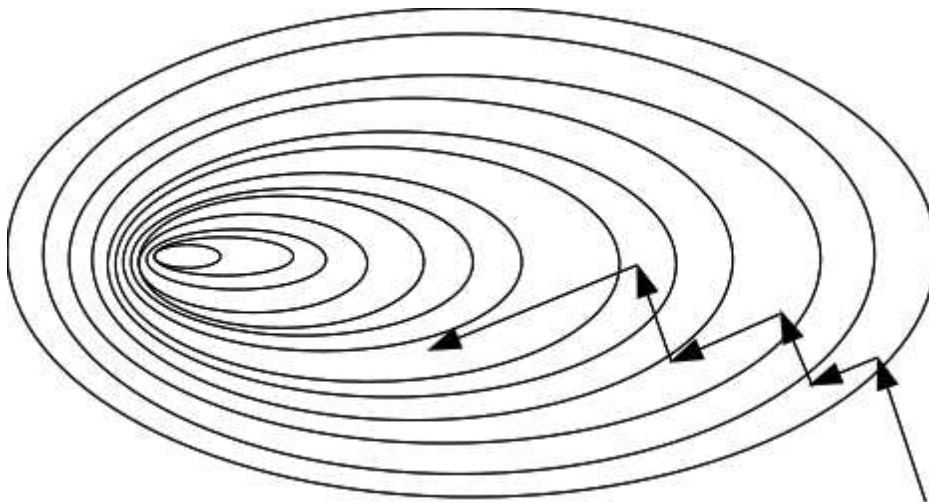
Figure 4.1.2: Schematic representation of the BFGS algorithm

2 Implementation

Automatic parametrization of the ligand field term in Momec has been implemented with a combination of Perl scripts for the initialization of the parametrization and the actual parametrization code in the C++ programming language. The use of Perl scripts allowed for increased flexibility during the development of the input format (see Pt. III Ch. 3) and due to its simple syntax, changes to the code could be implemented quickly.

2.1 Implementation of a Parametrization Setup Routine with Perl

As discussed, a force field parametrization involves several steps: a set of reference data has to be selected, the parameters and their functional form have to be identified, a suitable parametrization algorithm has to be chosen and the resulting force field has to be validated against data which is not part of the training set (cross-validation). The Perl scripts used during the parametrization of the ligand field term in Momec primarily deal with the first two objectives, namely the reference data and the parameters for the parametrization.

As the ligand field term adds an additional energy for transition metal ions, X-ray geometries of transition metal compounds with different degrees of distortion from the regular octahedral geometry were used for the reference data set. Detailed information about the different training sets used during the parametrization will be given in Ch. 3 of this Part. As discussed in Pt. III Ch. 3, the reference information is incorporated in the SD file format, which also allows for different weighting factors for every interaction. Listing 4.2.1 recalls the format explained previously and shows an excerpt of the stretches section of a reference SD file.

```
>  <MOMEC_REF_STRETCHES_V2>
1  R[U1]=2.29646@1.0  C=1,2
2  R[U1]=2.04872@1.0  C=1,3
3  R[U1]=2.08575@1.0  C=1,4
4  R[U1]=2.06225@1.0  C=1,5
5  R[U1]=2.04997@1.0  C=1,6
6  R[U1]=2.34478@1.0  C=1,7
7  R[U1]=1.46898@0.0  C=2,8
8  R[U1]=1.47210@0.0  C=2,10
9  R[U1]=0.74690@0.0  C=2,20
```

Listing 4.2.1: Excerpt of the stretches reference information in a SD file

Tags which specify reference information begin with the "MOMEC_REF" keyword. In the listing above, one line represents a single stretch interaction with its respective unit (U1 = Ångstroms in the example) given in brackets. The actual value (= bond length) is followed by the "@" symbol and the weight for this interaction[1]. The weight is followed by the connectivity of the interaction, which is printed mainly due to technical reasons to ease interaction with the Perl scripts, but also as a reference for the user. In the example above, the atom with number 1 is the transition metal whereas atoms 2–7 are the coordinating ligand atoms, bonded to atom 1.

Preparation of the reference data set has been mainly done by hand, since extracting the data from the CSD database[226], checking for errors in the structure, removing the counterions, generating the SD files needed for the parametrization and setting the weights requires chemical intuition and can only be automated in parts of the process. Future plans include to use the experimental errors given in the files from the CSD database and to derive an automatic weighting scheme for stretches, bends and torsions from these values.

The actual setup of the parametrization with Perl scripts has been implemented in a two step process. In the first step, the user calls a setup script, which initializes the directory structure, scans the reference files and creates a control file. The user is then able to edit the control file and thus specifies which parameters to optimize. The actual parametrization is started with a second script and does not need any user interaction.

2.1.1 The Parametrization Setup

The setup script accepts a single command line parameter, which is the location of a setup command file. The command file structure is given in Listing 4.2.2:

---

[1]   In the ligand field parametrization, weights were set to one, when one of the bonding partners of a stretch or the central atom of a bend is a metal. This is due to the fact that the ligand field code only affects the positions of the metal and its coordinating ligand atoms.

```
sdfiles=/path/to/reference/sd/files
workdir=/path/to/working/directory
forcefield=/path/to/initial/force/field/files
multi=10
rms=0.0001
popt=simplex
weight=const
mc_steps=500
unscaled_history=0
calc=opt
chunks=1
jac_hess=0
lf=1
debug=0
```

Listing 4.2.2: Command file structure for the parametrization setup script

The individual options are:

- *sdfiles* points to the path where the reference SD files used during the parametrization will be copied from.

- *workdir* sets the working directory for the parametrization, where all files generated during the process are stored.

- *forcefield* points to a folder containing a Momec force field which is then used as a starting point for the parametrization.

- *multi* specifies the maximum number of parallel Momec instances during a single parametrization step (integer value).

- *rms* specifies the convergence criterion for a Momec geometry optimization in Ångstroms. The RMS shift in Momec is the root mean square of all elements of the Jacobian matrix (floating-point value).

- *popt* specifies, which parametrization algorithm to use during the parametrization (possible values: "simplex", "bfgs" or "frpr", see Ch. 1 of this Part).

- *weight* specifies the weighting scheme (possible values: "const" for a scaling of weights with $w_{stretches} > w_{bends} > w_{torsions} > w_{UV/VIS-transitions}$ or "uni" for no scaling).

- *mc_steps* activates an initial Monte Carlo search with the given number of steps prior to the actual parametrization specified by *popt*. The parameter set yielding the lowest error is then used as a starting point for the actual parametrization (integer value).

- *unscaled_history* when set the parameters printed in the history file are not scaled. The progress of a parametrization including all parameter sets and the respective error values is printed in a history file in table form. Since parameters used during the parametrization are scaled to a value between 0 and 1 (which will be explained in detail below), the values in the history file can be printed unscaled for improved readability (boolean value).

- *calc* sets the calculation mode for Momec during a parametrization (possible values: "opt" for geometry optimization or "sp" for single point).

- *chunks* sets the number of chunks used during a parametrization (the concept of chunks will be explained later) (integer value).

- *jac_hess* switches to the Jacobian/Hessian parametrization method (see Pt. V Ch. 2) (boolean value).

- *lf* turns on the ligand field calculation for a parametrization (boolean value).

- *debug* turns on debug messages (boolean value).

Running the setup script creates a new directory, where all necessary executables of the Momec program, needed library files, Perl scripts, the reference SD files and the force field files are copied to. After loading the initial force field, the SD files are parsed one at a time and all interactions with a weight greater than zero are collected in a list. Setting a weight greater than zero enables the interaction and the corresponding parameters in the force field. A list of all possible force field parameters is written to the control file (see 4.2.3). In addition to the weighted interactions the setup script also scans for missing parameters in the force field. A single point calculation is performed on every reference structure and if stretch or bend parameters necessary for a complete description of the molecule are missing in the force field, the parameters are collected in a second list, which is then written to the control file. Missing force constants are set to a default value of 1.0 mdyn/Ångstrom for stretch interactions and 0.1 mdyn/rad for bend interactions and missing equilibrium values are set to the average of all the values present in the reference data set.

An example for the control file produced by the setup script is given in Listing 4.2.3:

```
> <MOMEC_PARAMETRIZATION_VARIABLES>
chunk1      STR   CT    CT            k=5.000       r0=1.500
chunk2      STR   CT    NT            k=6.000       r0=1.490
chunk3      BEN   CT    CT    H       k=0.360       a0=1.909
chunk4      NBD   CT                  r_vdW=1.900   epsi=0.044_const
> </MOMEC_PARAMETRIZATION_VARIABLES>
> <MOMEC_FORCEFIELD_AUTO_CONSTANTS>
STR   H     ND          k=1.000   r0=0.8011250
BEN   OW    CT    OW    k=0.100   a0=2.2613500
> </MOMEC_FORCEFIELD_AUTO_CONSTANTS>
> <MOMEC_PARAMETRIZATION_COMMANDS>
  debug=0
  multi=1
  mc_steps=1
  chunks=4
  weight=const
  popt=simplex
  unscaled_history=1
  calc=opt
  lf=0
> </MOMEC_PARAMETRIZATION_COMMANDS>
```

Listing 4.2.3: Control file generated after the execution of the setup script

The control file consists of three sections, which are marked by tags as in the SD file format, allowing for an easy incorporation of the parametrization control structure in a combined SD file in the future. The first section contains all parameters which should be optimized during the parametrization. A line consists of the chunk, in which the parameter should be parametrized, the interaction type[2], the corresponding atom types and the force field parameters followed by the starting values. If a value is followed by "_const", the parameter is fixed and thus excluded from the parametrization. A chunked parametrization proceeds as follows: As force field parameters are independent of each other to first order, each parameter can be parametrized independently of all other parameters[3]. Dividing the parameter set into smaller chunks reduces the time needed to converge to a force field and increases the overall performance of a parametrization. Also, only the reference data for the parameters in the chunk are included which may reduce the number of structures to calculate in each step, e. g. in the example above only structures which have a CT-CT bond will be used to parametrize the CT-CT

---

[2]   STR for stretch, MSTR for Morse stretch, BEN for bend, TOR for torsion, NBD for non-bonded, CHG for charge, LF for ligand field

[3]   This is true e. g. for stretch parameters, which affect different regions of a molecule. Coupled parameters, e. g. non-bonded interactions, have to be parametrized at the same time.

stretch interaction in chunk 1. Even if the resulting force field of a chunked parametrization may not be as good as the result of a full parametrization from a quantitative point of view, iterating multiple times will improve the overall result and may still be faster than a complete parametrization over all parameters (see Chapter 3 of this Part for detailed results).

The second section of the control file gives the list of missing parameters in the force field and the respective parameter values, which will be added automatically, but which will not be included in the parametrization process. Completing a force field in that way helps to generate meaningful structures and avoids convergence problems. Parameters added in this way have to be parametrized with additional reference data afterwards to generate optimal values.

The third section repeats the settings given in the command file and is given mainly for reference. Since the control file does not change during the parametrization process, it can be archived together with the actual parametrization results and all information regarding the setup of the parametrization is therefore kept in one place for review purposes.

2.2 The Implementation of the Parametrization Algorithm in C++

When the parametrization is set up, a second Perl script, the run script, starts the actual process. After the additional force field parameters ("MOMEC_FORCEFIELD_AUTO_CONSTANTS" of the control file) are written to the force field files used during the parametrization, the actual parametrization algorithm implemented in C++ is called. The code is based on an earlier implementation by Martin[227]. The general parametrization procedure is given in Figure 4.2.1:
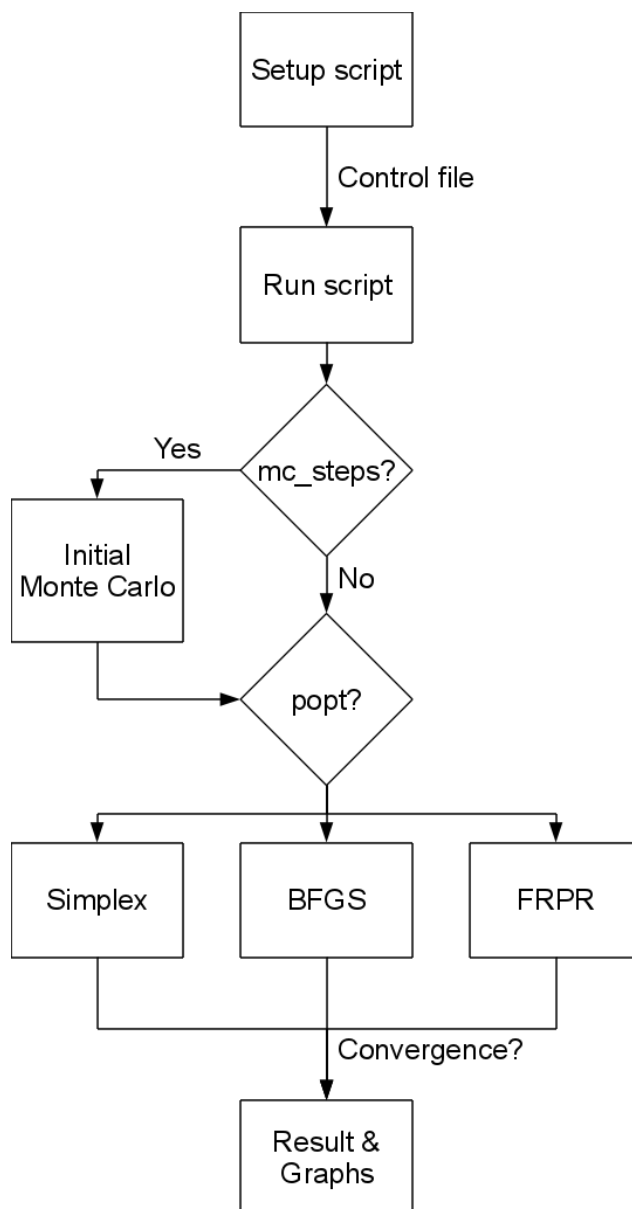
Figure 4.2.1: General parametrization work flow

When the "mc_steps" option is given in the command file, an initial Monte Carlo parametrization will be done before calling the actual algorithm. The Monte Carlo routine returns the parameter set with the minimum error value compared to the reference data found during the random search. This

set is then used as a starting point for the subsequent parametrization. As the parameters are scaled, each Monte Carlo step generates a random number between 0 and 1 for each parameter. The scaling of the parameters is done in order to ensure consistent step sizes for all parameters for the different parametrization algorithms. The maximum value for each parameter is chosen according to its nature, e. g. the maximum value for an equilibrium bond length is set to 4 Ångstroms, which equals to a scaled value of 1 in the parametrization.

After the Monte Carlo steps, the parametrization algorithm is started (for references see Ch. 1 of this Part). For each data point, the force field is adjusted to reflect the parameters of the current step and Momec is called to generate the new structures or properties from the reference data, either via a geometry optimization or single point. The resulting values are passed back to the parametrization algorithm, the error function is evaluated for each interaction and the total error calculated according to Eq. 4.1.1 is used to generate the next step of the parametrization. For a single point, this procedure is straightforward and repeated until convergence with respect to the parameters is achieved. For a geometry optimization however, problems concerning the convergence of the individual geometry optimizations may arise. Since the parametrization algorithm varies the parameters only with respect to the minimization of the error function, non-physical parameters may occur and this may lead to non-converging structures during the Momec geometry optimizations. In order to make the parametrization "aware" of this problem, several approaches have been tested.

A first approach was to add a penalty function, which adds an additional value for each unconverged structure to the error function after calculating the difference between reference and calculated structure. The aim was to make data points involving unconverged structures unfavorable for the parametrization algorithm. However, adding a large penalty value to the total RMS error "disoriented" the algorithm and often resulted in non-converging parametrizations. On the other hand, adding small penalty values had almost no effect on the parametrization process.

A more successful approach was to add penalties to individual interactions. Lower and upper boundary values for an interaction were defined and if e. g. a stretch was found to be outside of these boundaries after a geometry optimization, a penalty value was added to the total RMS value. The penalty function used is given in Eq. 4.2.1 for the lower boundary case:

$$
p_{abs} = |p_{calc} - p_{min}|
$$
$$
p_{norm} = p_{abs} - 5.0
$$
$$
p_{penalty} = \frac{x_{scale}}{1 + exp(-1.0 * p_{norm})}
$$

(4.2.1)

The absolute values p_{abs} were normalized to the lower end of the exponential function at a value of -5.0 and the penalty function was scaled according to the parameter type by x_{scale} (100 in the case of a bond stretch). To include the force constant in this approach, an additional boundary condition for the strain energy in one interaction was defined, compared to the energy calculated from the parameter

set, and a penalty was added to the total RMSD value using the equation 4.2.1. While this approach helped to keep the individual interactions in a reasonable parameter range, the convergence problems were only resolved to some extent.

Another approach to the problem was attempted by using the "best" geometry of a non-converged optimization. Since the geometry optimization in molecular mechanics minimizes the strain energy of a given molecule, the "best" geometry in a non-converged optimization should be the one with the lowest energy. This approach was tested and whenever a geometry optimization failed, the structure with the lowest energy was returned to the parametrization routines in favor of the geometry of the last step, after which the optimization was aborted. However, since the geometry optimizations were always started from the crystal structure of the molecule, which also represents the reference structure for the parametrization, the lowest energy structure was in many cases the structure after the first optimization step. While the structure is changed after one step, it is still very close to the crystal structure and therefore, the value of the error function is low. The overall parametrization therefore favors non-converged structures, and this approach did not solve the convergence problems.

The convergence problems were finally solved by modifying the actual algorithm of the parametrization, which is described in detail using the example of the simplex algorithm.
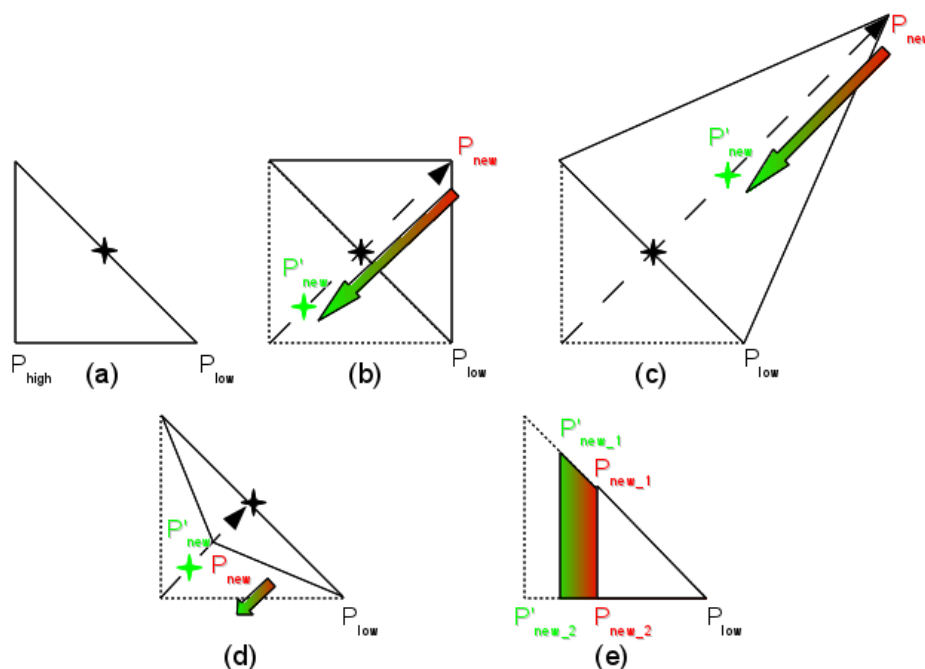
Figure 4.2.2: Possible simplex operations for the modified version of the simplex algorithm, which avoids convergence failures in Momec. The new point p_{new} (depicted in red, no geometry convergence) is shifted back along the vector towards p_{high} until a converging point p_{new} (green) is found.

The starting simplex polyhedron shown in Fig. 4.2.2 consists of a point p_{high} with the highest error value, a point p_{low} with the lowest error value and $N - 1$ points in between. All of these points represent parameter sets and all of these sets are assumed to produce converging structures for the

full reference data set[4]. The reflection of p_{high} through the barycenter of the polyhedron generates a new point p_{new}, where convergence of a Momec geometry optimization is not guaranteed. At this point, the algorithm is modified as follows: the convergence of the parameter set p_{new} is checked: if all structures converge, the point is valid and the algorithm continues in its regular fashion; if the parameter set leads to unconverged structures, the selected point is shifted along the reflection vector towards p_{high}, at which the convergence is guaranteed. The calculation is restarted at point p'_{new} and convergence is checked again. This procedure is repeated while reducing the size of the shift towards p_{high} every time, until a point for which all structures converge is found. In the worst case, this point is almost identical to p_{high}, but the simplex continues with a different simplex operation and still contains valid parameter values. The same procedure was implemented for the other simplex operations, namely the reflection + expansion, the contraction and the mixing of a fraction of p_{low} into all other points. Figure 4.2.2 shows the modified simplex operations.

The BFGS algorithm can in principle be modified in a similar way. However, since the calculation of one point involves deriving the gradient for every parameter, recalculation of the gradient at a different point drastically increases the computational effort. Instead of a calculation of all structures for one parameter set (simplex algorithm), the derivatives for N parameters would have to be calculated, which involves N calculations for all structures. As the derivatives are calculated numerically[227], the number of calculations is even higher. Therefore, the checks for unconverged structures were only implemented in the line search part of the BFGS algorithm, while the calculation of the gradients was not modified.

---

[4] This can be ensured by a Monte Carlo parametrization prior to the actual simplex parametrization. The Monte Carlo results are also checked for unconverged structures in every step and the parameter set producing only converged structures and giving the lowest error is passed to the simplex algorithm.

3 Results and Discussion

The algorithms and the options to define the general procedure of the automatic parametrization evolved in the course of this thesis which allowed for an increase in the complexity of the parametrization tasks. The initial parametrizations did not take any ligand field effect into account, but simply tested the parametrization algorithms on standard force field parameters like a carbon-carbon stretch interaction. The incremental parametrization approach already mentioned in Ch. 2 of this Part was tested and the proper functioning of the ligand field code was confirmed with a number of hypothetical test structures. The procedure was tested on a single X-ray structure and UV/VIS data was included as reference data for the parametrization. Finally, a larger ligand field reference data set was used in the automatic parametrization and leave-one-out tests were carried out for verification of the obtained force field. Timings for the individual parametrizations are not presented at this point, since run times are highly dependent on the computer hardware and the version of the code. Since both the hardware and the code changed during the course of this project, individual timings are not comparable to each other and can not be seen as significant.

3.1 Parametrization without a Ligand Field Term

The parametrization algorithms were initially tested with a series of 17 transition metal compounds coordinated by cyclam-based ligands (see appendix B for CSD reference codes, literature and structures)[1]. The weights in these structures were set only for stretch interactions which involve the CT-CT (sp^3 carbon-sp^3 carbon) and CT-NT (sp^3 carbon-sp^3 nitrogen) atom types, both of which are already well defined in the original Momec force field[56–61] (see Appendix C for details). However, the starting parameters of the parametrization were also modified from their optimal positions in order to test the parametrization algorithm. The overall parametrization therefore included only four parameters, since both stretch interactions were described by a harmonic potential. Additional parameters were added as constants to the force field in order to increase the overall accuracy of the parameter set and avoid convergence problems (see Table 4.3.1). These parameters were not changed during the parametrization process. Four parametrizations have been carried out with this reference data set. The results are shown in Table 4.3.2.

---

[1] Most of the parametrizations presented in this Chapter were done together with Markus Rössler during his research internship.

Table 4.3.1: Additions to the starting force field for the parametrization of the set of 17 transition metal complexes coordinated by cyclam-based ligands. All parameters shown are only added to the force field and not modified in the course of the parametrization.

interaction type	atom 1	atom 2	atom 3	k [mdyn/(Å or rad)]	r_0 [(Å or rad)]
stretch	NT	NT		1.000	1.169
stretch	H	ND		1.000	0.801
stretch	CON	OC		1.000	1.289
stretch	NI2	OW		1.000	2.155
stretch	CO2	CT		1.000	1.910
stretch	CO2	OW		1.000	2.208
stretch	CR3	OW		1.000	1.970
bend	CO3	NT	NT	0.100	2.173
bend	NT	NT	NT	0.100	3.061
bend	NT	CR3	OC	0.100	1.571
bend	OC	CR3	OC	0.100	3.142
bend	CON	OC	CR3	0.100	2.298
bend	CON	ND	H	0.100	2.068
bend	ND	CON	OC	0.100	2.018
bend	H	ND	H	0.100	2.078
bend	OC	CON	OCO	0.100	2.163
bend	CT	OW	CU2	0.100	2.239
bend	OW	CT	OW	0.100	2.261
bend	OR	CT	OW	0.100	2.011
bend	NT	NI2	OW	0.100	1.750
bend	OW	NI2	OW	0.100	2.331
bend	H	OW	NI2	0.100	1.973
bend	CT	CO2	NT	0.100	1.615
bend	NT	CO2	OW	0.100	1.527
bend	CT	CO2	OW	0.100	3.106
bend	CO2	CT	OW	0.100	2.090
bend	CO2	CT	CT	0.100	2.166
bend	CO2	OW	H	0.100	2.210
bend	OW	CR3	OW	0.100	2.354
bend	NT	CR3	OW	0.100	1.767
bend	CR3	OW	H	0.100	2.015

Table 4.3.2: Results of the automatic parametrization with the simplex or BFGS algorithm on a set of 17 transition metal compounds coordinated by cyclam-based ligands. Starting values for the initial force field are given in parentheses.

algorithm	k(CT-CT) [mdyn/Å]	r_0(CT-CT) [Å]	k(CT-NT) [mdyn/Å]	r_0(CT-CT) [Å]	RMSD
simplex	9.800 (5.000)	1.505 (1.500)	5.351 (6.000)	1.479 (1.490)	0.109 (0.175)
BFGS	4.989 (5.000)	1.496 (1.500)	5.989 (6.000)	1.482 (1.490)	0.109 (0.175)
simplex	2.825 (1.000)	1.495 (2.000)	1.670 (2.000)	1.461 (2.000)	0.109 (1.401)
BFGS	0.447 (1.000)	1.373 (2.000)	0.568 (2.000)	1.363 (2.000)	0.141 (1.401)

The RMSD (see Ch. 1 of this Part) was calculated with the reference information of 119 CT-CT stretches and 150 CT-NT stretches with a relative weight of 110. Bends and torsions which involve the CT-CT and CT-NT motif were also included with a relative weight of 5 and 1, respectively. However, since the parametrization did not include any degrees of freedom for the bends and torsions, the effects on these interactions during the parametrization are minor and will not be discussed here.

As can be seen from Table 4.3.2, both simplex and BFGS algorithm perform equally well when starting from the already well defined parameters of the Momec force field. The overall RMSD value improves slightly and the r_0 values do not deviate much from the starting values. However, the force constants derived by the automatic parametrization differ when comparing the two algorithms. The BFGS algorithm returns force constants which are near their original values, whereas the simplex algorithm returns force constants which differ notably from their starting values. Since the parametrization space is small and no reference energy criterion, which affects the value of the force constant was included, both sets of parameters perform almost equally well.

If the starting parameters are modified from the values of the original Momec force field, the situation changes notably. While the simplex algorithm still converges to a set of parameters, which gives a RMSD value in the same region as before, the BFGS algorithm gives a result which is slightly worse. This can be explained by the fact, that multiple minima exist on the parameter surface and since the starting values are far from the minimum of the original values, the BFGS converged to another minimum. Prepending an additional Monte Carlo simulation before the actual BFGS parametrization can increase the chance of finding a minimum, which is near the global minimum of the parameter surface from a qualitative point of view.

To compare the parametrized interactions with a reference data, a graph showing the calculated values vs. the reference values is plotted after every parametrization by the automatic parametrization run script. The graphs for the stretches in the cyclam parametrizations are shown in Fig. 4.3.1.
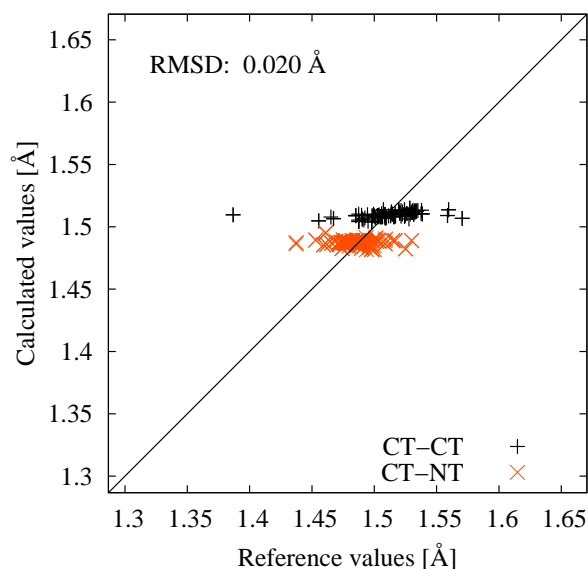
(a) Simplex parametrization starting from the original Momec force field (Appendix C)
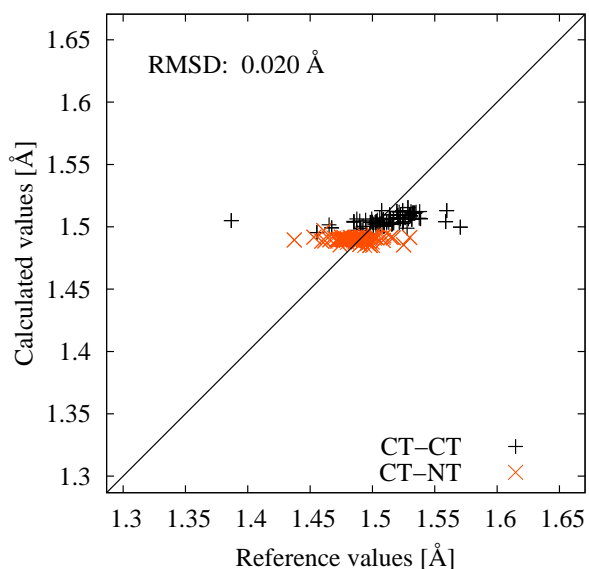
(b) BFGS parametrization starting from the original Momec force field (Appendix C)
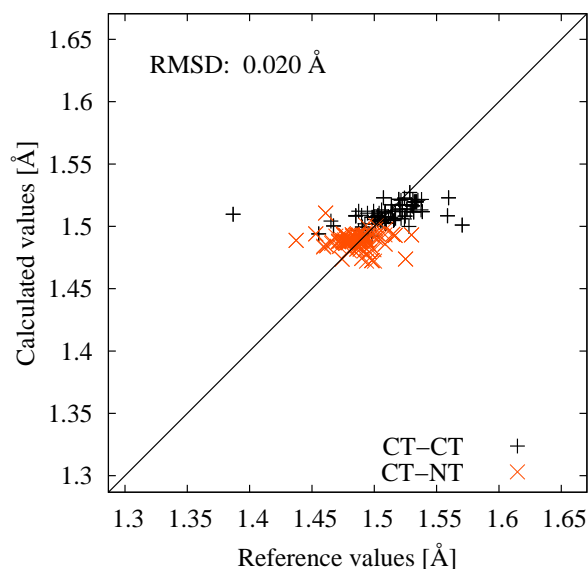
(c) Simplex parametrization starting from the modified Momec force field
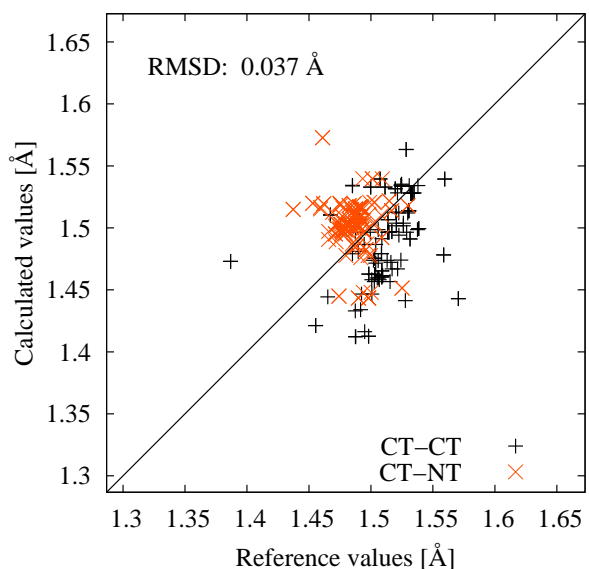
(d) BFGS parametrization starting from the modified Momec force field

Figure 4.3.1: Comparison between final geometries of an automatic parametrization and reference geometries of a set of 17 transition metal complexes coordinated by cyclam-based ligands.

As the force constants for both the CT-CT and CT-NT stretches have a high value in the case of the two parametrizations starting from the original force field (Figs. 4.3.1a and 4.3.1b), the resulting distribution of the calculated bond lengths is narrow. Starting from the modified version of the force field converges the parametrization to a set of parameters with smaller force constants (Figs. 4.3.1c and 4.3.1d), which broadens the distribution and increases the flexibility of the stretch interactions. As stated above, including an energy criterion in the parametrization may have had an effect on the optimization of the force constant and may have produced a narrower distribution of the calculated bond lengths.

3.1.1 Incremental Parametrization

In order to test the concept of chunks, explained earlier in Ch. 2 of this part, the same set of transition metal complexes coordinated by cyclam-based ligands was used in a chunked parametrization. The final values of the parametrization variables are shown in comparison to the results of a parametrization with all variables optimized at the same time in Table 4.3.3. Bend interactions which involve CT and NT atom types have been included in this parametrization to increase the number of possible chunks.

Table 4.3.3: Final values of the parametrization variables during the chunked parametrization of a set of 17 transition metal compounds coordinated by cyclam-based ligands (values from a parametrization with all variables at the same time are given in parentheses).

chunk	interaction type	atom 1	atom 2	atom 3	k [mdyn/(Å or rad)]	r_0 or θ_0 [(Å or rad)]
1	stretch	CT	CT		5.999 (5.118)	1.500 (1.502)
2	stretch	CT	NT		4.631 (6.303)	1.476 (1.480)
3	bend	CT	CT	H	0.360 (0.488)	1.909 (1.920)
4	bend	H	CT	NT	0.360 (0.377)	1.909 (1.894)
5	bend	CT	CT	NT	0.450 (0.466)	1.911 (1.891)
6	bend	CT	CT	CT	0.450 (0.448)	1.911 (1.908)
7	bend	CT	NT	CT	0.450 (0.462)	1.911 (1.893)
8	bend	CT	NT	H	0.397 (0.428)	1.883 (1.880)

The constants automatically added to the force field were identical to the parametrization shown in Section 3.1 of this Part. The original Momec force field (see Appendix C) was used for all other interactions in the molecule. The weights were again only set for interactions which involve the CT and NT atom types and stretches were scaled by a factor of 110, bends by a factor of 5 and torsions by a factor of 1.

As can be seen from Table 4.3.3, the final values from both parametrizations are within the same region, which proves that the force field interactions are independent from each other and therefore can be parametrized individually in this case.

The overall accuracy of the resulting force fields is shown in Figure 4.3.2.
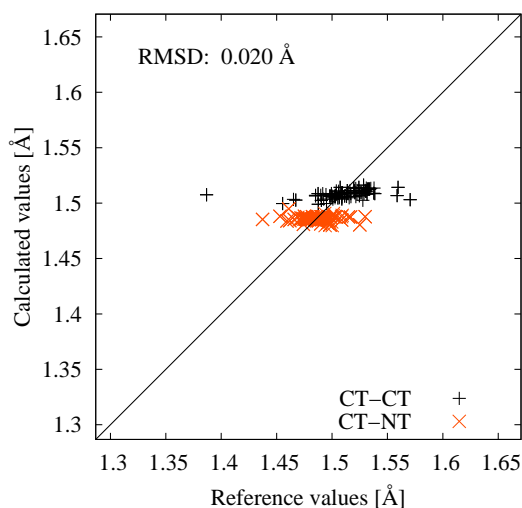
(a) Chunked parametrization: Stretches
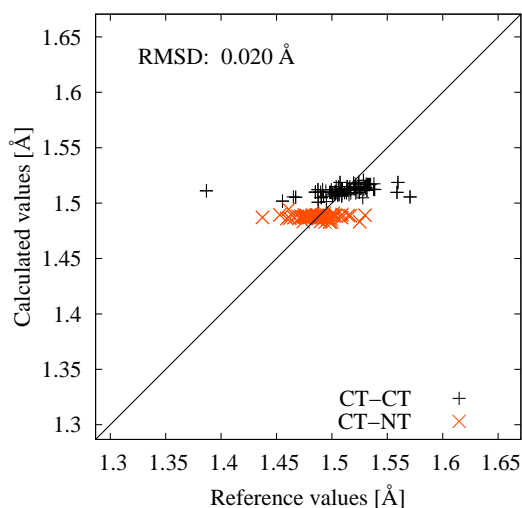
(b) Complete parametrization: Stretches
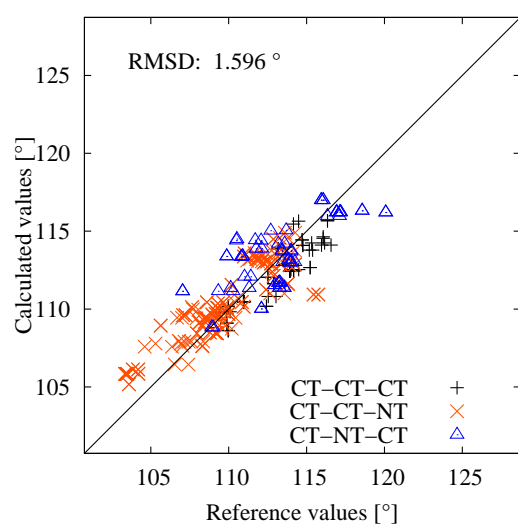
(c) Chunked parametrization:

Bends without hydrogen atoms
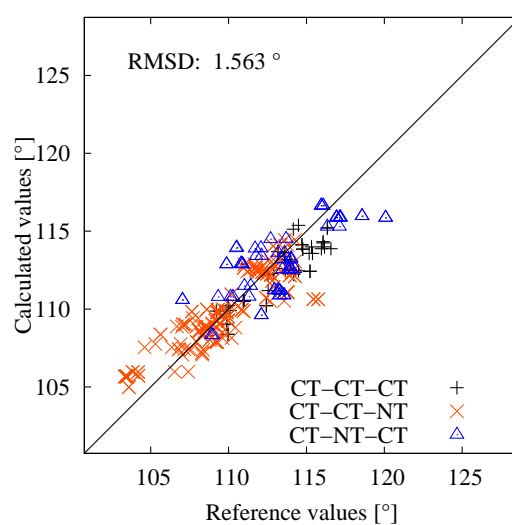
(d) Complete parametrization:

Bends without hydrogen atoms
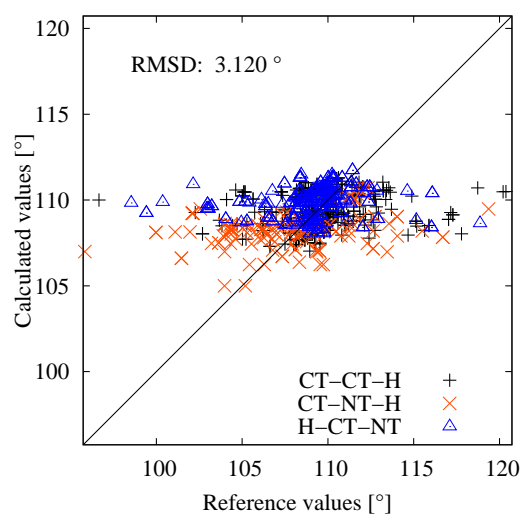
(e) Chunked parametrization:

Bends with hydrogen atoms
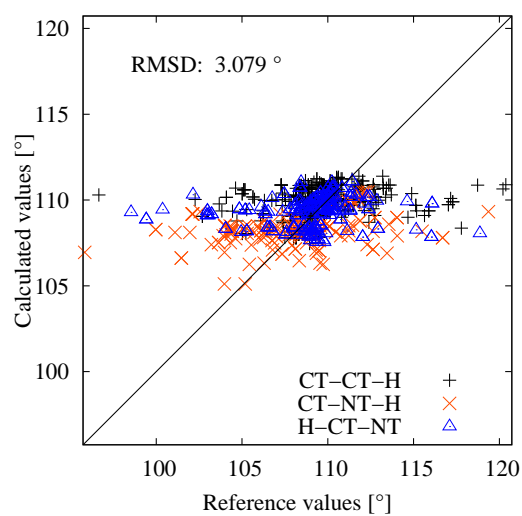
(f) Complete parametrization:

Bends with hydrogen atoms

Figure 4.3.2: Comparison between final geometries of chunked and complete parametrizations of a set of 17 transition metal complexes coordinated by cyclam-based ligands.

As can be seen from the plots, the resulting geometries from both parametrizations are practically the same. Since both parametrizations start from the original Momec force field, where all interactions involved in the parametrization already have highly optimized parameters, this test can certainly not be seen as proof that this method will always lead to acceptable results. However, taking this result as a proof of concept justifies the implementation of this method. Parametrizing variables, which are highly sensitive to changes and easily lead to convergence failures can be effectively treated with this method. The advantage of the chunked parametrization lies in the automatic process, since the user has to specify the course of the parametrization only once opposed to optimizing one parametrization after the other by hand.

3.2 Ligand Field Model Structure Parametrization

In order to test the functionality of the ligand field code in a parametrization, a set of highly symmetric model structures was used as reference data. The test structures consist of a Cu^{II} transition metal center (atom type CU2) coordinated to six nitrogen ligands (atom type NT) in an octahedral coordination geometry. One of the three NT-CU2-NT axes is elongated (CU2-NT distance: 2.5 Å) whereas the other two axes are left at a shorter value (CU2-NT distance: 2.0 Å) in order to mimic a tetragonal distortion.

During the test parametrization the following parametrization variables were used (the final values after the parametrization are tabulated), Table 4.3.4:

Table 4.3.4: Parametrization variables with final values for the test parametrization of the CU2-NT ligand field interaction of a highly symmetrical Cu^{II} transition metal complex surrounded by six nitrogen ligands.

interaction type	atom 1	atom 2	α [1/Å]	D [kJ/mol]	r_0 [Å]
Morse stretch	CU2	NT	0.544	561.228	2.115

interaction type	atom 1			r_{vdW} [Å]	ϵ
non-bonded	CU2			0.023	0.001
non-bonded	NT			2.221	0.079

interaction type	atom 1	atom 2	a_4 [cm^{-1}Å^4]	a_5 [cm^{-1}Å^5]	a_6 [cm^{-1}Å^6]
ligand field e_σ	CU2	NT	97754	108302	98562
ligand field e_{ds}	CU2	NT	27997	10736	24972

The parametrization used the simplex algorithm and weights were set for the six CU2-NT stretches and the NT-CU2-NT bend interactions. The weights were scaled to a value of 110 for the stretches and 5 for the bends during the parametrization. The parameters of fourth, fifth and sixth order for the σ-interaction and d-s-mixing of the original implementation of the ligand field potential were used (see Eq. 3.3.7) together with an additional Morse potential for the CU2-NT bond. Although the original ligand field potential allows for a total of seven variables per AOM parameter, only three variables were chosen at this point, because of a theoretically suggested $1/r^{-5}$ dependence for octahedral complexes [188,189] (see also Ch. 2 of this part).

Table 4.3.5 shows the comparison of the reference and calculated geometries:

Table 4.3.5: Comparison between reference geometry and calculated geometry which results from the final force field of the automatic parametrization shown in Table 4.3.4.

interaction type	atom 1	atom 2	atom 3	n_{ref} [Å or rad]	n_{calc} [Å or rad]
stretch (short)	CU2	NT		2.000	2.000
stretch (long)	CU2	NT		2.500	2.499
bend (90°)	NT	CU2	NT	1.571	1.571
bend (180°)	NT	CU2	NT	3.142	3.142

The structure is a perfect match to the reference structure. For this model compound, the automatic parametrization found a set of parameters which can model the distorted geometry.

The test was extended to a set of three structures with slightly different geometries. The long CU2-NT bond in the two additional structures was elongated or shortened, respectively, by 0.02 Å, so that the parametrization should be able to find a minimum which models all three structures with a median value of 2.50 Å for the long CU2-NT bond. Table 4.3.6 shows the resulting parametrization values and Table 4.3.7 the corresponding geometries.

Table 4.3.6: Parametrization variables with final values for the test parametrization of the CU2-NT ligand field interaction of three highly symmetrical Cu^{II} transition metal complexes surrounded by six nitrogen ligands.

interaction type	atom 1	atom 2	α [1/Å]	D [kJ/mol]	r_0 [Å]
Morse stretch	CU2	NT	0.537	566.599	2.166

interaction type	atom 1		r_{vdW} [Å]	ϵ
non-bonded	CU2		0.003	0.001
non-bonded	NT		2.228	0.064

interaction type	atom 1	atom 2	a_4 [cm^{-1}Å^4]	a_5 [cm^{-1}Å^5]	a_6 [cm^{-1}Å^6]
ligand field e_σ	CU2	NT	97714	105385	96677
ligand field e_{ds}	CU2	NT	31538	29653	12923

Table 4.3.7: Comparison between reference geometry and calculated geometry which results from the final force field of the automatic parametrization shown in Table 4.3.6. Only stretch interactions are shown, as the bend interactions were reproduced with exactly the same values as in the reference structure (see also Table 4.3.5).

interaction type	atom 1	atom 2	n_{ref} [Å or rad]	n_{calc} [Å or rad]
stretch (short) mol1	CU2	NT	2.000	2.000
stretch (long) mol1	CU2	NT	2.500	2.500
stretch (short) mol2	CU2	NT	2.000	2.000
stretch (long) mol2	CU2	NT	2.520	2.500
stretch (short) mol3	CU2	NT	2.000	2.000
stretch (long) mol3	CU2	NT	2.480	2.500

As can be seen from Table 4.3.7, the automatic parametrization again yielded a force field which reproduces the tetragonal distortion in this set of model compounds with a combined effect of a Morse stretch function and a ligand field interaction. We have taken this result as a proof of concept that an automatic parametrization of the ligand field interaction is feasible.

3.3 Ligand Field Single Molecule Parametrization

The insights on the parametrization gained during the experiments described in the preceding sections were used to parametrize a force field based on a "real" Cu^{II} crystal structure. The molecule $[Cu([9]aneN_3)_2]^{2+\,[228]}$ (refcode DUSJAC01, see Appendix B Fig. 6.3.2h) shows a Jahn-Teller distorted geometry with one long axis (CU2-NT distances: 2.296 and 2.345 Å) and two short axes (CU2-NT distances: 2.049 and 2.062 Å and 2.086 and 2.050 Å, respectively) and therefore has the same general coordination geometry as the model structures used in the preceding section.

In the first parametrization done with the geometry of this molecule as reference data, the same parametrization conditions as described in the preceding section, namely the original implementation of the ligand field potential with parameters for e_σ and e_{ds} of fourth, fifth and sixth order, an additional Morse stretch and the non-bonded interactions as parametrization variables, were used. The weights were also scaled with a factor of 110 for the stretches and 5 for the bends and were only set of the CU2-NT bonds and NT-CU2-NT bend interactions. Table 4.3.8 shows the final force field parameters when a simplex algorithm is used during the parametrization:

Table 4.3.8: Parametrization variables with final values for the test parametrization of the CU2-NT ligand field interaction of the DUSJAC01 reference structure (see Appendix B Fig. 6.3.2h).

interaction type	atom 1	atom 2	α [1/Å]	D [kJ/mol]	r_0 [Å]
Morse stretch	CU2	NT	0.695	557.265	2.205

interaction type	atom 1			r_{vdW} [Å]	ϵ
non-bonded	CU2			1.120	0.032
non-bonded	NT			2.086	0.041

interaction type	atom 1	atom 2	a_4 [cm^{-1}Å^4]	a_5 [cm^{-1}Å^5]	a_6 [cm^{-1}Å^6]
ligand field e_σ	CU2	NT	81587	113187	97858
ligand field e_{ds}	CU2	NT	82711	31748	40148

Comparing the final parameters to the ones obtained during the parametrization of the model structures, the overall range is quite similar. The resulting geometry produced by the force field is compared to the reference geometry in Figure 4.3.3.

(a) Stretch interactions

(b) Bend interactions
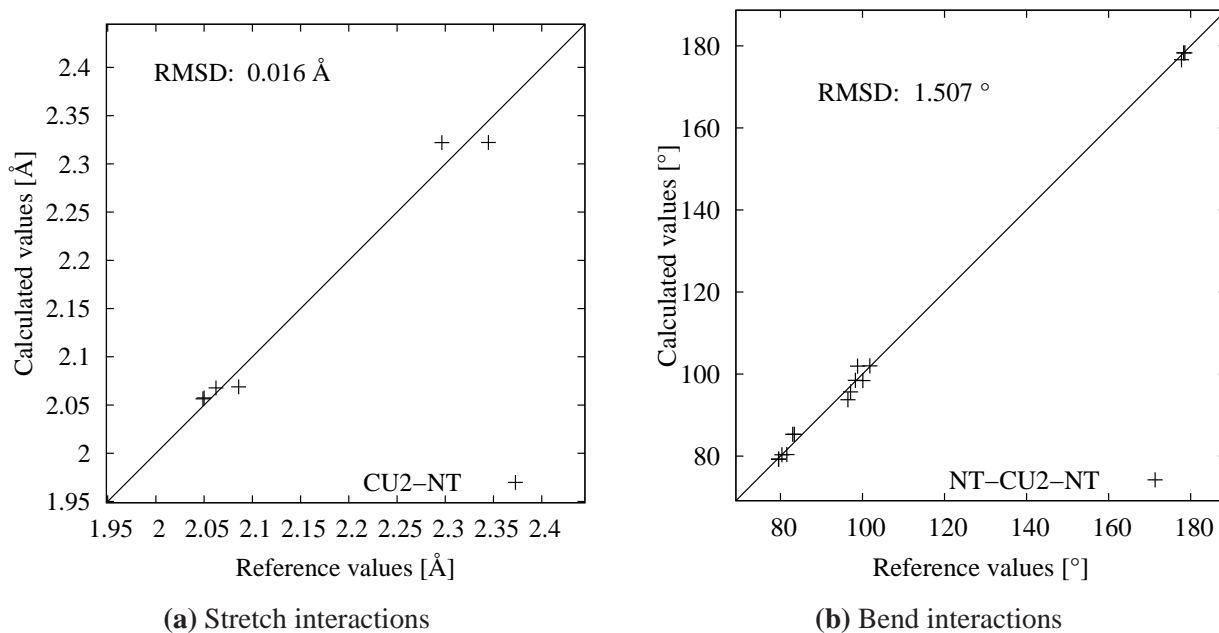
Figure 4.3.3: Calculated vs. reference data plots for the parametrization of DUSJAC01 with the original implementation of the ligand field potential.

As can be seen from the figures, the overall agreement with the reference structure is good and both short and long bonds are reproduced by the calculation within acceptable error.

As the parametrization only involved the ligand field parameters of fourth, fifth and sixth order, the parametrization was repeated and parameters a_2 to a_6 were allowed to vary for the automatic parametrizer in order to enhance the flexibility of the ligand field potential. The parametrization results and the comparison of the structural data to the reference geometry are shown in Table 4.3.9 and Figure 4.3.4, respectively.

Table 4.3.9: Parametrization variables with final values for the test parametrization of the CU2-NT ligand field interaction of the DUSJAC01 reference structure (see Appendix B Fig. 6.3.2h). The ligand field potential is expanded to include parameters a_{2-6}.

interaction type	atom 1	atom 2	α [1/Å]	D [kJ/mol]	r_0 [Å]
Morse stretch	CU2	NT	1.556	589.389	2.187

interaction type	atom 1			r_{vdW} [Å]	ϵ
non-bonded	CU2			0.049	0.000
non-bonded	NT			2.040	0.066

interaction type	atom 1	atom 2	a_2 [cm^{-1}Å^2]	a_3 [cm^{-1}Å^3]	a_4 [cm^{-1}Å^4]
ligand field e_σ	CU2	NT	91540	100641	100765
ligand field e_{ds}	CU2	NT	21896	18996	20670

interaction type	atom 1	atom 2		a_5 [cm^{-1}Å^5]	a_6 [cm^{-1}Å^6]
ligand field e_σ	CU2	NT		105382	93251
ligand field e_{ds}	CU2	NT		28659	27858
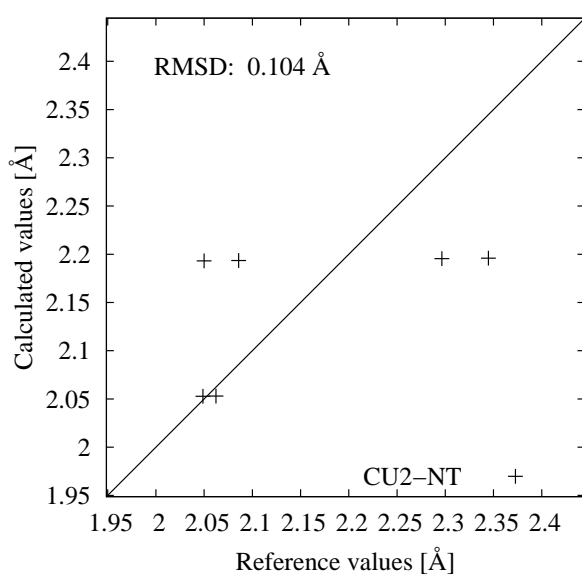
(a) Stretch interactions
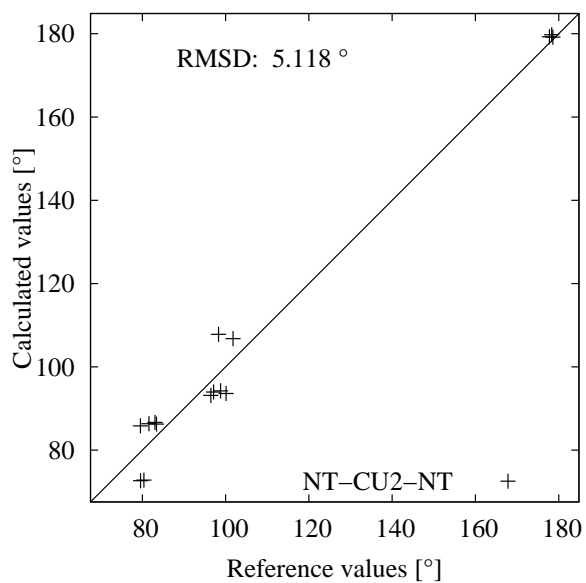
(b) Bend interactions

Figure 4.3.4: Calculated vs. reference data plots for the parametrization of DUSJAC01 with the original implementation of the ligand field potential with parametrization variables a_{2-6}.

Figure 4.3.4 shows that increasing the flexibility of the ligand field potential does not have a positive effect on the overall accuracy of the parametrization. In fact, the optimized structure calculated by the force field does not reproduce the crystal structure and the result is worse compared to the restricted version of the ligand field. Instead of an elongated geometry, the complex is modeled as a compressed

octahedral structure, showing four long and two short bonds. Expanding the flexibility leads to an over-parametrization of the problem and the two potentials, ligand field and Morse stretch, are no longer balanced in the resulting force field. This is a general problem of the form of the potential, as already discussed in Ch. 2 of this part.

In order to make the ligand field parametrization more robust, the original form of the potential was substituted by a Morse and "Gauss-like" descriptions (see Ch. 2 for details). As these potentials already have a minimum at an equilibrium bond length, the additional Morse stretch describing the classical steric interaction between the metal and the ligand is no longer needed and the total energy (steric + LFSE) can be described with just one potential. The parametrization described in the following paragraph therefore only included the ligand field variables in the parametrization and an additional Morse stretch was only added after the ligand field was already parametrized to verify, that all effects have been accurately described with the ligand field potential.

The parameters and resulting geometry information of the Morse (see Eq. 3.3.8) parametrization of the molecule are shown in Table 4.3.10 and Figure 4.3.5. The parametrization used the Monte Carlo routines to find a suitable set of starting parameters[2] for the ligand field terms (500 steps each). The weights were again set for CU2-NT stretches and NT-CU2-NT bends and were not scaled in this parametrization, therefore having the value of one in all cases.

Table 4.3.10: Parametrization variables with final values for the test parametrization of the CU2-NT ligand field interaction of the DUSJAC01 reference structure (see Appendix B Fig. 6.3.2h) with a Morse ligand field approach.

interaction type	atom 1	atom 2	α [1/Å]	D [cm^{-1}]	r_0 [Å]
1) ligand field e_σ (Morse description)	CU2	NT	13.368	6501	2.060
2) ligand field e_{ds} (Morse description)	CU2	NT	8.032	12902	2.314

interaction type	atom 1	atom 2	α [1/Å]	D [kJ/mol]	r_0 [Å]
3) Morse stretch	CU2	NT	1.078	76.543	2.446

---

[2] As the implementation of the Morse potential changed the functional form of the ligand field, the choice of starting parameters was difficult and therefore, the Monte Carlo routines were used in order to generate converging structures

(a) Stretch interactions

(b) Bend interactions
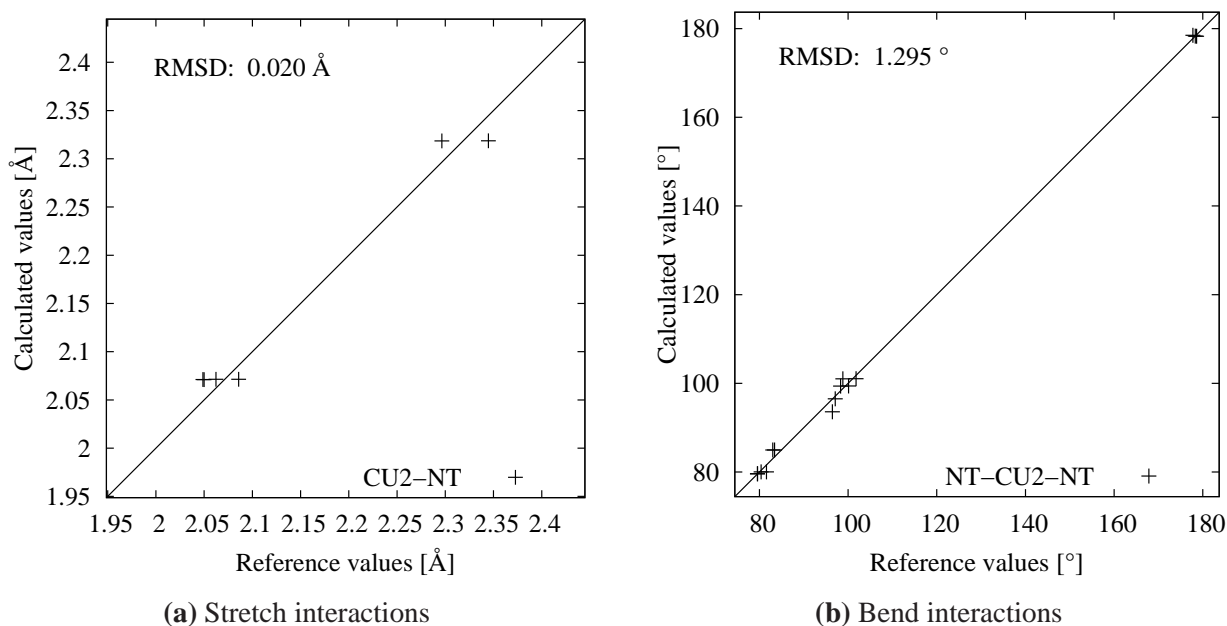
Figure 4.3.5: Calculated vs. reference data plots for the parametrization of DUSJAC01 with the Morse implementation of the ligand field potential.

As can be seen from Fig. 4.3.5, the accuracy of the parametrization is as good as with the original implementation of the ligand field potential when only parameters of fourth, fifth and sixth power (see Fig. 4.3.3) are used. The parametrization has been done in three steps, parametrizing only the e_σ interaction first, adding an e_{ds} term in the second step and adding an additional Morse stretch term in the third step. The RMSD values obtained after these individual parametrizations are 0.026 after e_σ, 0.022 after e_{ds} and 0.022 after the additional Morse stretch. The overall accuracy is therefore already good with a single Morse description of the ligand field e_σ interaction and does not improve much by adding terms for e_{ds} and the classical Morse stretch.

The same parametrization has been done with the "Gauss-like" implementation of the ligand field. Parametrization variables and resulting geometry information are shown in Table 4.3.11 and Figure 4.3.6:

Table 4.3.11: Parametrization variables with final values for the test parametrization of the CU2-NT ligand field interaction of the DUSJAC01 reference structure (see Appendix B Fig. 6.3.2h) with a "Gauss-like" ligand field approach.

interaction type	atom 1	atom 2	D [cm⁻¹]	a^a	b^a	c^a
1) ligand field e_σ ("Gauss-like" description)	CU2	NT	5923	1.092	1.967	2.154
2) ligand field e_{ds} ("Gauss-like" description)	CU2	NT	3633	4.524	2.080	2.893

interaction type	atom 1	atom 2		α [1/Å]	D [kJ/mol]	r_0 [Å]
3) Morse stretch	CU2	NT		0.297	34.815	2.162

[a] Please note, that no unit is given for parameters a, b and c, as the "Gauss-like" potential (Eq. 3.3.9) does not allow an easy deduction of the units of the individual parameters. As the AOM parameters represent an energy, D is assumed to have the unit cm^{-1} whereas the remaining variables including r are treated as unitless.

(a) Stretch interactions

(b) Bend interactions
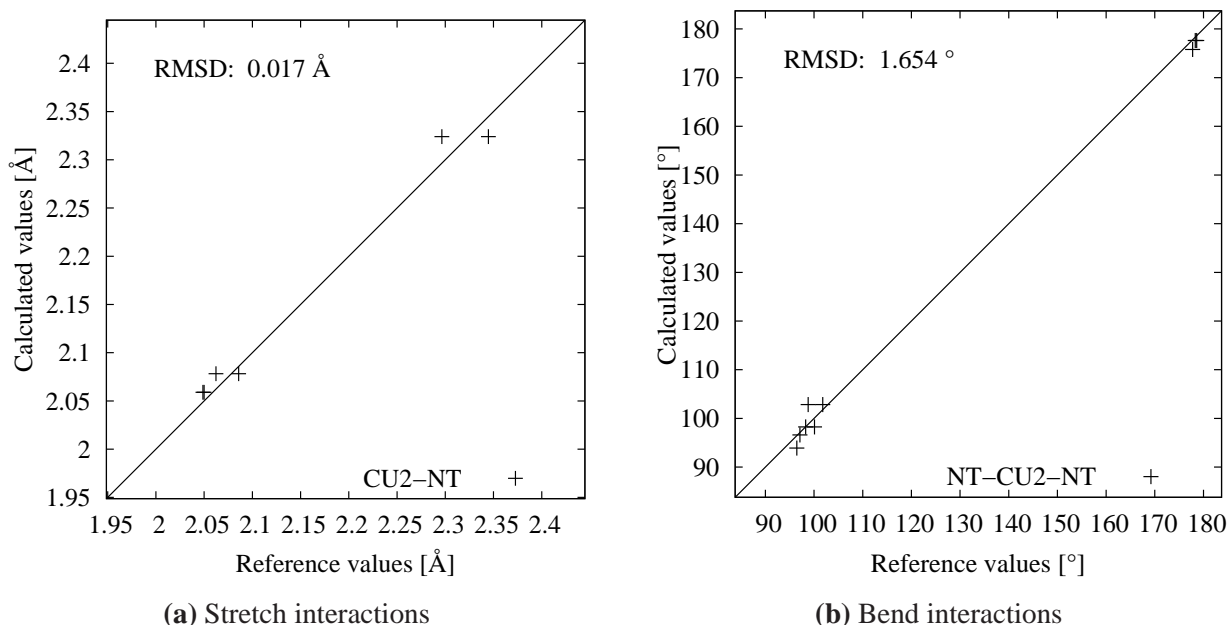
Figure 4.3.6: Calculated vs. reference data plots for the parametrization of DUSJAC01 with the "Gauss-like" implementation of the ligand field potential.

As with the Morse description of the ligand field potential, the reference structure is reproduced within acceptable error. The "Gauss-like" description is also a bit more flexible, as the short bonds do not all have the same bond length (see Fig. 4.3.5), but the small differences in bond length are also reproduced with the "Gauss-like" form of the potential. Again, the parametrization involved a three step procedure with a preceding Monte Carlo simulation for the ligand field parameters. The RMSD

values found after each individual step were 0.0285 after the parametrization of e_σ, 0.026 after e_{ds} and 0.026 after the additional Morse stretch.

Parametrization of a single reference molecule with all three descriptions of the ligand field potential implemented so far show that the original implementation by Deeth et al. can only give accurate results if both ligand field potential and an additional Morse stretch are precisely balanced. As soon as this balance is no longer given or the system has too many degrees of freedom, the description of the distorted coordination geometry breaks down. On the contrary, the ligand field description with a Morse or a "Gauss-like" potential has the advantage of a defined minimum on the parameter surface, which makes automatic parametrization easier and does not need an additional term for balance. This is a significant advantage during the automatic parametrization procedure and therefore, these approaches have been used during the parametrizations of larger reference data sets shown below.

3.3.1 Ligand Field Single Molecule Parametrization with UV/VIS Data

As discussed in greater detail in Ch. 2 of Pt. III, the eigenvalues of the symmetrical 5×5 ligand field matrix correspond to the d-orbital energy levels. While a routine, which derives the point group of the molecule and the corresponding splitting of the d-orbitals into terms is still missing in the current implementation of the ligand field code, the splitting in a simple Cu^{II} case is analogous to the levels of the d-orbitals and thus, the energies can be compared to experimental findings. Therefore, a parametrization with geometry and UV/VIS reference data of a single transition metal complex has been done.

The molecule $[Cu(dien)_2]^{2+}$ [229] (refcode ETACUB, see Appendix B Fig. 6.3.2i) shows a Jahn-Teller distorted geometry and four transitions to the singly occupied $d_{x^2-y^2}$ orbital [230] (see Table 4.3.13). The parametrization was carried out with the original implementation of the ligand field potential with variables a_{4-6} for the e_σ and e_{ds} parameters, an additional Morse stretch term and the non-bonding parameters for CU2 and NT. In addition to the weights set for the stretches and bends which involve the transition metal atom, weights were also set for the UV/VIS transitions. The weights were scaled internally to a ratio of 115 (stretches) to 5 (bends) to 10^{-7} (transitions) during the parametrization to account for the different scales of the data.

Tables 4.3.12 and 4.3.13 and Figure 4.3.7 show the results of the parametrization.

Table 4.3.12: Parametrization variables with final values for the test parametrization of the CU2-NT ligand field interaction of the ETACUB reference structure (see Appendix B Fig. 6.3.2i) with the original implementation of the ligand field term and geometry plus UV/VIS data[230] for reference.

interaction type	atom 1	atom 2	α [1/Å]	D [kJ/mol]	r_0 [Å]
Morse stretch	CU2	NT	0.572	548.586	2.027

interaction type	atom 1			r_{vdW} [Å]	ϵ
non-bonded	CU2			1.125	0.062
non-bonded	NT			2.215	0.063

interaction type	atom 1	atom 2	a_4 [cm^{-1}Å^4]	a_5 [cm^{-1}Å^5]	a_6 [cm^{-1}Å^6]
ligand field e_σ	CU2	NT	29289	76228	88560
ligand field e_{ds}	CU2	NT	100264	44297	45717

(a) Stretch interactions

(b) Bend interactions

(c) UV/VIS transitions
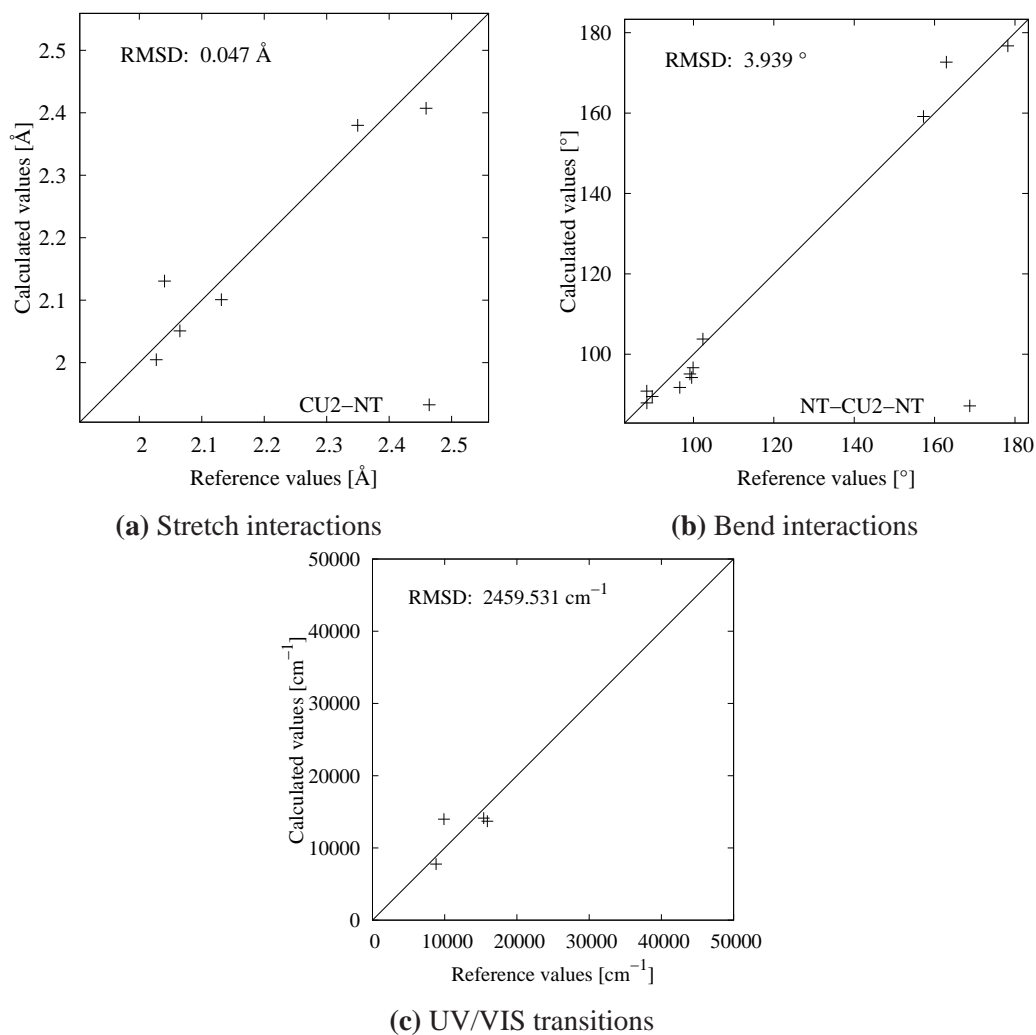
Figure 4.3.7: Calculated vs. reference data plots for the parametrization of ETACUB with the original implementation of the ligand field potential with geometry and UV/VIS as reference data.

Table 4.3.13: Comparison between reference and calculated bond lengths and UV/VIS transitions for the parametrization of ETACUB.

| bond	r_{ref} [Å]	r_{calc} [Å]	from	to	n_{ref} [cm^{-1}]	n_{calc} [cm^{-1}]
Cu–N1	2.350	2.380	d_{z^2}	$d_{x^2-y^2}$	8800	7763
Cu–N2	2.040	2.131	d_{xy}	$d_{x^2-y^2}$	9900	13977
Cu–N3	2.459	2.407	d_{xz}	$d_{x^2-y^2}$	15400	14121
Cu–N4	2.131	2.101	d_{yz}	$d_{x^2-y^2}$	15900	13694
Cu–N5	2.027	2.005				
Cu–N6	2.065	2.051				

While the Morse stretch and non-bonded parameters do not change much when including UV/VIS data compared to previous parametrizations (see Table 4.3.8), the ligand field parameters show a large variation. The overall accuracy concerning the geometry is worse compared to the parametrization of DUSJAC01 (Fig. 4.3.3), but both calculated geometry and UV/VIS transitions show a definite trend towards the reference data. Subsequent tests with larger reference data sets including UV/VIS data not shown here did not give acceptable results concerning the modelling of the geometry and the calculation of the d-d-transitions. To model both properties of the molecule accurately at the same time, the form of the ligand field potential would have to be extended and/or, two sets of parameters would be needed, one describing the geometry and one modeling the UV/VIS transitions. Both sets should be independent from each other, i. e. the parameter set for the geometry should not influence the calculation of the d-d-transitions and vice versa. This can be achieved when different force fields are used for the geometry optimization and a subsequent single point to calculate the d-d-transitions. Further attempts to correctly predict the d-orbital transitions, also including systems with different transition metals than Cu^{II}, will be carried out in the future.

3.4 Ligand Field Parametrization of Multiple Molecules

The set of Cu^{II} complexes used by Deeth et al. in the first LFMM publication[9] was used as a larger training set for the automatic parametrization. The set includes 13 tetra-, penta- and hexacoordinate complexes, where the Cu^{II} transition metal ion is coordinated by aliphatic nitrogen donor ligands (for detailed structures see Appendix B). As a tetragonal distortion of the molecule is only seen in the penta- and hexacoordinate cases of the training set, the parametrization is a good test case for the automatic algorithms, since both distorted and non-distorted geometries have to be reproduced by a single set of ligand field parameters.

The initial parametrization was carried out with the original implementation of the ligand field potential. However, even with 1000 Monte Carlo steps and a subsequent simplex optimization, a suitable set

of parameters describing all 13 structures with acceptable accuracy could not be found. The RMSD values of the original publication by Deeth[9] are therefore used as a reference for the original form of the ligand field potential. Deeth used a linear approximation for the σ interaction of the ligand field. The structures were optimized to an RMSD of 0.071 Å for the bond stretches and 3.041° for the valence angles. The results of our own parametrizations which involve the Morse and "Gauss-like" description of the ligand field potential are shown in this Section.

Table 4.3.14 shows the final force field parameters of the parametrization with a Morse description of the ligand field potential and Figure 4.3.8 shows the corresponding plots for the CU2-NT stretches and NT-CU2-NT bends.

Table 4.3.14: Parametrization variables with final values for the test parametrization of the CU2-NT ligand field interaction of a set of 13 reference structures (see Appendix B Figs. 6.3.2a to 6.3.2m) with a Morse ligand field approach.

interaction type	atom 1	atom 2	α [1/Å]	D [cm^{-1}]	r_0 [Å]
1) ligand field e_σ (Morse description)	CU2	NT	7.796	8413	2.037
2) ligand field e_{ds} (Morse description)	CU2	NT	7.072	38909	3.845

interaction type	atom 1	atom 2	α [1/Å]	D [kJ/mol]	r_0 [Å]
3) Morse stretch	CU2	NT	0.023	5.177	2.450

(a) Stretch interactions

(b) Bend interactions
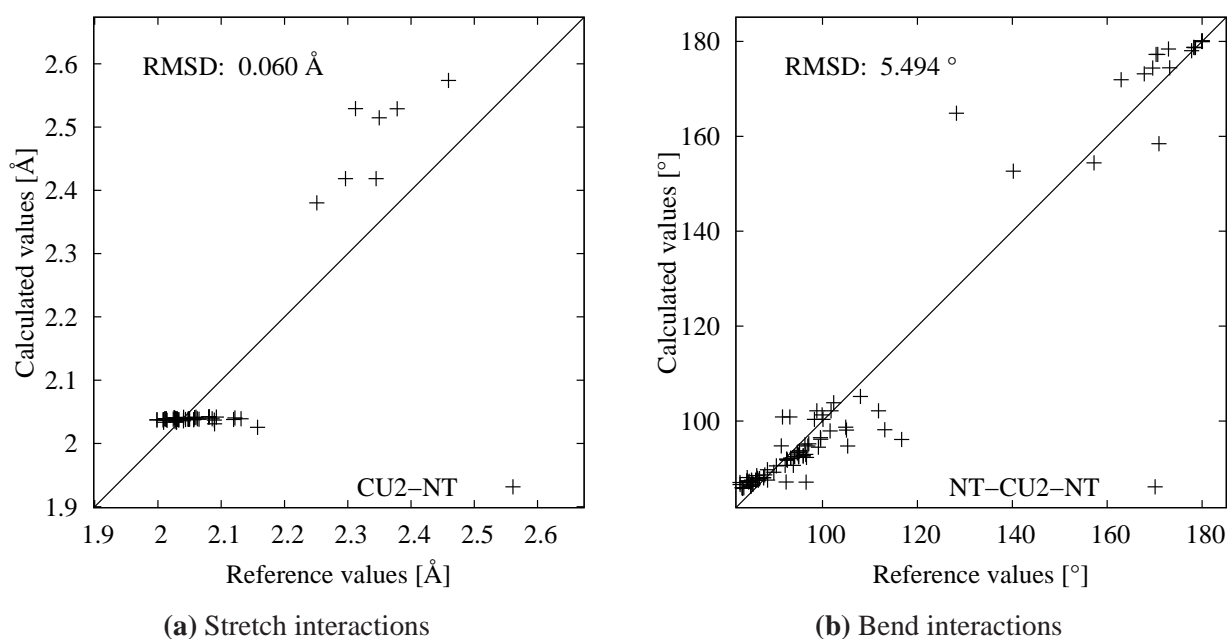
Figure 4.3.8: Calculated vs. reference data plots for the parametrization of a set of 13 reference structures with a CU2-NT ligand field interaction described by a Morse potential.

As can be seen in the plots, the overall agreement of the calculated structure with experimental findings is acceptable. The trend of the Morse potential giving one set of short bonds and a number of different long bonds, which was already shown during the discussion of the parametrization of a single molecule (see Fig. 4.3.5), is confirmed in the parametrization of the larger set. Describing the ligand field interaction with a Morse potential does not lead to the needed flexibility near the equilibrium bond length and therefore, all short bonds are described with a single calculated bond length. With larger bond lengths the stiffness of the potential decreases and allows for an increased flexibility in the calculated bond lengths.

Table 4.3.15 shows the final values of the parametrization with the same set of compounds and the "Gauss-like" description of the ligand field potential. The comparison between calculated and reference data is given in Fig. 4.3.9.

Table 4.3.15: Parametrization variables with final values for the test parametrization of the CU2-NT ligand field interaction of a set of 13 reference structures (see Appendix B Figs. 6.3.2a to 6.3.2m) with a "Gauss-like" ligand field approach.

interaction type	atom 1	atom 2	D [cm^{-1}]	a	b	c
1) ligand field e_σ ("Gauss-like" description)	CU2	NT	35308	8.975	1.568	2.692
2) ligand field e_{ds} ("Gauss-like" description)	CU2	NT	-5231	9.276	1.520	0.245

interaction type	atom 1	atom 2		α [1/Å]	D [kJ/mol]	r_0 [Å]
3) Morse stretch	CU2	NT		0.887	23.696	1.971

(a) Stretch interactions

(b) Bend interactions
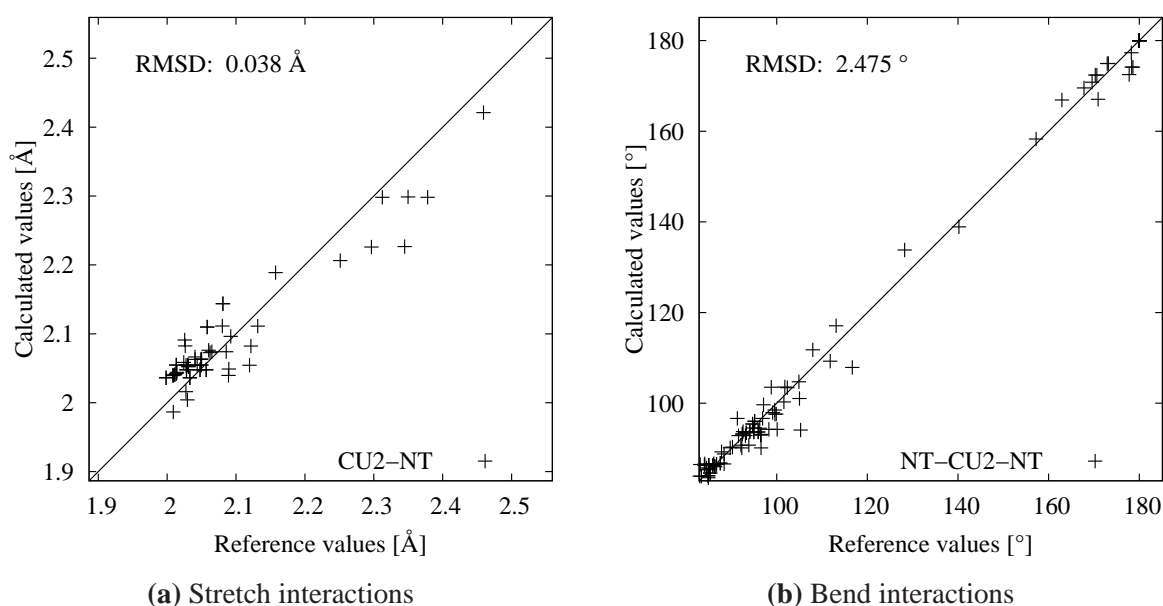
Figure 4.3.9: Calculated vs. reference data plots for the parametrization of a set of 13 reference structures with a CU2-NT ligand field interaction described by a "Gauss-like" potential.

As the figures show, the "Gauss-like" description of the ligand field potential increases the overall accuracy compared to the experimental structures. Both stretches and bends are described more accurately and the increased flexibility of the "Gauss-like" potential can clearly be seen in Fig. 4.3.9a. Compared to the results of the parametrization which involves a Morse description of the ligand field (see Fig. 4.3.8a), the shorter bonds are no longer described by a single calculated bond length, but the distribution is broader and more accurate compared to experimental findings. Also, the overall convergence rate of the potential is faster and fewer Monte Carlo steps are needed to find a suitable set of parameters.

With the force field given in Table 4.3.15, a series of leave-one-out tests was carried out. Although the parametrization data set is diverse and small, we present these tests as a proof of concept for future parametrizations which involve ligand field interactions.

Before carrying out the actual leave-one-out tests, the force field was once again relaxed. Starting from the parameters given in Table 4.3.15, all variables were included in a simplex parametrizations at the same time. The parametrization converged to a slightly better force field, which will not be shown here in detail. This force field was then used as a starting point for the leave-one-out tests.

Table 4.3.16 shows the results of the tests.

Table 4.3.16: RMSD values of stretches and bends of the individual leave-one-out test molecules of a set of 13 Cu^{II} transition metal complexes. RMSD values of the full force field are given in parentheses.

compound left out	RMSD$_{stretches}$ [Å]	ΔRMSD$_{stretches}$ [Å]	RMSD$_{bends}$ [°]	ΔRMSD$_{bends}$ [°]
CEDHAU	0.032 (0.032)	0.000	1.750 (1.734)	0.016
CEFBEU	0.060 (0.042)	0.018	0.905 (0.566)	0.339
CHXCUA	0.037 (0.037)	0.000	0.617 (0.624)	-0.007
CMENOX	0.023 (0.026)	-0.003	0.274 (0.226)	0.048
CUENCL	0.051 (0.045)	0.006	2.862 (2.924)	-0.062
DAPRCU	0.018 (0.018)	-0.000	0.142 (0.149)	-0.007
DMEDCU	0.020 (0.030)	-0.010	6.434 (0.510)	**5.924**
DUSJAC01	0.174 (0.049)	**0.125**	3.840 (3.141)	0.699
ETACUB	0.025 (0.024)	0.001	1.969 (1.957)	0.012
ETEACU	0.030 (0.030)	0.000	1.027 (1.015)	0.012
JIBZUP	0.036 (0.035)	0.001	3.811 (3.819)	-0.008
LATSII	0.040 (0.038)	0.002	1.907 (1.905)	0.002
TENCUB	0.030 (0.035)	-0.005	4.824 (4.185)	0.639

The table shows the RMSD values of stretches and bends, respectively, of a single molecule each,

which was not included in the parametrization. Given in parentheses are the RMSD values of the same molecule from the complete force field, where all molecules were used as reference data. With two exceptions, leaving one molecule out of the training set does not lead to drastic effects on the RMSD value and therefore, the robustness and consistency of the resulting force field is retained. The two exceptions, DMEDCU and DUSJAC01, have been examined in detail. Looking at the geometry optimized structure of DMEDCU after the parametrization without the X-ray structure of the molecule shows a distortion of the five-membered ring involving the CU2-NT-CT-CT-NT moiety (see Fig. 6.3.2h). The ring is no longer planar in the calculated structure and therefore, the angles around the Cu^{II} transition metal center are distorted, which explains the large deviation compared to the full force field. The other exception, DUSJAC01 (see Fig. 6.3.2h), represents a highly symmetric complex. Looking at the individual bond lengths of the geometry optimized molecule shows a tetragonal elongation, but the axes are perturbed compared to the result of the full force field. In the crystal structure, the long axis is along the N2-Cu-N7 bond whereas in the calculated structure the long axis is found along the N4-Cu-N6 bond. If the axes are reordered to match the crystal structure, a RMSD value of 0.054 is obtained, which gives a change in RMSD compared to the full force field of 0.005. This value is in line with the remaining values. Omitting the structure of DUSJAC01 seems to remove the information of the position of the elongated axis and therefore, the geometry optimized structure does no longer retain the order of the axes.

Summarizing the results of the parametrization of the ligand field potential, the "Gauss-like" description represents the best approach for an automatic parametrization of the interaction we have found so far. The Morse potential gives similar results, but is less flexible concerning especially the modeling of the short bonds in a complex. The original implementation of the ligand field potential gives rise to convergence problems, since it always has to be correctly balanced with an additional Morse potential. Also, it does not show a defined minimum on the parameter surface. Two potentials working in different directions at the same time represent a difficult problem for the parametrization algorithms.

Part V

Outlook

1 Parametrizations based on DFT-Optimized Structures

The parametrizations shown in the preceding Part of this thesis are all based on X-ray structure reference data. Therefore, the resulting force field will yield optimized structures which are comparable to X-ray geometries. However, as the aim of this project was to identify a method which can predict exchange coupling constants between transition metal centers in a fast and reliable way, an X-ray structure geometry may not be the desired starting structure. As already discussed in detail in Pt. II Ch. 4, the X-ray structure of a molecule is not necessarily at a minimum on the PES of a DFT method. Therefore, from the point of view of a theoretical chemist, the exchange coupling constant should be calculated from the DFT-optimized structure[1].

In order to transfer this approach to the MM-optimization of molecules, the force field parametrization can be based on DFT- optimized structures. The parametrization process thus involves an additional step, namely the geometry optimization of the structures of the reference data set by DFT, prior to the actual force field parametrization. As the exchange coupling constants are calculated by B3LYP and a combination of TZVP and 6-31G* basis, the geometry optimization should also be based on this combination of method and basis set to assure the compatibility of the PES of the two calculations.

First tests towards a DFT-based force field were carried out with a set of Cu^{II} transition metal complexes[2]. The structures were optimized with the B3LYP functional together with the SVP or TZVP basis sets. However, with a set of 33 different Cu^{II} complexes, neither of the functional/basis set combinations gave acceptable results. While some of the calculations did not lead to a minimum structure, others showed large discrepancies to the X-ray structure. Identifying a method which yields consistent results for a large set of different transition metal complexes, was not possible in the course of this work.

However, as a proof of concept, a set of three Cu^{II} structures geometry optimized with B3LYP/SVP has been identified and used in a ligand field parametrization. The molecules CUENCL, DUSJAC01 and ETACUB (see Appendix B, Figs. 6.3.2e, 6.3.2h and 6.3.2i) all show a tetragonally distorted Cu^{II} center surrounded by six aliphatic nitrogen donors and have already been used in the parametrization

---

[1] The X-ray structure however contains the distortions induced by crystal lattices, which are not reproduced by the DFT geometry optimization. It is therefore a matter of error estimation to decide whether the X-ray structure or the DFT-optimized structure should be used for the calculation of exchange coupling constants.

[2] The DFT optimizations were done together with Mariam Veschgini during her research internship.

117

based on X-ray structures in Pt. IV Ch. 3. The force field parameters after the parametrization are shown in Table 5.1.1.

Table 5.1.1: Parametrization variables with final values for the parametrization of the CU2-NT ligand field interaction of a set of three DFT-optimized reference structures (CUENCL, DUSJAC01, ETACUB, see Appendix B Figs. 6.3.2e, 6.3.2h and 6.3.2i) with a "Gauss-like" ligand field approach.

interaction type	atom 1	atom 2	D [cm^{-1}]	a	b	c
ligand field e_σ ("Gauss-like" description)	CU2	NT	2658	4.651	2.182	1.684

The resulting force field was then used to optimize the geometry of the complex JIBZUP (see Appendix B, Fig. 6.3.2k), which has a Cu^{II} center coordinated by five aliphatic nitrogen donors with a tetragonal distortion. The geometry was also optimized by DFT and both structures are shown in Fig. 5.1.1 in an overlay plot:
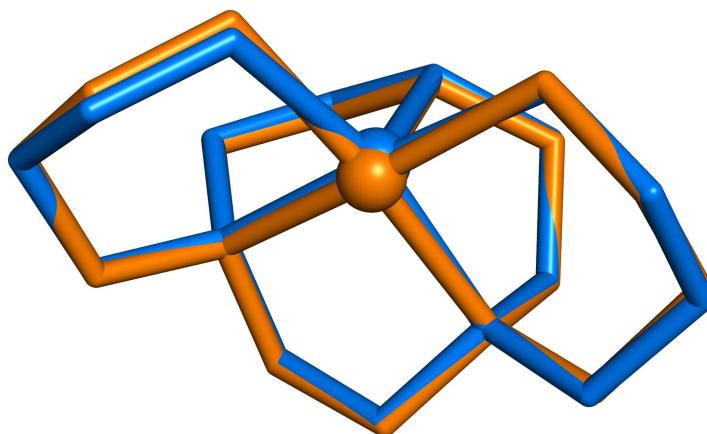
Figure 5.1.1: Overlay of DFT optimized (blue) and MM optimized (orange) structures of JIBZUP (see Appendix B, Fig. 6.3.2k for details). Hydrogen atoms are omitted for clarity.

The copper-nitrogen bond lengths for the X-ray structure, DFT-optimized structure, MM-optimized structure with ligand field and MM-optimized structure without the ligand field are given in Table 5.1.2:

Table 5.1.2: Copper-nitrogen bond lengths of JIBZUP (see Appendix B, Fig. 6.3.2k for details) calculated with DFT or MM optimizations in comparison to the X-ray structure.

structure	r_{Cu-N1} [Å]	r_{Cu-N2} [Å]	r_{Cu-N3} [Å]	r_{Cu-N4} [Å]	r_{Cu-N5} [Å]
X-ray	2.060	2.080	2.251	2.025	2.027
DFT-optimized	2.144	2.147	2.269	2.113	2.102
MM-optimized (LF)	2.137	2.142	2.356	2.137	2.131
MM-optimized (no LF)	2.164	2.205	2.202	2.271	2.016

As can be seen from the table, the DFT-optimized structure shows an elongation in the short Cu^{II}-N bond lengths whereas the long Cu^{II}-N bond has virtually the same length in both structures. The MM-optimized structure including the ligand field term (see Table 5.1.1) accurately resembles the DFT-optimized structure. Turning off the ligand field term and optimizing the structure only with the terms of the original force field, but no explicit Cu^{II}-N stretch term, yields a structure which does not resemble the DFT-optimized structure. The ligand field term therefore has an important effect for the correct description of the molecule in this particular case. Given the right parametrization based on DFT-optimized structures, a MM geometry optimization therefore can be used to accurately predict DFT geometries with small computational effort.

2 The "Maximum Force Field" Approach: Jacobian and Hessian Matrix Information as Reference Data

During the parametrizations of the ligand field term, one of the major problems encountered has been the overall convergence of the ligand field parameters, or, when the original implementation of the ligand field potential was used, the correct balancing of ligand field and classical stretch term. Many of these convergence problems were found to be caused by non-converging geometry optimizations due to non-matching parameters. As already discussed in Pt. IV Ch. 2, the parametrization algorithm is not aware of Momec geometry convergence problems. Although modifications to the algorithm, e.g. the additions to the simplex algorithm showed in Pt. IV Ch. 2, introduced a certain level of awareness for convergence problems, the fundamental problem of the additional complexity of the geometry optimization remains the same. Therefore, we have tested a method involving the use of the Jacobian and Hessian matrices, which uses only single point calculations.

Looking at the information present in the Jacobian matrix first, one can use the fact that the first derivatives of the energy with respect to the atomic coordinates have to be zero at a minimum structure. Therefore, the reference Jacobian matrix is zero for every matrix element. The single point calculations done with varying parameters will also only give zero for all matrix elements, if a minimum structure is found. This represents a valuable information, but cannot be used as the only reference date during the parametrization, since setting the force constant of an interaction to zero would automatically induce Jacobian matrix elements with a value of zero.

The second derivatives of the energy with respect to the atomic coordinates, the Hessian matrix, contains information about the force constants of individual interactions, e.g. stretches, bends and torsions. Those can be estimated by QC methods (see Pt. IV Ch. 1 for details), but this would involve another time-consuming calculation. However, the structure of a reference molecule can also be expressed with an overdetermined maximum force field. Given a hypothetical three-atomic molecule *A-B-A'*, the connectivity can be described using two bond lengths r_{A-B} and $r_{B-A'}$ and an additional bend interaction $a_{A-B-A'}$. The equilibrium values for the harmonic potentials are set to the exact values from the crystal structure and the force constants are estimated from literature known values. The Hessian matrix deduced from this information is then used as a reference for the succeeding parametrization.

The combination of Jacobian and Hessian reference matrix elements now represents the full set of reference data. If multiple molecules should be included in the parametrization, an additional set of Jacobian and Hessian matrix in the maximum force field scheme just described is added to the reference data set.

The actual parametrization is then started with a reduced number of parameters, e. g. in the example presented above, the bonds *A-B* and *B-A'* would both be represented by a single stretch interaction STR(A-B). Both equilibrium bond lengths and force constants are therefore included in the parametrization and will relax to a median value, which gives a Jacobian and Hessian closest to the reference matrices. The parametrization in this simple case would therefore be a parameter reduction from a set of three interactions (two stretches, one bend) in the maximum force field to a set of two interactions (one stretch, one bend) in the parametrized force field.

Extending this scheme to the ligand field approach opens up another aspect, i. e. parameter substitution. Assuming an octahedral nitrogen-coordinated Cu^{II} compound with tetragonal distortion, each individual Cu-N bond length will be described by a different set of parameters in the maximum force field and thus, the tetragonally elongated geometry of the reference molecule will be retained in the optimized strcuture. In the parametrization, the individual Cu-N parameters will be replaced with a single ligand field parameter and, if needed, an additional stretch parameter, thus reducing a set of six interactions to a set of one or two interactions and also substituting a classical harmonic description by a ligand field term. Since all information about the molecule is given by the Jacobian and Hessian matrices, we are confident, that this approach can be used for an initial estimation of ligand field parameters. The parameters are then used as starting values for a second parametrization, which uses the geometry optimization as described in earlier Chapters of this thesis, in order to further refine the force field.

3 Future Developments

The combination of the ligand field parametrization shown in Pt. IV, reference data based on DFT-optimized structures discussed in Ch. 1 of this Part and the calculation of exchange coupling constants with DFT single points shown in Pt. II creates the possibility of a virtual screening of transition metal compounds, which are potential candidates for single molecule magnets (SMMs). Although a successful parametrization of oligonuclear compounds, e. g. from the test-set used in Pt. II, has not been completed, the results shown in the preceding Chapters of this work suggest that such a parametrization is possible with the tools developed here. Apart from the convergence problems and possible approaches to solve the problem, which were already discussed in Ch. 2 of this Part, a major point for the improvement of the parametrization process is the functional form of the ligand field potential. The "Gauss-like" approach shown in Pt. III Ch. 3 yields promising results, but further improvements to the functional form will have to be made in order to correctly describe not only the geometry but also the electronic transitions of a transition metal complex with molecular mechanics methods. The new functional form has to be tested with different transition metals as well, since the Cu^{II} ion represents the simplest possible case of an one electron system. Also, the parametrizations shown in this work are entirely based on compounds where no π-bonding effect is found between the d-orbitals of the metal and the ligand orbitals. The automatic parametrization may therefore break down when more than one sets of ligand field parameters is used at the same time. If that is the case, the number of parameters which describe the functional form of the ligand field effect may have to be reduced.

As discussed before, support for different electronic states and their corresponding terms has to be implemented in order to be able to treat the full range of transition metal ions. Also, the treatment of intermediate spin systems (Fe^{III}, Fe^{II}), is not fully supported yet but can be quickly implemented, e. g. with an additional flag in the parametrization command file.

To further improve the overall performance of the parametrizations shown in this thesis, the implementation of the ligand field code will be revised and improved using modern C++ libraries. The parametrization algorithms and the Perl scripting environment will be integrated into the main Momec program and rewritten in C++, in order to support massively parallel computation and further automation. This will help to generate new force fields in a more robust and also faster way and will make the parametrization in Momec an easy to use tool for the everyday chemist.

Part VI

Appendices

1 List of Abbreviations

5Z quintuple zeta

[9]aneN$_3$ 1,4,7-triazacyclononane

[14]aneN$_4$ 1,4,8,11-tetraazacyclotetradecane

adt *N,N*-bis(2-aminoethyl)diethylenetriamine

AO atomic orbital

AOM angular overlap model

apt 1,4-bis(3-aminopropyl)-1,4,7-triazacyclononane

bipym 2,2'-bipyrimidine

CASSCF complete active space SCF

CD circular dichroism

CFT crystal field theory

CGTO contracted Gaussian type orbital

chn 1,3-diaminocyclohexane

CI configuration interaction

cit citrate

cyclam 1,4,8,11-tetraazacyclotetradecane

DFT density functional theory

deen *N,N*-diethylethylenediamine

diammac 6,13-dimethyl-1,4,8,11-tetraazacyclotetradecane-6,13-diamine

dien diethylenetriamine

dmed   (dimethylamino)ethylamine

DTNE   1,2-bis(1,4,7-triazacyclonon-1-yl)ethane

DZ   double zeta

ECP   effective core potential

en   ethylenediamine

EPR   electron paramagnetic resonance

ESR   Elektronenspinresonanz

Et$_5$dien   1,1,4,7,7-pentaethyldiethylenetriamine

G03   Gaussian 03

G09   Gaussian 09

GGA   generalized gradient approximation

GTO   Gaussian type orbital

GUI   graphical user interface

Hacac   2,4-pentanedione

H$_2$Dopn   3,9-dimethyl-4,8-diazaundeca-3,8-diene-2,10-dione dioxime

H$_3$BBAC   N,N-bis(2-hydroxybenzyl)aminoacetic acid

H$_3$sabhea   N-salicyclidene-2-(bis(2-hydroxyethyl)amino)ethylamine

HF   Hartree-Fock

KS   Kohn-Sham

LDA   local density approximation

LFMM   ligand field molecular mechanics

LFSE   ligand field stabilization energy

LFT   ligand field theory

maltolato   3-oxy-2-methyl-4H-pyran-4-onato-O^3,O^4

MCD   magnetic circular dichroism

med	*N*-methylethylenediamine
Me₃tacn	N,N',N''-trimethyl-1,4,7-triazacyclononane
MM	molecular mechanics
MO	molecular orbital
MOE	Molecular Operating Environment
nen	*N*-ethylethylenediamine
OAc	acetate
oxpn	N,N'-bis(3-aminopropyl)oxamide
papd	2,5,8,11,14-pentaazapentadecane
PES	potential energy surface
PGTO	primitive Gaussian type orbital
pz	pyrazolyl
QC	quantum chemistry
QZ	quadruple zeta
RMSD	root mean square deviation
SCF	self-consistent field
SMM	single molecule magnet
STO	Slater type orbital
SVL	Scientific Vector Language
tcn	1,4,7-triazacyclononane
tetren	tetraethylenepentamine
tmpa	tris(2-pyridylmethyl)amine
tn	1,3-diaminopropane
tpen	N,N,N',N'-tetrakis(2-pyridylmethyl)ethylenediamine
TP⁻	hydrotris(pyrazolyl)borate

TPP   tetraphenylphosphonium

tren   tris(2-aminoethyl)amine

TZ   triple zeta

ZFS   zero-field splitting

2 Appendix A - List of Transition Metal Complexes used for the Calculation of Exchange Coupling Constants

2.1 Polynuclear

(a) [HO-Cr(cyclam)-NC-Cr(CN)$_5$]$^-$
(TPP$^+$ counterion)

(b) [HO-Cr(cyclam)-NC-Cr(CN)$_5$]$^-$
(Na$^+$ counterion)

(c) *trans*-Cr[MnL^1]$_2$Cl

(d) *trans*-Fe[MnL^1]$_2$Cl

(e) *trans*-Fe[MnL^1]$_2$PF$_6$
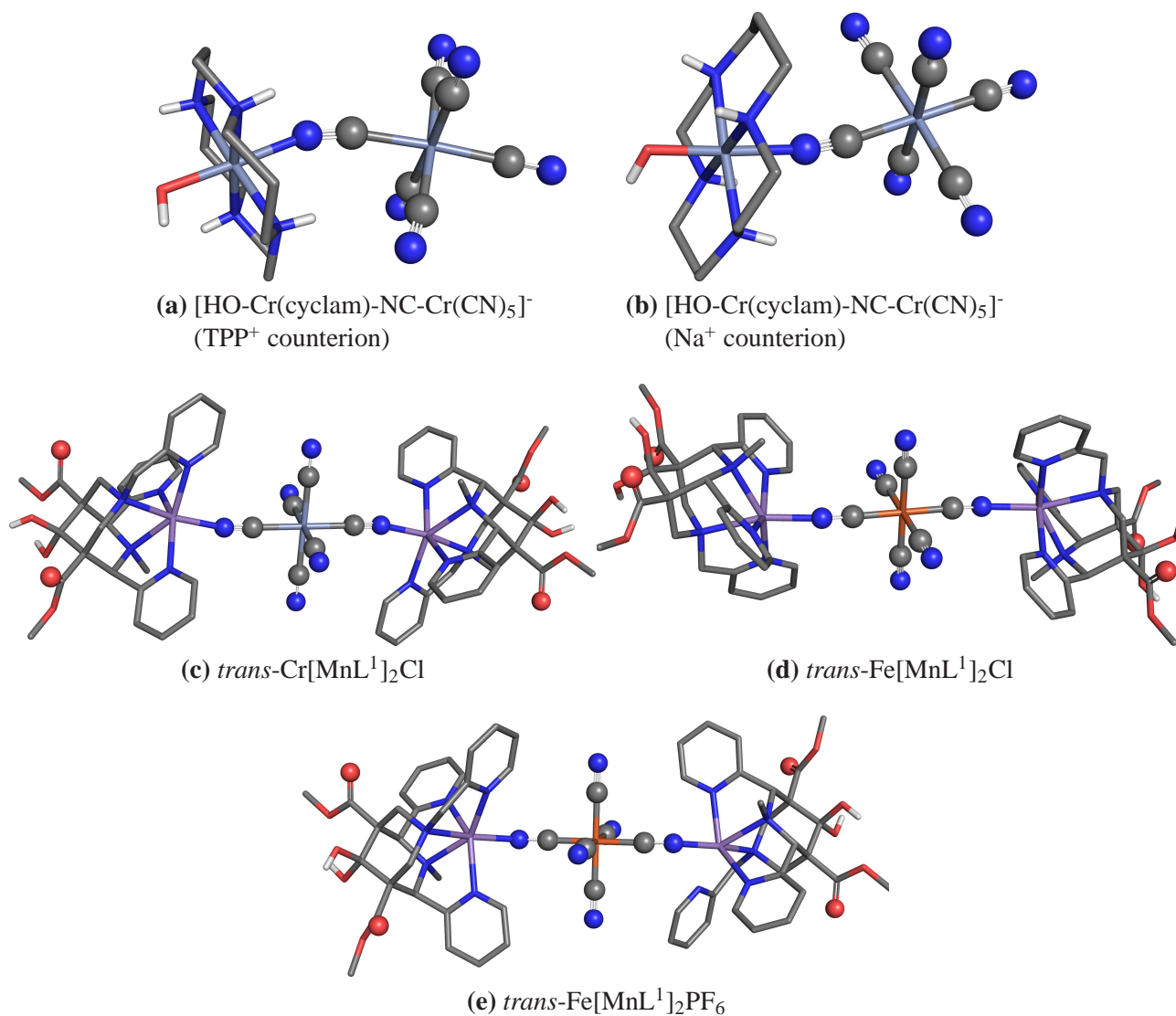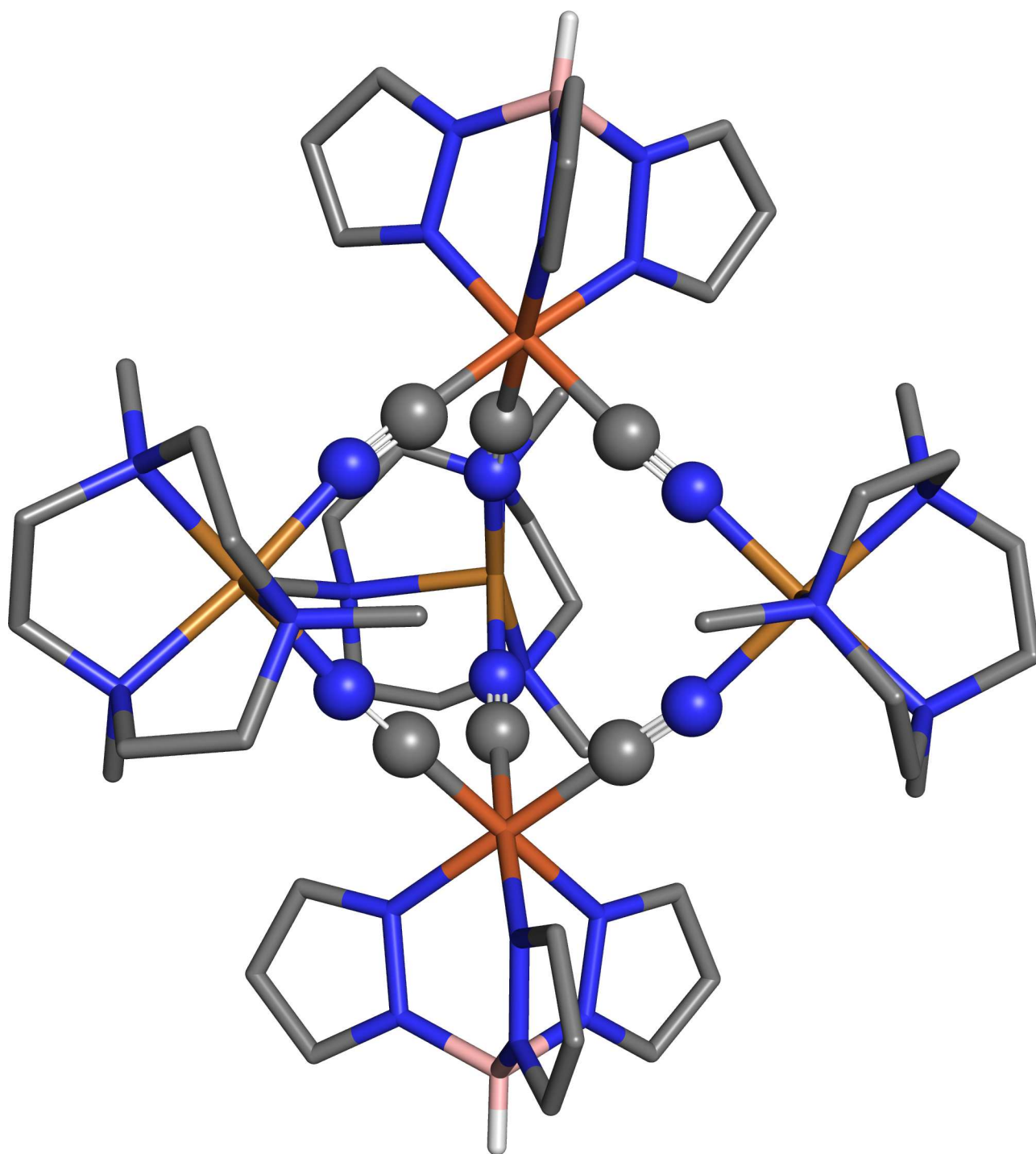
Figure 6.2.1

(f) [Tp$_2$(Me$_3$tacn)$_3$Cu$_3$Fe$_2$(CN)$_6$]$^{4+}$

Figure 6.2.1

2.2 Dinuclear

(a) $[Cu_2(MeC(OH)(PO_3)_2)_2]^{4-}$

(b) $[(Et_5dien)_2Cu_2(\mu\text{-}C_2O_4)]^{2+}$

(c) $[Mn(Me_6\text{-}[14]ane\text{-}N_4)Cu(oxpn)]^{2+}$

(d) $[(\mu\text{-}OCH_3)VO(maltolato)]_2$

(e) $[Fe_2OCl_6]^{2-}$

(f) $[MnMn(\mu\text{-}O)_2(\mu\text{-}OAc)DTNE]^{2+}$

(g) $[Cu_2(\mu\text{-}OH)_2(bipym)_2]^{2+}$

(h) $[(Dopn)Cu(OH_2)Cr(OCH_3)L]^{2+}$
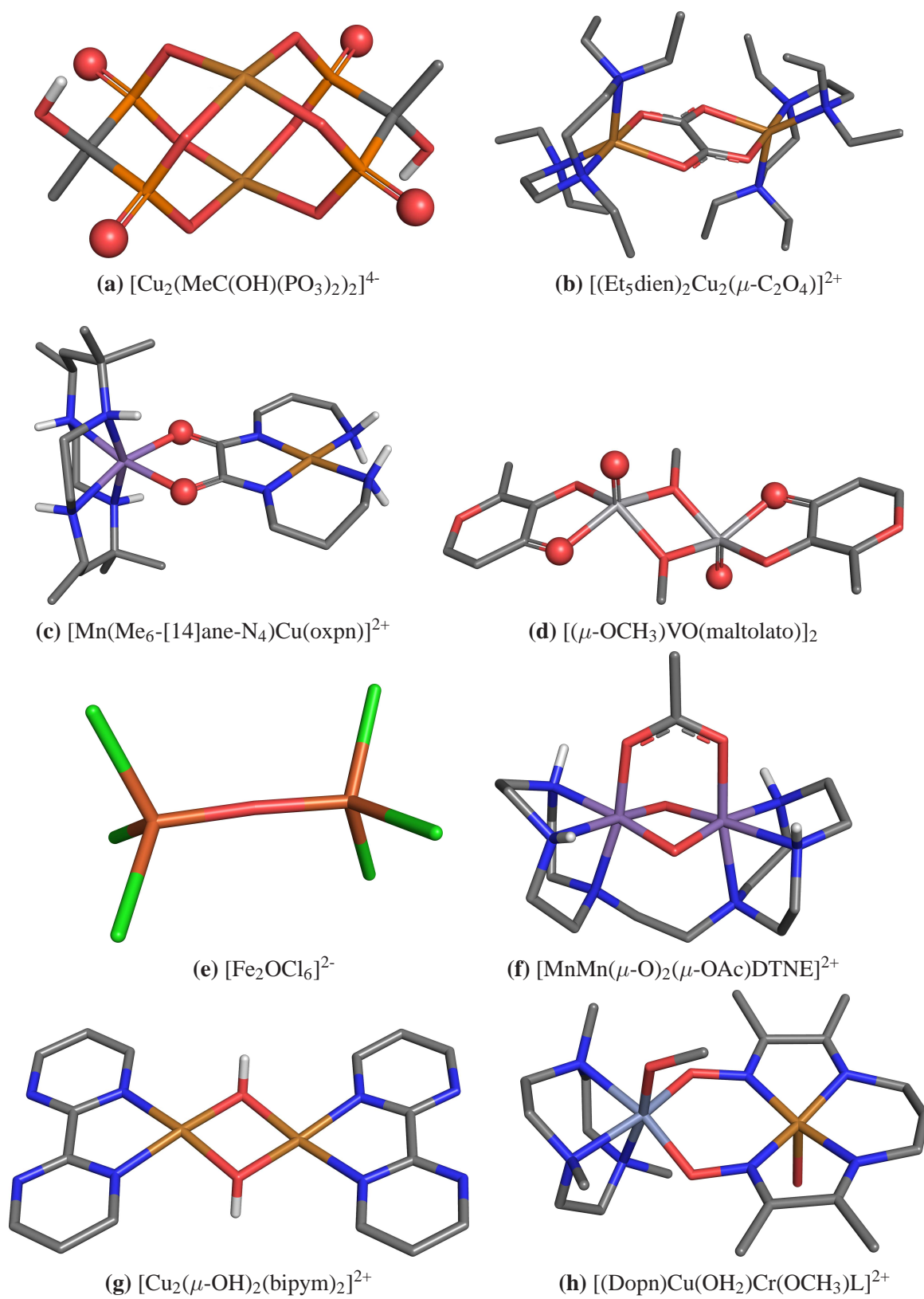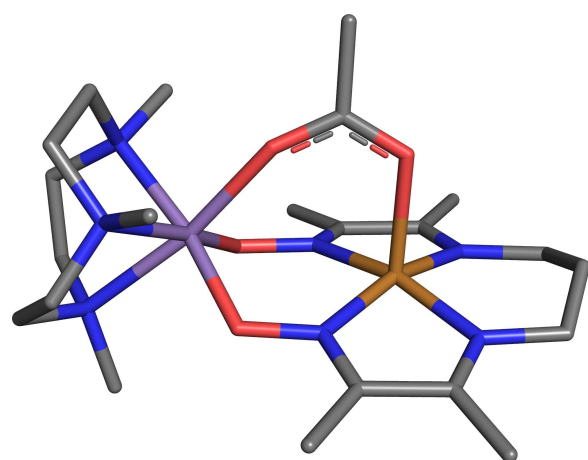
Figure 6.2.2

(i) [(Dopn)Cu(μ-CH$_3$COO)MnL]$^{2+}$
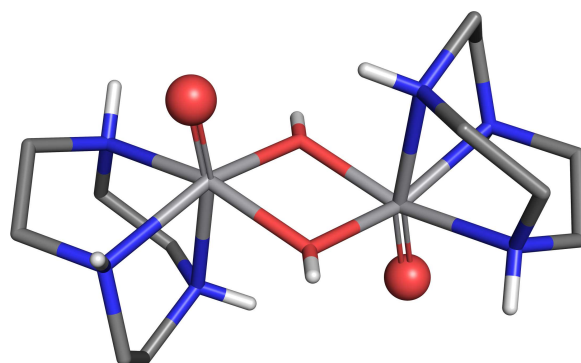
(j) [V$_2$O$_2$(μ-OH)$_2$([9]aneN$_3$)$_2$]$^{2+}$
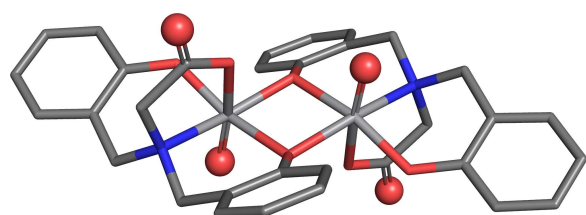
(k) [Et$_3$NH]$_2$[(VO)$_2$(BBAC)$_2$]
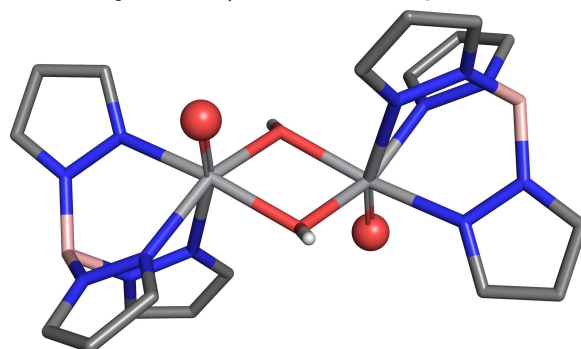
(l) [HB(pz)$_3$VO(OH)$_2$]$_2$
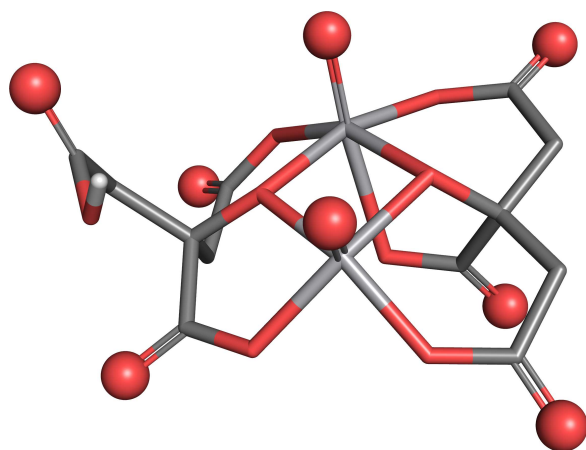
(m) [(VO)$_2$(cit)(Hcit)]$^{3-}$
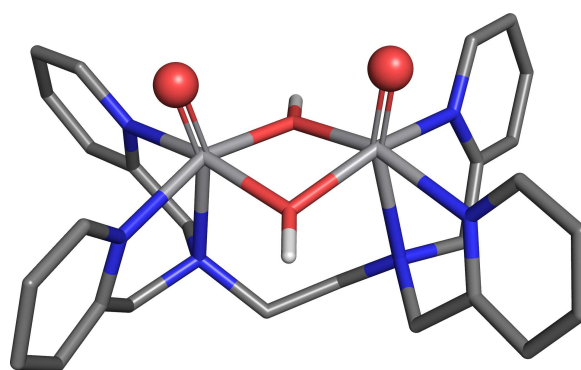
(n) [V$_2$O$_2$(μ-OH)(tpen)]$^{2+}$

Figure 6.2.2
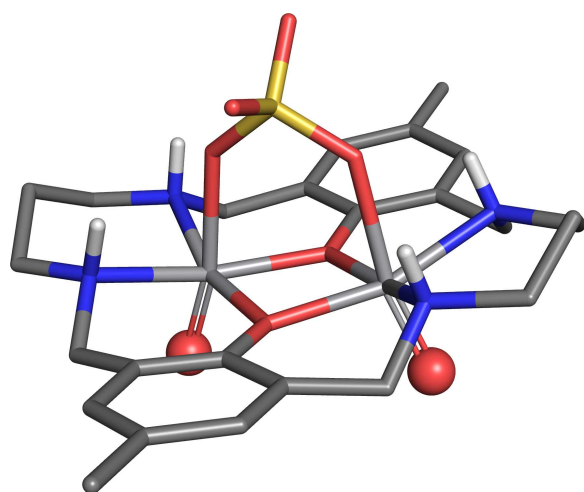
(o) [(VO)$_2$L(μ-SO$_4$)]
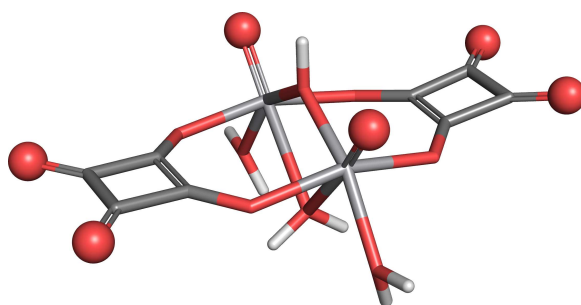
(p) [V$_2$O$_2$(OH)(C$_4$O$_4$)$_2$(H$_2$O)$_3$]$^-$
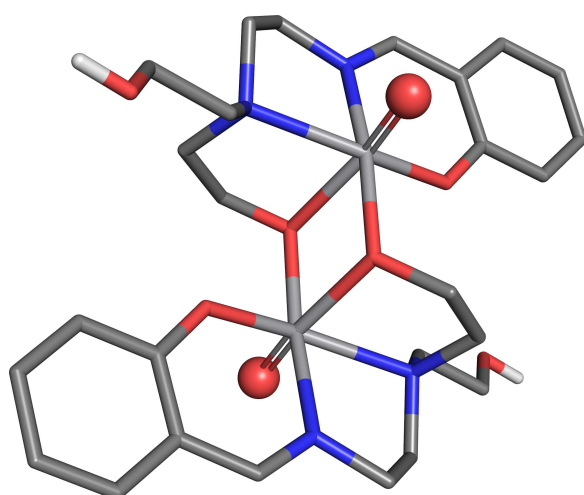
(q) [(VO(Hsabhea))$_2$]
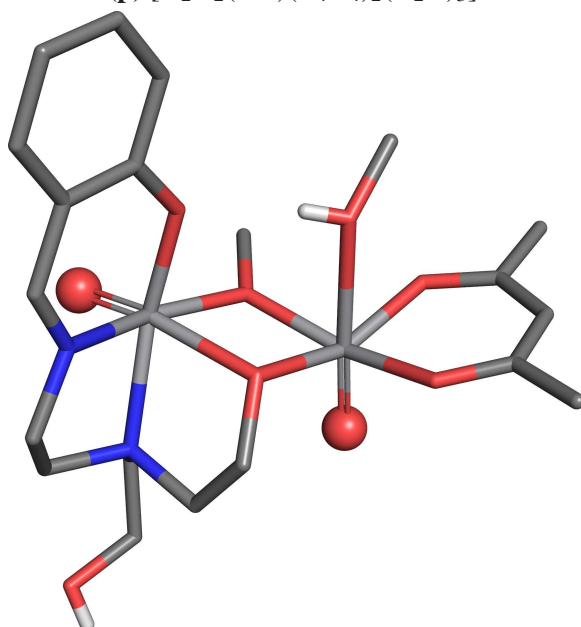
(r) [(VO(Hsabhea))(VO(acac)(HOMe))(μ_2-OMe)]
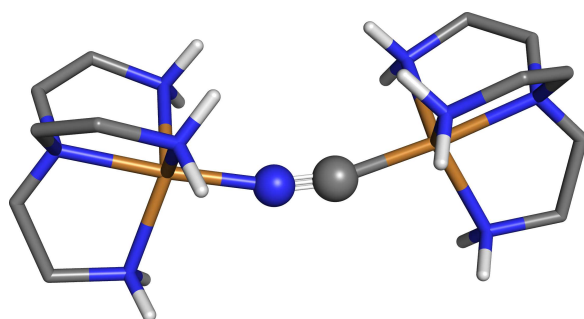
(s) [Cu$_2$(tren)$_2$CN]
(ClO$_4$ counterions not shown)
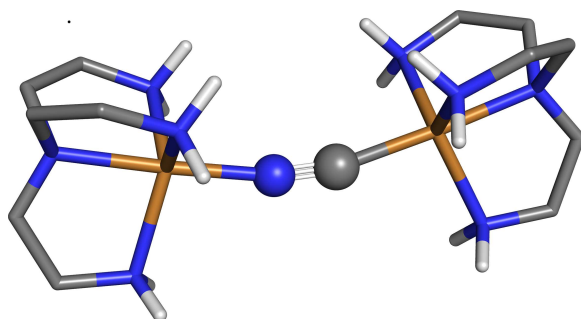
(t) [Cu$_2$(tren)$_2$CN]
(BF$_4$ counterions not shown)

Figure 6.2.2

(u) [Cu$_2$(tren)$_2$CN]
(ClO$_4$/PF$_6$ counterions not shown)

(v) [Cu$_2$(tmpa)$_2$CN]
(ClO$_4$ counterions not shown)

(w) [Cu$_2$(tmpa)$_2$CN]
(BF$_4$ counterions not shown)

(x) [Cu$_2$(tmpa)$_2$CN]
(BF$_4$ counterions and CH$_3$CN present in the crystal not shown)

(y) [Ni$_2$(tetren)$_2$CN]
([Cr(CN)$_6$] counterion not shown)
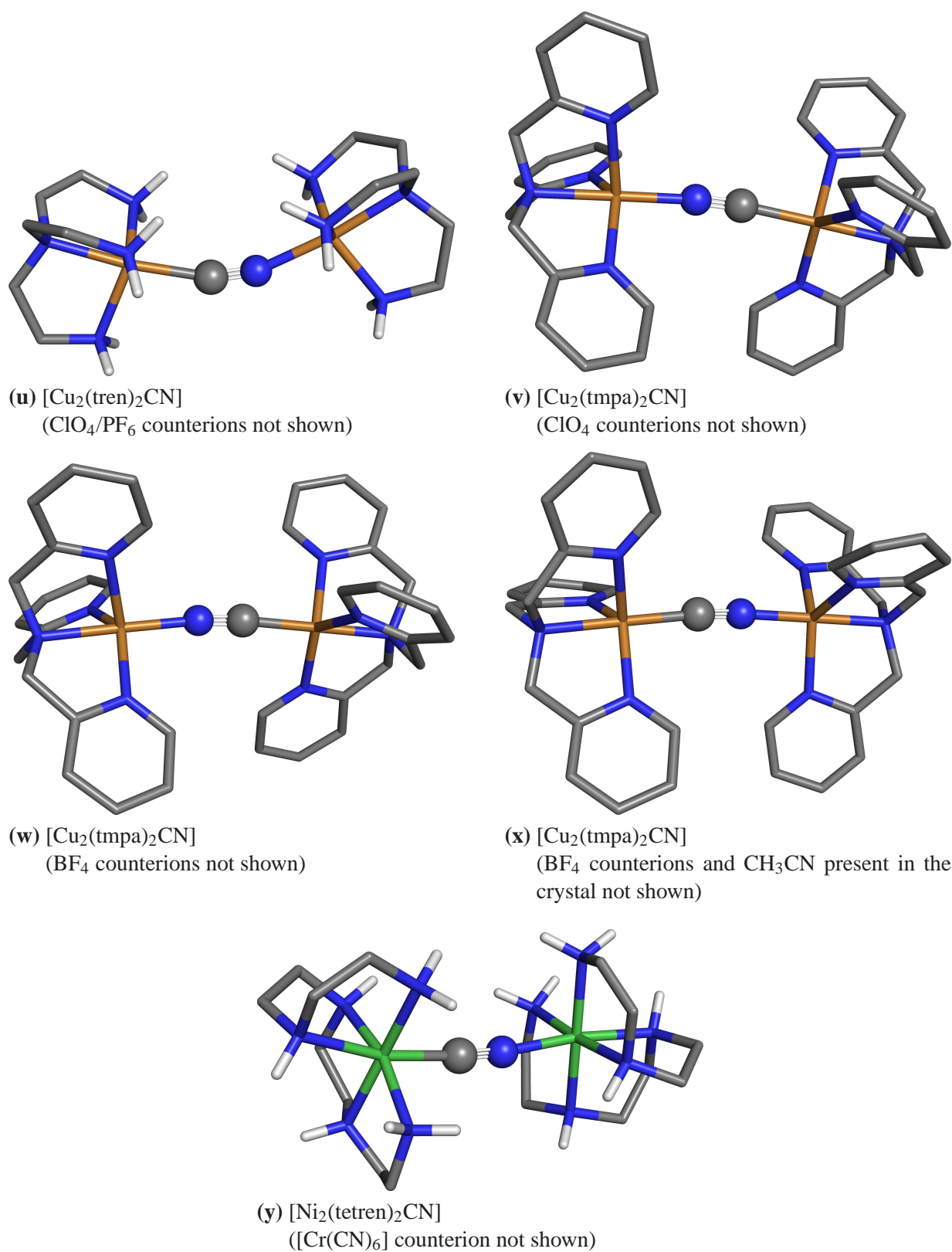
Figure 6.2.2

3 Appendix B - List of Transition Metal Complexes used for Parametrizations

3.1 Cyclam-based
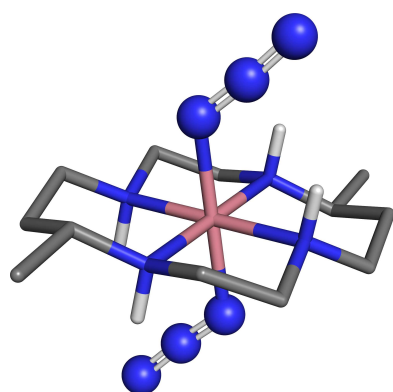
(a) *trans*-[Co(L)(N$_3$)$_2$]$^+$ L=C-*meso*-5,12-dimethyl-1,4,8,11-tetraazacyclotetradecane (AZMTCO[231])
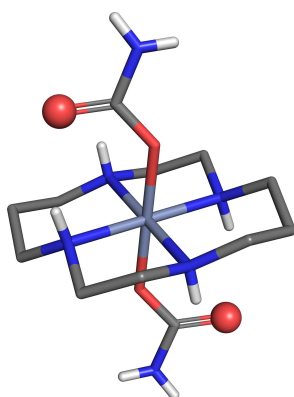
(b) *trans*-[Cr([14]aneN$_4$)(OCONH$_2$)$_2$]$^+$ (BINPET[232])

(c) [Co([14]aneN$_4$)]$^{2+}$ (COANEC[233])
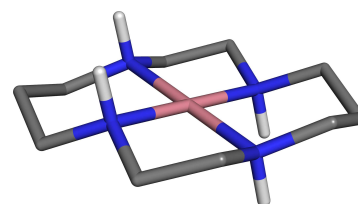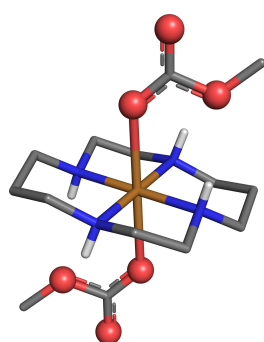
(d) *trans*-[Cu([14]aneN$_4$)(O$_2$COCH$_3$)$_2$] (DOHXON[234])
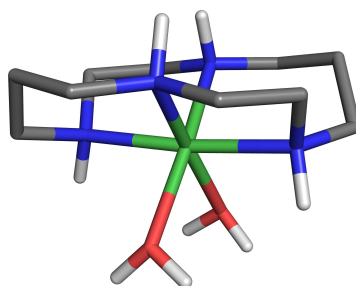
(e) *cis*-[Ni([14]aneN$_4$)(OH$_2$)$_2$]$^{2+}$ (FAGVUE[235])
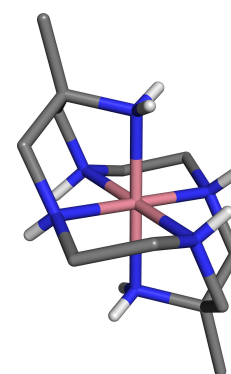
(f) *trans*-[Co(diammac)]$^{3+}$ (FEBZOB[236])

Figure 6.3.1

(g) [Co(diammac)]$^{3+}$
(FEBZOB10[237])

(h) [Cu([14]aneN$_4$)]$^{2+}$
(HAFSUC[238])

(i) *cis*-[Cr(diammac)]$^{3+}$
(HAHLOR[239])

(j) *trans*-
[Co([14]aneN$_4$)(OH$_2$)(COCH$_3$)]$^{2+}$
(PASGAR[240])

(k) *trans*-
[Fe(diammac)]$^{3+}$
(SANLAU[241])

(l) *cis*-
[Co([14]aneN$_4$)(en)]$^{3+}$
(TZCECO[242])

(m) *cis*-
[Cr([14]aneN$_4$)(en)]$^{3+}$
(WAMWOW[243])

(n) *cis*-
[Cr([14]aneN$_4$)(OH$_2$)(OH)]$^{2+}$
(WESLAH[244])

(o) *trans*-[Ni(OH$_2$)$_2$(cyclam)]$^{2+}$
(ZIQXOM[245])

(p) *trans*-
[Fe(diammac)]$^{3+}$
(ZUSCIZ[246])

(q) *trans*-
[Cr([14]aneN$_4$)(OH$_2$)(OH)]$^{2+}$
(ZUZSOC[247])
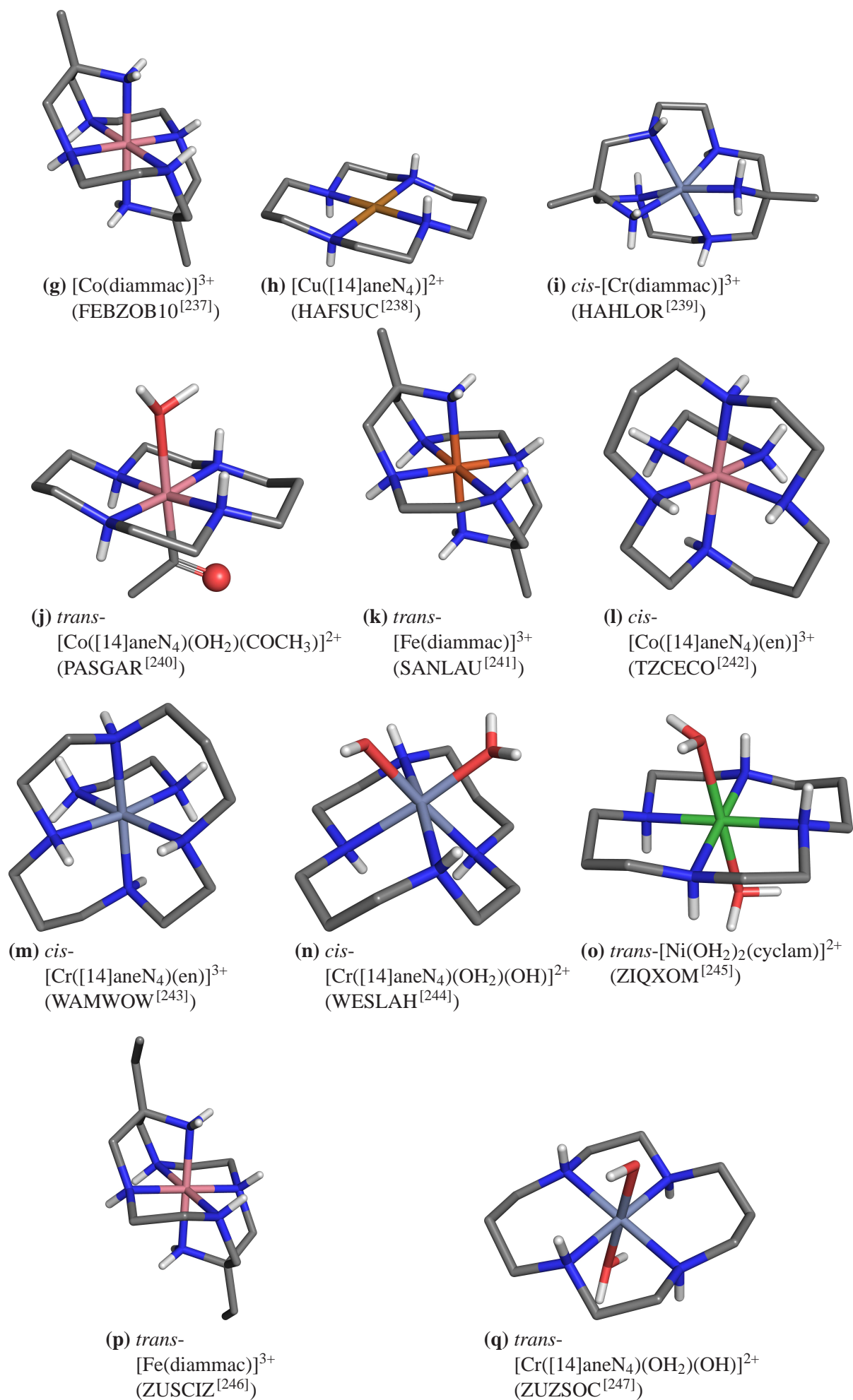
Figure 6.3.1

3.2 Cu^{II}

Please note: axial ligands, which may be present in the crystal of the complexes shown here, have been left out for the parametrization process. The structures are therefore identical to the training set used by Deeth et al.[9]. It is assumed, that the additional ligands do not have a pronounced effect on the parametrization of the CU2-NT ligand field interaction.

(a) $[Cu(en)_2]^{2+}$ (CEDHAU[248])

(b) $[Cu(deen)_2]^{2+}$ (CEFBEU[249])

(c) $[Cu(chn)_2]^{2+}$ (CHXCUA[250])

(d) $[Cu(med)_2]^{2+}$ (CMENOX[251])

(e) $[Cu(en)_3]^{2+}$ (CUENCL[252])

(f) $[Cu(tn)_2]^{2+}$ (DAPRCU[253])

Figure 6.3.2

(g) [Cu(dmed)$_2$]$^{2+}$
(DMEDCU[254])

(h) [Cu(tcn)$_2$]$^{2+}$
(DUSJAC01[228])

(i) [Cu(dien)$_2$]$^{2+}$
(ETACUB[229])

(j) [Cu(nen)$_2$]$^{2+}$
(ETEACU[255])

(k) [Cu(apt)$_2$]$^{2+}$
(JIBZUP[256])

(l) [Cu(papd)$_2$]$^{2+}$
(LATSII[257])

(m) [Cu(adt)$_2$]$^{2+}$
(TENCUB[258])
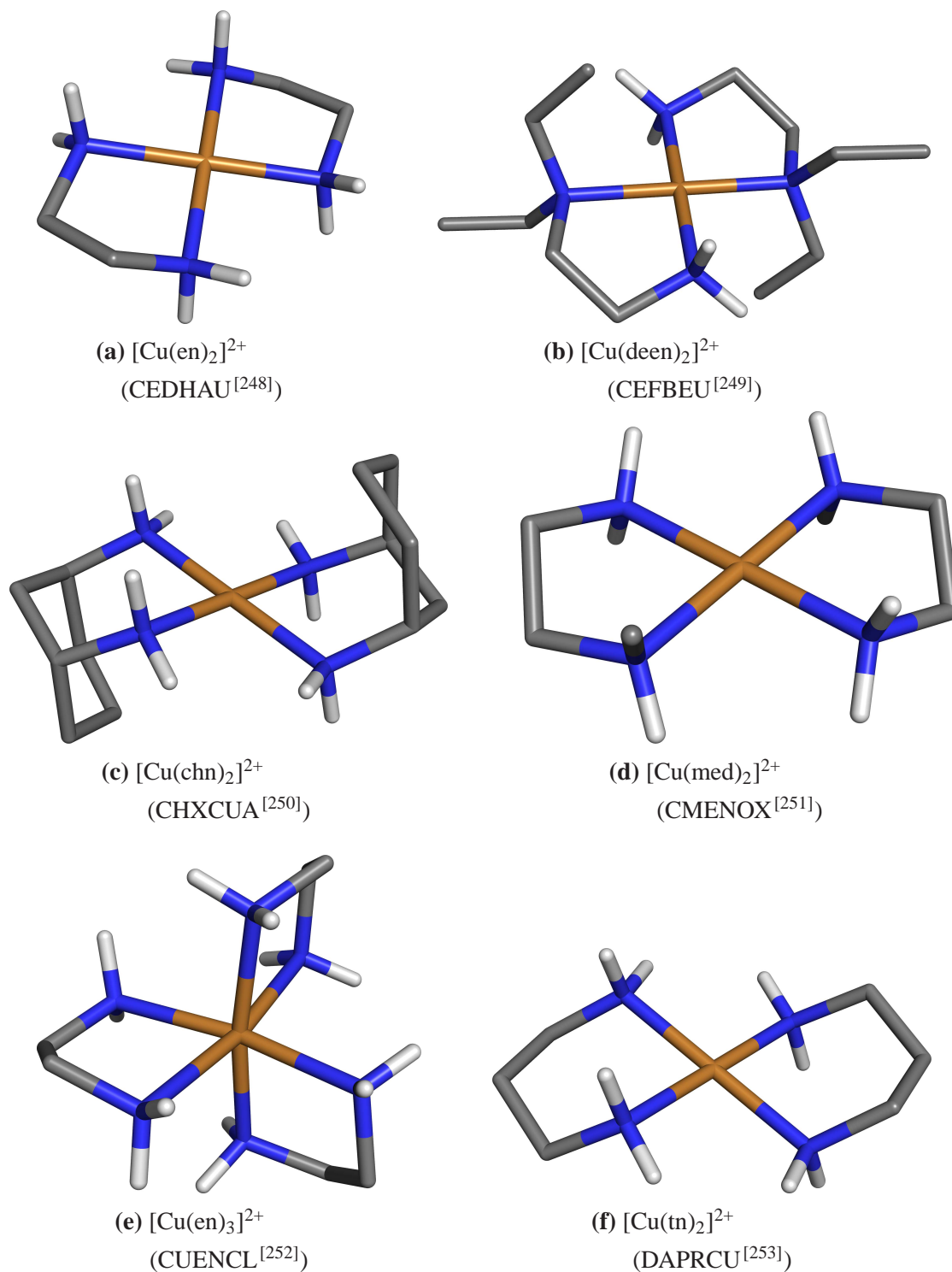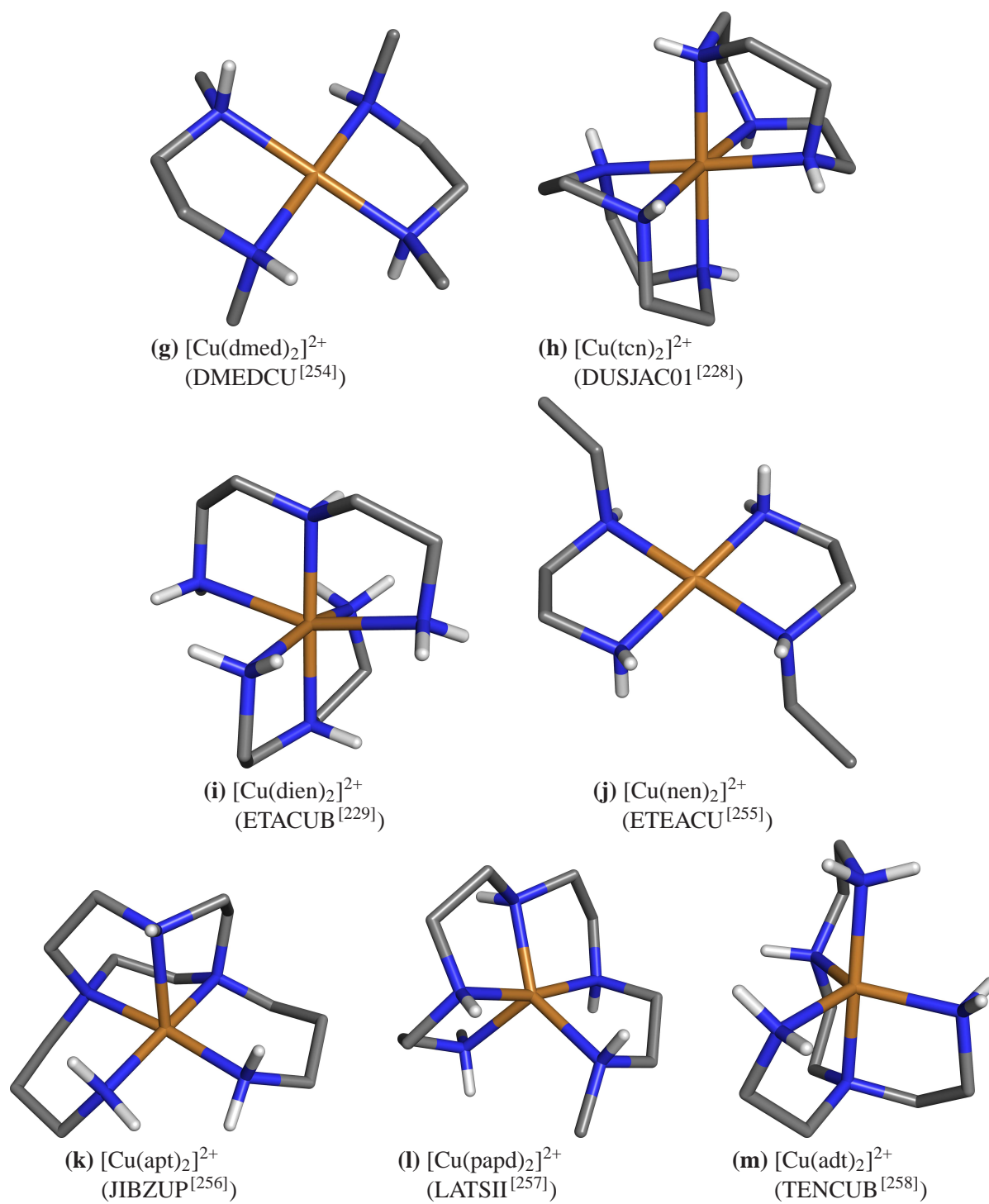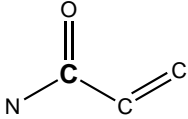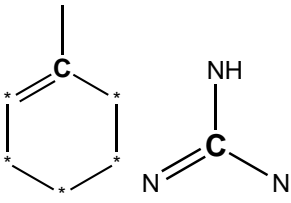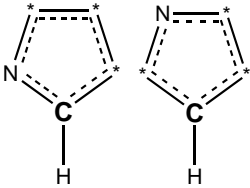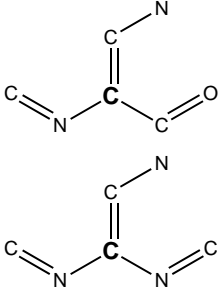
Figure 6.3.2

4 Appendix C - Momec Force Field Parameters (April 2011)[56–61]
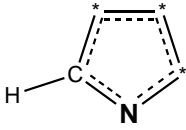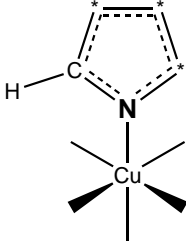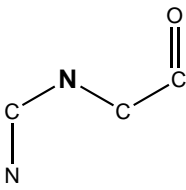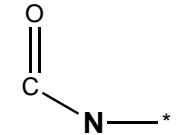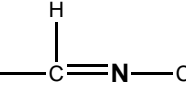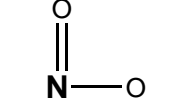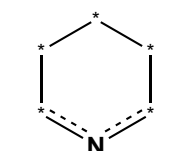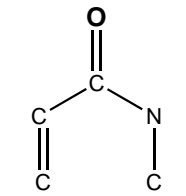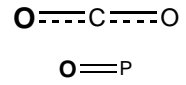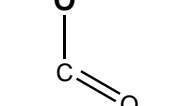
4.1 Atom Types
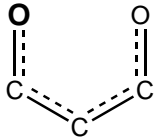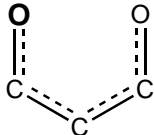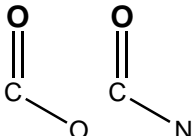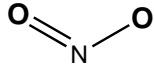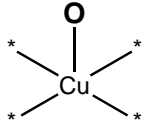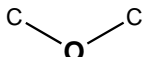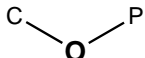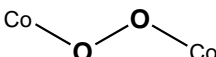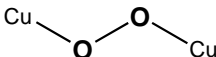
atom 1	chemical environment	mass [u]	harmonic	multiple harmonic	1,3- interaction	twist
H	hydrogen	1.010	1	0	0	0
LP	lone pair	3.000	1	0	0	0
C		12.010	1	0	0	0
C3		12.010	1	0	0	0
CA		12.010	1	0	0	0
CAH		12.010	1	0	0	0
CB		12.010	1	0	0	0
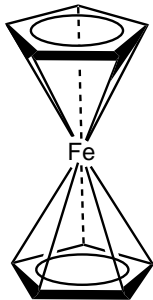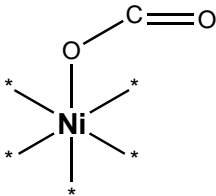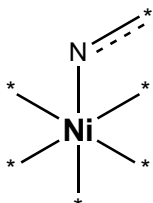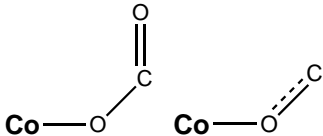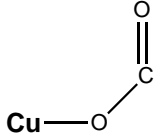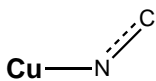
atom 1	chemical environment	mass [u]	harmonic	multiple harmonic	1,3- interaction	twist
CCC		12.010	1	0	0	0
CCO		12.010	1	0	0	0
CFC		12.010	1	0	0	0
CI		12.010	1	0	0	0
CK		12.010	1	0	0	0
CMC		12.010	1	0	0	0
COC		12.010	1	0	0	0
CON		12.010	1	0	0	0
CT	carbon	12.010	1	0	0	0
N*		14.010	1	0	0	0
N3		14.010	1	0	0	0
NA		14.010	1	0	0	0

atom 1	chemical environment	mass [u]	harmonic	multiple harmonic	1,3- interaction	twist
NAH		14.010	1	0	0	0
NAX		14.010	1	0	0	0
NB		14.010	1	0	0	0
ND		14.010	1	0	0	0
NI		14.010	1	0	0	0
NOO		14.010	1	0	0	0
NP		14.010	1	0	0	0
NT	nitrogen	14.010	1	0	0	0
O		16.000	1	0	0	0
O2		16.000	1	0	0	0
OC		16.000	1	0	0	0

atom 1	chemical environment	mass [u]	harmonic	multiple harmonic	1,3- interaction	twist
OCC		16.000	1	0	0	0
OCCT		16.000	1	0	0	0
OCO		16.000	1	0	0	0
OH		16.000	1	0	0	0
ONO		16.000	1	0	0	0
OP		16.000	1	0	0	0
OR		16.000	1	0	0	0
OS		16.000	1	0	0	0
OW	oxygen	16.000	1	0	0	0
OXCO		16.000	1	0	0	0
OXCU		16.000	1	0	0	0
P	phosphorus	30.970	1	0	0	0
SW	sulfur	32.060	1	0	0	0
CL	chlorine	35.450	1	0	0	0

atom 1	chemical environment	mass [u]	harmonic	multiple harmonic	1,3-interaction	twist
TI3	titanium(III)	47.880	0	1	1	0
TI4	titanium(IV)	47.880	0	1	1	0
V3	vanadium(III)	50.940	0	1	1	0
CR2	chromium(II)	52.000	0	1	1	0
CR3	chromium(III)	52.000	0	1	1	0
MN3	manganese(III)	54.940	0	1	1	0
FE	iron	55.850	0	1	1	0
FE2H	high-spin iron(II)	55.850	0	1	1	0
FE2L	low-spin iron(II)	55.850	0	1	1	0
FE3H	high-spin iron(III)	55.850	0	1	1	0
FE3L	low-spin iron(III)	55.850	0	1	1	0
FECP		55.850	0	1	1	0
NI2	nickel(II)	58.700	0	1	1	0
NI2C		58.700	0	1	1	0
NI2P		58.700	0	1	1	0
NI2T	tetracoordinated nickel(II)	58.700	0	1	1	0
CO2	cobalt(II)	58.930	0	1	1	0
CO2T	tetracoordinated cobalt(II)	58.930	0	1	1	0
CO3	cobalt(III)	58.930	0	1	1	0
CO3C		58.930	0	1	1	0

atom 1	chemical environment	mass [u]	harmonic	multiple harmonic	1,3-interaction	twist
CU1	copper(I)	63.550	0	1	1	0
CU2	copper(II)	63.550	0	1	1	0
CU2C		63.550	0	1	1	0
CU2P		63.550	0	3	3	0
CU2T	tetracoordinated copper(II)	63.550	0	1	1	0
ZN2	zinc(II)	65.380	0	1	1	0
ZN2T	tetracoordinated zinc(II)	65.380	0	1	1	0
BR	bromine	79.900	1	0	0	0
Y3	yttrium(III)	88.910	0	1	1	0
RH3	rhodium(III)	102.910	0	1	1	0
I	iodine	126.900	1	0	0	0
LA3	lanthanum(III)	138.910	0	1	1	0
CE3	cerium(III)	140.120	0	1	1	0
PR3	praseodymium(III)	140.910	0	1	1	0
ND3	neodymium(III)	144.240	0	1	1	0
PM3	promethium(III)	146.920	0	1	1	0
SM3	samarium(III)	150.360	0	1	1	0
EU3	europium(III)	151.970	0	1	1	0
GD3	gadolinium(III)	157.250	0	1	1	0
TB3	terbium(III)	158.930	0	1	1	0
DY3	dysprosium(III)	162.500	0	1	1	0
HO3	holmium(III)	164.930	0	1	1	0
ER3	erbium(III)	167.260	0	1	1	0
TM3	thulium(III)	168.930	0	1	1	0
YB3	ytterbium(III)	173.040	0	1	1	0
LU3	lutetium(III)	174.970	0	1	1	0
PT2	platinum(III)	195.080	0	1	1	0
PT4	platinum(IV)	195.080	0	1	1	0
U6	uranium(III)	238.030	0	1	1	0

4.2 Stretch Interactions

atom 1	atom 2	k [mdyn/Å]	r$_0$ [Å]	atom 1	atom 2	k [mdyn/Å]	r$_0$ [Å]
C	CB	6.210	1.419	CI	NT	6.700	1.317
C	NA	5.810	1.388	CK	H	5.000	0.970
C	O	7.920	1.229	CK	N*	6.120	1.371
C3	N3	8.000	1.107	CK	NB	7.350	1.304
CA	CA	7.400	1.377	CO2	NP	0.820	2.100
CA	CFC	7.400	1.377	CO2	NT	0.820	2.120
CA	CON	7.400	1.377	CO2T	ND	0.820	1.780
CA	CT	5.000	1.500	CO2T	NP	0.820	1.960
CA	H	5.000	0.970	CO3	NI	1.750	1.905
CA	NA	5.940	1.381	CO3	NP	1.750	1.865
CA	NP	6.500	1.335	CO3	NT	1.750	1.905
CA	NT	6.690	1.340	CO3C	NP	1.750	1.865
CAH	CA	1.500	1.380	CO3C	NT	1.750	1.915
CAH	CAH	1.300	1.335	CO3C	OC	1.400	1.860
CAH	CI	4.500	1.450	CO3C	OCC	1.400	1.880
CAH	CT	3.000	1.490	CO3P	OXCO	1.750	1.840
CAH	H	5.000	0.970	COC	CT	5.000	1.500
CAH	NAH	1.500	1.340	COC	OCC	7.400	1.275
CAH	NAX	2.500	1.340	COC	OCCT	7.400	1.275
CAH	NI	4.500	1.440	CON	CT	5.000	1.500
CB	CB	7.220	1.370	CON	ND	6.500	1.310
CB	N*	6.060	1.374	CON	OCO	9.000	1.260
CB	NA	6.410	1.354	CR3	NP	1.000	1.985
CB	NB	5.750	1.391	CR3	NT	1.100	2.045
CCO	OC	8.000	1.290	CR3	OC	0.750	1.935
CCO	OCO	9.000	1.220	CT	CT	5.000	1.500
CE3	O2	0.053	2.370	CT	CTO	5.000	1.500
CE3	OH	0.053	2.370	CT	CTOC	5.000	1.500
CFC	CFC	5.000	1.470	CT	H	5.000	0.970
CFC	COC	5.000	1.470	CT	N*	4.690	1.475
CFC	NP	6.500	1.335	CT	NAH	3.000	1.450
CI	CA	5.000	1.460	CT	ND	6.000	1.490
CI	CI	15.000	1.526	CT	NOO	5.000	1.530
CI	CT	5.000	1.500	CT	NT	6.000	1.490
CI	H	3.900	0.950	CT	OP	3.500	1.410
CI	NI	7.200	1.270	CT	OR	5.000	1.400

atom 1	atom 2	k [mdyn/Å]	r$_0$ [Å]	atom 1	atom 2	k [mdyn/Å]	r$_0$ [Å]
CT	OW	0.500	1.340	ER3	O2	0.074	2.150
CT	SW	2.640	1.820	ER3	OH	0.074	2.150
CTO	CTO	5.000	1.505	EU3	O2	0.067	2.245
CTO	CTOC	5.000	1.510	EU3	OH	0.067	2.245
CTOC	CTOC	5.000	1.490	FE3H	OC	1.000	1.990
CTOC	NOO	5.000	1.528	FE3H	OW	0.500	1.900
CTOC	NTO	6.000	1.480	FE3L	C3	1.700	1.923
CU1	NI	0.700	2.000	FE3L	NP	1.700	1.925
CU1	NT	0.100	2.220	FE3L	NT	1.700	1.950
CU2	ND	0.600	1.920	GD3	O2	0.069	2.226
CU2	NP	0.600	1.940	GD3	OH	0.069	2.226
CU2	NT	0.600	1.970	GD3	OW	0.069	2.226
CU2	OC	0.800	1.900	H	NA	6.030	0.910
CU2	ONO	0.100	2.500	H	NT	5.640	0.910
CU2	OP	0.100	2.150	H	OP	5.000	0.910
CU2	OW	0.100	2.500	H	OW	5.000	0.910
CU2	SW	0.600	2.290	HO3	O2	0.073	2.178
CU2C	ND	0.600	1.920	HO3	OH	0.073	2.178
CU2C	NP	0.600	1.940	HO3	OW	0.073	2.178
CU2C	NT	0.600	1.970	LA3	O2	0.049	2.409
CU2C	OC	0.800	1.900	LA3	OH	0.049	2.409
CU2C	OW	0.100	2.500	LA3	OW	0.049	2.409
CU2C	SW	0.600	2.290	LU3	O2	0.076	2.038
CU2P	NAH	0.900	1.940	LU3	OH	0.076	2.038
CU2P	NAX	0.300	2.300	LU3	OW	0.076	2.038
CU2P	ND	0.600	1.920	MN3	OC	0.300	1.950
CU2P	NP	0.600	1.940	NAH	H	5.000	0.910
CU2P	NT	0.600	1.970	NAH	NAH	1.500	1.360
CU2P	OC	0.800	1.900	NAH	NAX	1.500	1.360
CU2P	ONO	0.100	2.500	ND3	O2	0.058	2.320
CU2P	OP	0.100	2.150	ND3	OH	0.058	2.320
CU2P	OW	0.100	2.500	ND3	OW	0.058	2.320
CU2P	OXCU	0.600	1.830	NI	CT	4.000	1.420
CU2T	ND	0.600	1.890	NI2	NT	0.600	2.090
CU2T	NP	0.600	1.940	NI2C	NP	0.600	2.025
DY3	O2	0.072	2.195	NI2C	NT	0.600	2.035
DY3	OH	0.072	2.195	NI2C	OC	0.650	2.040
DY3	OW	0.072	2.195	NI2P	NP	0.600	2.025

atom 1	atom 2	k [mdyn/Å]	r_0 [Å]	atom 1	atom 2	k [mdyn/Å]	r_0 [Å]
NI2P	NT	0.600	2.050	SM3	OW	0.064	2.258
NI2T	ND	0.600	1.760	TB3	O2	0.071	2.213
NI2T	NP	0.600	1.855	TB3	OH	0.071	2.213
NOO	ONO	6.500	1.213	TI3	OC	0.800	2.080
OC	CT	8.000	2.000	TI3	OW	0.500	2.035
OXCO	OXCO	3.250	1.470	TI4	OCC	1.500	1.980
OXCU	OXCU	3.250	1.430	TI4	OCCT	1.500	2.040
P	O2	7.297	1.448	TI4	OW	0.500	1.722
P	OH	3.197	1.665	TM3	O2	0.075	2.215
P	OS	3.197	1.686	TM3	OH	0.075	2.215
PM3	O2	0.062	2.285	V3	OC	0.500	1.920
PM3	OH	0.062	2.285	V3	OW	0.500	1.980
PR3	O2	0.056	2.345	Y3	O2	0.074	2.160
PR3	OH	0.056	2.345	Y3	OH	0.074	2.160
PR3	OW	0.056	2.345	YB3	O2	0.076	2.095
PT2	NB	2.540	2.010	YB3	OH	0.076	2.095
PT2	NT	2.540	2.030	YB3	OW	0.076	2.095
RH3	NT	1.750	2.050	ZN2	ND	0.350	2.000
SM3	O2	0.064	2.258	ZN2	NP	0.350	2.100
SM3	OH	0.064	2.258	ZN2	NT	0.350	2.220

4.3 Bend Interactions

atom 1	atom 2	atom 3	k [mdyn/rad]	a_0 [rad]	atom 1	atom 2	atom 3	k [mdyn/rad]	a_0 [rad]
CB	C	NA	0.970	1.943	CAH	CA	H	0.450	2.122
CB	C	O	1.110	2.248	CFC	CA	H	0.450	2.094
NA	C	O	1.110	2.105	CFC	CA	NP	0.970	2.094
FE3L	C3	N3	0.450	3.141	CI	CA	CA	0.250	2.094
CA	CA	CA	0.970	2.094	CON	CA	NP	0.970	2.094
CA	CA	CFC	0.970	2.094	CT	CA	NP	0.450	2.094
CA	CA	CON	0.970	2.094	H	CA	NP	0.450	2.094
CA	CA	CT	0.450	2.094	NA	CA	NA	0.970	2.152
CA	CA	H	0.450	2.094	NA	CA	NT	0.970	2.025
CA	CA	NP	0.970	2.094	NA	CA	NT	0.970	2.091
CA	CA	NT	0.450	2.094	CAH	CAH	CA	0.150	2.122
CAH	CA	CA	0.450	2.024	CAH	CAH	CAH	0.100	1.850

atom 1	atom 2	atom 3	k [mdyn/rad]	a_0 [rad]	atom 1	atom 2	atom 3	k [mdyn/rad]	a_0 [rad]
CAH	CAH	CI	0.650	2.304	NP	CO2	NP	0.023	1.571
CAH	CAH	CT	0.650	2.274	NT	CO2	NT	0.017	1.571
CAH	CAH	H	0.450	2.215	NP	CO3	NP	0.050	1.571
CAH	CAH	NAH	0.150	1.955	NP	CO3	NT	0.050	1.571
CAH	CAH	NAX	0.150	1.955	NT	CO3	NT	0.050	1.571
CI	CAH	NAH	0.650	2.112	NP	CO3C	NP	0.050	1.571
CT	CAH	NAH	0.650	2.112	NP	CO3C	NT	0.050	1.571
CT	CAH	NAX	0.650	2.112	NT	CO3C	NT	0.050	1.571
NAH	CAH	CA	0.150	2.292	NT	CO3C	OC	0.045	1.571
NAH	CAH	H	0.350	2.094	NT	CO3C	OCC	0.045	1.571
NAH	CAH	NAH	0.150	1.955	OC	CO3C	OC	0.040	1.571
C	CB	CB	1.180	2.080	OCC	CO3C	OCC	0.040	1.571
C	CB	NB	0.970	2.269	CCC	COC	CFC	0.350	2.094
CB	CB	N*	0.970	1.854	CCC	COC	CT	0.350	2.094
CB	CB	NA	0.970	2.229	CCC	COC	OCC	0.970	2.094
CB	CB	NB	0.970	1.911	CCC	COC	OCCT	0.970	2.094
NA	CB	N*	0.970	2.199	CFC	COC	OCC	0.350	2.094
COC	CCC	COC	0.970	2.094	CFC	COC	OCCT	0.350	2.094
COC	CCC	H	0.970	2.094	CT	COC	OCC	0.350	2.094
CT	CCO	OC	0.250	2.067	CT	COC	OCCT	0.350	2.094
CT	CCO	OCO	0.250	2.067	CA	CON	ND	0.250	2.067
OC	CCO	CCO	0.800	1.993	CA	CON	OCO	0.250	2.067
OC	CCO	OC	0.250	2.094	CT	CON	ND	0.250	2.067
OC	CCO	OCO	0.250	2.149	CT	CON	OCO	0.250	2.067
OCO	CCO	CCO	0.950	2.115	ND	CON	OCO	0.250	2.094
CA	CFC	CA	0.970	2.094	NP	CR3	NP	0.025	1.571
CA	CFC	CFC	0.450	2.094	NP	CR3	NT	0.025	1.571
CA	CFC	COC	0.350	2.094	NT	CR3	NT	0.025	1.571
CA	CFC	NP	0.970	2.094	CA	CT	CA	0.450	1.911
CFC	CFC	NP	0.450	2.094	CA	CT	CT	0.450	1.911
CA	CI	H	0.450	2.094	CA	CT	H	0.360	1.909
CAH	CI	H	0.450	2.094	CA	CT	ND	0.450	1.911
CAH	CI	NI	0.150	2.094	CA	CT	NT	0.450	1.911
NI	CI	CA	0.150	2.094	CA	CT	OP	0.450	1.911
NI	CI	H	0.450	2.094	CA	CT	OW	0.450	1.911
H	CK	N*	0.490	2.148	CAH	CT	CA	0.450	1.911
H	CK	NB	0.490	2.148	CAH	CT	CAH	0.450	1.960
NB	CK	N*	0.970	1.960	CAH	CT	CT	0.450	1.960

atom 1	atom 2	atom 3	k [mdyn/rad]	a_0 [rad]	atom 1	atom 2	atom 3	k [mdyn/rad]	a_0 [rad]
CAH	CT	H	0.360	1.909	H	CTO	H	0.320	1.911
CAH	CT	NT	0.450	1.911	ND	CU2	ND	0.013	1.571
CAH	CT	OP	0.450	1.911	ND	CU2	NP	0.013	1.571
CAH	CT	OW	0.450	1.911	ND	CU2	NT	0.013	1.571
CCO	CT	CCO	0.450	1.911	ND	CU2	OW	0.007	1.571
CCO	CT	CT	0.450	1.911	NP	CU2	NP	0.013	1.571
CCO	CT	H	0.360	1.909	NP	CU2	NT	0.013	1.571
CCO	CT	ND	0.450	1.911	NP	CU2	ONO	0.007	1.571
CCO	CT	NT	0.450	1.911	NP	CU2	OW	0.007	1.571
COC	CT	H	0.350	1.909	NP	CU2	SW	0.013	1.571
CON	CT	CON	0.450	1.911	NT	CU2	NT	0.013	1.571
CON	CT	CT	0.450	1.911	NT	CU2	ONO	0.007	1.571
CON	CT	H	0.360	1.909	NT	CU2	OW	0.007	1.571
CON	CT	NT	0.450	1.911	NT	CU2	SW	0.013	1.571
CT	CT	CT	0.450	1.911	ONO	CU2	ONO	0.002	3.141
CT	CT	H	0.360	1.909	ONO	CU2	OW	0.002	1.571
CT	CT	N*	0.500	1.909	ONO	CU2	SW	0.007	1.571
CT	CT	NAH	0.450	1.911	OW	CU2	OW	0.002	3.141
CT	CT	ND	0.450	1.911	OW	CU2	SW	0.007	1.571
CT	CT	NOO	0.450	1.911	SW	CU2	SW	0.013	1.571
CT	CT	NT	0.450	1.911	ND	CU2C	ND	0.013	1.571
CT	CT	OW	0.450	1.911	ND	CU2C	NP	0.013	1.571
CT	CT	SW	0.690	1.911	ND	CU2C	NT	0.013	1.571
H	CT	H	0.320	1.902	ND	CU2C	OC	0.015	1.571
H	CT	N*	0.360	1.909	ND	CU2C	OW	0.007	1.571
H	CT	ND	0.360	1.909	NP	CU2C	NP	0.013	1.571
H	CT	NT	0.360	1.909	NP	CU2C	NT	0.013	1.571
H	CT	OW	0.360	1.909	NP	CU2C	ONO	0.007	1.571
H	CT	SW	0.450	1.911	NP	CU2C	OW	0.007	1.571
NAH	CT	H	0.360	1.909	NP	CU2C	SW	0.013	1.571
NAH	CT	OP	0.450	1.885	NT	CU2C	NT	0.013	1.571
NAH	CT	OW	0.450	1.885	NT	CU2C	OC	0.015	1.571
NI	CT	CT	0.450	1.911	NT	CU2C	ONO	0.007	1.571
NI	CT	H	0.450	1.911	NT	CU2C	OW	0.007	1.571
NI	CT	H	0.450	1.911	NT	CU2C	SW	0.013	1.571
NT	CT	NT	0.450	1.911	OC	CU2C	OC	0.017	1.571
OS	CT	H	0.485	1.911	OC	CU2C	OW	0.009	1.571
CT	CTO	CTO	0.450	1.920	ONO	CU2C	ONO	0.002	3.141

atom 1	atom 2	atom 3	k [mdyn/rad]	a_0 [rad]	atom 1	atom 2	atom 3	k [mdyn/rad]	a_0 [rad]
ONO	CU2C	OW	0.002	1.571	CA	NA	CB	0.970	1.958
ONO	CU2C	SW	0.007	1.571	CA	NA	H	0.490	2.059
OW	CU2C	OW	0.002	3.141	CAH	NAH	CAH	0.150	1.842
OW	CU2C	SW	0.007	1.571	CAH	NAH	CT	0.650	2.243
SW	CU2C	SW	0.013	1.571	CAH	NAH	CU2P	0.050	2.147
ND	CU2P	ND	0.013	1.571	CAH	NAH	H	0.350	2.094
ND	CU2P	NP	0.013	1.571	CAH	NAH	NAH	0.200	1.885
ND	CU2P	NT	0.013	1.571	CU2P	NAH	NAH	0.200	2.269
ND	CU2P	OW	0.007	1.571	NAH	NAH	CT	0.650	2.094
NP	CU2P	NP	0.013	1.571	NAH	NAH	H	0.350	2.094
NP	CU2P	NT	0.013	1.571	NAX	NAH	CAH	0.200	1.885
NP	CU2P	ONO	0.007	1.571	NAX	NAH	CT	0.650	2.094
NP	CU2P	OW	0.007	1.571	CAH	NAX	CU2P	0.100	2.147
NP	CU2P	SW	0.013	1.571	CAH	NAX	NAH	0.200	1.823
NT	CU2P	NT	0.013	1.571	CU2P	NAX	NAH	0.100	2.304
NT	CU2P	OC	0.015	1.571	CB	NB	CK	0.970	1.841
NT	CU2P	ONO	0.007	1.571	PT2	NB	CB	0.300	2.221
NT	CU2P	OW	0.007	1.571	PT2	NB	CK	0.300	2.221
NT	CU2P	SW	0.013	1.571	CT	ND	CON	0.250	2.067
OC	CU2P	OC	0.017	1.571	CU2	ND	CON	0.200	2.094
OC	CU2P	OW	0.009	1.571	CU2	ND	CT	0.200	2.094
ONO	CU2P	ONO	0.002	3.141	CU2C	ND	CON	0.200	2.094
ONO	CU2P	OW	0.002	1.571	CU2C	ND	CT	0.200	2.094
ONO	CU2P	SW	0.007	1.571	CU2P	ND	CON	0.200	2.094
OW	CU2P	OW	0.002	3.141	CU2P	ND	CT	0.200	2.094
OW	CU2P	SW	0.007	1.571	NI2T	ND	CON	0.200	2.094
SW	CU2P	SW	0.013	1.571	NI2T	ND	CT	0.200	2.094
ND	CU2T	ND	0.013	1.571	CI	NI	CT	0.450	2.094
ND	CU2T	NP	0.013	1.571	CI	NI	CU2P	0.100	2.356
NP	CU2T	NP	0.013	1.571	CT	NI	CI	0.450	2.007
NP	FE3L	NP	0.042	1.571	CT	NI	CU2P	0.200	1.920
NP	FE3L	NT	0.042	1.571	CU1	NI	CI	0.100	2.356
NT	FE3L	NT	0.042	1.571	CU1	NI	CT	0.100	1.912
CB	N*	CK	0.970	1.859	NP	NI2	NT	0.025	1.571
CB	N*	CT	0.970	2.196	NT	NI2	NT	0.025	1.571
CK	N*	CT	0.970	2.248	NP	NI2C	NP	0.025	1.571
C	NA	CA	0.970	2.206	NP	NI2C	NT	0.025	1.571
C	NA	H	0.490	2.039	NP	NI2C	OC	0.026	1.571

atom 1	atom 2	atom 3	k [mdyn/rad]	a_0 [rad]	atom 1	atom 2	atom 3	k [mdyn/rad]	a_0 [rad]
NT	NI2C	NT	0.025	1.571	CO2	NT	CT	0.200	1.920
NT	NI2C	OC	0.026	1.571	CO2	NT	H	0.100	1.915
OC	NI2C	OC	0.027	1.571	CO3	NT	CA	0.200	1.920
NP	NI2P	NP	0.025	1.571	CO3	NT	CT	0.200	1.920
NP	NI2P	NT	0.025	1.571	CO3	NT	H	0.100	1.915
NT	NI2P	NT	0.025	1.571	CO3C	NT	CA	0.200	1.920
ND	NI2T	ND	0.025	1.571	CO3C	NT	CT	0.200	1.920
NT	NI2T	ND	0.025	1.571	CO3C	NT	H	0.100	1.915
NT	NI2T	NT	0.025	1.571	CR3	NT	CT	0.200	1.920
CT	NOO	ONO	0.450	2.059	CR3	NT	H	0.100	1.915
ONO	NOO	ONO	0.650	2.164	CT	NT	CT	0.450	1.911
CA	NP	CA	0.970	2.094	CT	NT	H	0.450	1.909
CA	NP	CFC	0.970	2.094	CU1	NT	CT	0.200	1.920
CFC	NP	CFC	0.970	2.094	CU1	NT	H	0.100	1.915
CO2	NP	CA	0.200	2.094	CU2	NT	CA	0.200	1.920
CO2	NP	CFC	0.200	2.094	CU2	NT	CT	0.200	1.920
CO3	NP	CA	0.200	2.094	CU2	NT	H	0.100	1.915
CO3	NP	CFC	0.200	2.094	CU2C	NT	CA	0.200	1.920
CO3	NP	CT	0.200	2.094	CU2C	NT	CT	0.200	1.920
CO3C	NP	CA	0.200	2.094	CU2C	NT	H	0.100	1.915
CO3C	NP	CFC	0.200	2.094	CU2P	NT	CA	0.200	1.920
CO3C	NP	CT	0.200	2.094	CU2P	NT	CT	0.200	1.920
CR3	NP	CA	0.200	2.094	CU2P	NT	H	0.100	1.915
CR3	NP	CFC	0.200	2.094	FE3L	NT	CT	0.200	1.920
CU2	NP	CA	0.200	2.094	FE3L	NT	H	0.100	1.915
CU2	NP	CFC	0.200	2.094	H	NT	H	0.330	1.902
CU2C	NP	CA	0.200	2.094	NI2	NT	CT	0.200	1.920
CU2C	NP	CFC	0.200	2.094	NI2	NT	H	0.100	1.915
CU2P	NP	CA	0.050	2.094	NI2C	NT	CT	0.200	1.920
CU2P	NP	CFC	0.200	2.094	NI2C	NT	H	0.100	1.915
FE3L	NP	CA	0.200	2.094	NI2P	NT	CT	0.200	1.920
FE3L	NP	CFC	0.200	2.094	NI2P	NT	H	0.100	1.915
NI2C	NP	CA	0.200	2.094	NI2T	NT	CT	0.200	1.920
NI2C	NP	CFC	0.200	2.094	NI2T	NT	H	0.100	1.915
NI2P	NP	CA	0.200	2.094	PT2	NT	CT	0.200	1.920
NI2P	NP	CFC	0.200	2.094	PT2	NT	H	0.100	1.915
CA	NT	CT	0.450	1.911	RH3	NT	CT	0.200	1.920
CA	NT	H	0.450	1.909	RH3	NT	H	0.100	1.915

atom 1	atom 2	atom 3	k [mdyn/rad]	a_0 [rad]	atom 1	atom 2	atom 3	k [mdyn/rad]	a_0 [rad]
ZN2	NT	CT	0.200	1.920	CU2C	OP	H	0.100	1.915
ZN2	NT	H	0.100	1.915	CU2P	OP	CU2P	0.100	1.745
CO3	OC	CCO	0.050	2.094	CU2P	OP	H	0.100	1.915
CO3C	OC	CCO	0.050	2.094	H	OP	H	0.320	1.902
CR3	OC	CCO	0.400	1.998	CT	OR	CT	0.750	1.911
CU2C	OC	CCO	0.050	2.094	P	OS	CT	1.386	2.065
CU2P	OC	CCO	0.050	2.094	CU2	OW	H	0.100	1.915
CU2P	OC	CU2P	0.100	1.830	CU2C	OW	H	0.100	1.915
FE3H	OC	CCO	0.750	2.030	CU2P	OW	CU2P	0.100	1.745
MN3	OC	CCO	0.300	2.028	CU2P	OW	H	0.100	1.915
NI2C	OC	CCO	0.050	2.094	H	OW	H	0.320	1.902
TI3	OC	CCO	0.450	2.062	TI4	OW	CT	0.050	1.915
V3	OC	CCO	0.500	2.030	CO3	OX	OX	0.500	1.911
CO3C	OCC	COC	0.600	2.094	CU2P	OX	OX	0.500	1.911
TI4	OCC	COC	0.600	2.094	O2	P	OS	1.386	2.003
TI4	OCCT	COC	0.600	2.094	OH	P	O2	0.624	2.011
P	OH	H	0.624	2.039	OH	P	OS	0.624	1.764
CU2	ONO	NOO	0.320	2.094	OS	P	OS	0.624	1.716
CU2C	ONO	NOO	0.320	2.094	CT	SW	CT	0.500	1.740
CU2P	ONO	NOO	0.320	2.094	CU2	SW	CT	0.100	1.920
CT	OP	CU2P	0.200	2.094	CU2C	SW	CT	0.100	1.920
CU2	OP	H	0.100	1.915	CU2P	SW	CT	0.100	1.920

4.4 Torsion Interactions

atom 1	atom 2	atom 3	atom 4	k [mdyn/rad]	multiplicity	t_0 [rad]
**	C	CB	**	0.007	2.000	1.571
**	C	NA	**	0.009	2.000	1.571
**	CA	CA	**	0.050	2.000	1.571
**	CA	CFC	**	0.050	2.000	1.571
**	CA	CON	**	0.003	2.000	1.571
**	CA	CT	**	0.005	6.000	0.524
**	CA	NA	**	0.010	2.000	1.571
**	CA	NP	**	0.050	2.000	1.571
**	CA	NT	**	0.001	6.000	0.524
**	CA	OW	**	0.150	3.000	4.680

atom 1	atom 2	atom 3	atom 4	k [mdyn/rad]	multiplicity	t$_0$ [rad]
**	CA	CCO	**	0.005	2.000	1.571
**	CAH	CA	**	0.065	2.000	1.571
**	CAH	CAH	**	0.015	2.000	1.571
**	CAH	CI	**	0.025	2.000	1.571
**	CAH	CT	**	0.001	6.000	0.524
**	CAH	NAH	**	0.009	2.000	1.571
**	CAH	NAX	**	0.003	2.000	1.571
**	CAH	NI	**	0.003	2.000	1.571
**	CB	CB	**	0.028	2.000	1.571
**	CB	N*	**	0.011	2.000	1.571
**	CB	NA	**	0.014	2.000	1.571
**	CB	NB	**	0.009	2.000	1.571
**	CCC	COC	**	0.030	2.000	1.571
**	CCO	CCO	**	0.000	2.000	3.097
**	CCO	CT	**	0.001	6.000	0.524
**	CCO	OC	**	0.005	2.000	1.571
**	CFC	CFC	**	0.030	2.000	1.571
**	CFC	COC	**	0.030	2.000	1.571
**	CFC	NP	**	0.003	2.000	1.571
**	CI	NT	**	0.001	6.000	0.524
**	CI	CT	**	0.001	6.000	0.524
**	CI	CA	**	0.010	6.000	1.571
**	CK	N*	**	0.011	2.000	1.571
**	CK	N*	**	0.011	2.000	1.571
**	CK	NB	**	0.034	2.000	1.571
**	CK	NB	**	0.034	2.000	1.571
**	COC	CT	**	0.005	6.000	0.524
**	COC	OCC	**	0.030	2.000	1.571
**	COC	OCCT	**	0.030	2.000	1.571
**	CON	CT	**	0.001	6.000	0.524
**	CON	ND	**	0.005	2.000	1.571
**	CT	CT	**	0.002	3.000	0.000
**	CT	NAH	**	0.001	6.000	0.524
**	CT	ND	**	0.001	6.000	0.524
**	CT	NOO	**	0.003	6.000	0.524
**	CT	NT	**	0.001	3.000	0.000
**	CT	OP	**	0.001	3.000	0.000
**	CT	OW	**	0.008	3.000	0.000

atom 1	atom 2	atom 3	atom 4	k [mdyn/rad]	multiplicity	t_0 [rad]
**	CT	SW	**	0.001	3.000	0.000
**	CTO	CTO	**	0.011	3.000	0.000
**	CTO	CTOC	**	0.011	3.000	0.000
**	CTOC	CTOC	**	0.011	3.000	0.000
**	CU2P	NAH	**	0.005	2.000	0.262
**	CU2P	NP	**	0.005	2.000	0.262
**	NAH	NAH	**	0.020	2.000	1.571
**	NAH	NAX	**	0.065	2.000	1.571
**	NI	CI	**	0.025	2.000	1.571
**	NI	CI	**	0.025	2.000	1.571
**	NI	CT	**	0.000	2.000	0.524
**	O2	P	**	0.052	3.000	0.390
**	OH	P	**	0.052	3.000	0.635
**	OR	CT	**	0.008	3.000	0.000
**	OS	CT	**	0.080	3.000	0.050
**	OS	P	**	0.052	3.000	0.390
**	OXCO	OXCO	**	0.900	2.000	0.000
**	OXCU	OXCU	**	0.900	2.000	0.000
**	PT2	NB	**	0.000	2.000	2.094
**	PT2	NT	**	0.000	2.000	2.094
**	SAH	CAH	**	0.015	2.000	1.571

4.5 Non-bonded Interactions

atom 1	r_{vdW} [Å]	ϵ	atom 1	r_{vdW} [Å]	ϵ	atom 1	r_{vdW} [Å]	ϵ
C	1.900	0.044	CU2	0.000	0.000	O	1.700	0.055
C3	1.900	0.044	CU2C	0.000	0.000	OC	1.700	0.055
CA	1.900	0.044	CU2P	0.000	0.000	OCC	1.700	0.055
CAH	1.900	0.044	FE3L	0.000	0.000	OCCT	1.700	0.055
CB	1.900	0.044	H	1.440	0.024	OCO	1.700	0.055
CCC	1.900	0.044	N*	1.800	0.052	ONO	1.700	0.055
CCO	1.900	0.044	N3	1.800	0.052	OP	1.700	0.055
CFC	1.900	0.044	NA	1.800	0.052	OR	1.700	0.055
CI	1.900	0.044	NAH	1.800	0.052	OW	1.700	0.055
CK	1.900	0.044	NB	1.800	0.052	OXCU	1.700	0.055
CO2	0.000	0.000	ND	1.800	0.050	PT2	1.650	0.300

atom 1	r_vdW [Å]	ϵ	atom 1	r_vdW [Å]	ϵ	atom 1	r_vdW [Å]	ϵ
CO3	0.000	0.000	NI	1.800	0.050	PT4	0.000	0.000
CO3C	0.000	0.000	NI2	0.000	0.000	RH3	0.000	0.000
COC	1.900	0.044	NI2C	0.000	0.000	SAH	2.000	0.185
CON	1.900	0.044	NI2P	0.000	0.000	SW	2.000	0.185
CR2	0.000	0.000	NOO	1.800	0.050	TI4	0.000	0.000
CR3	0.000	0.000	NP	1.800	0.050	ZN2	0.000	0.000
CT	1.900	0.044	NT	1.800	0.050			

4.6 Out-of-plane Interactions

atom 1	atom 2	atom 3	atom 4	k [mdyn/rad]	atom 1	atom 2	atom 3	atom 4	k [mdyn/rad]
CA	CAH	CA	H	2.000	CCO	OC	OC	OC	0.500
CA	NP	CA	H	2.000	CI	NI	CAH	H	1.500
CA	NP	CA	CU2P	2.000	CO2T	ND	NI	NA	0.070
CAH	NAH	CAH	CU2P	2.000	COC	CCC	OCC	CFC	0.500
CA	NP	CT	H	2.000	COC	CCC	OCC	CT	0.500
CA	NP	CA	CCO	2.000	COC	CCC	OCCT	CFC	0.500
CAH	CAH	CA	NAH	2.000	COC	CCC	OCCT	CT	0.500
CAH	CAH	CAH	H	2.000	CCO	CA	OCO	OC	0.120
CAH	CAH	NAH	CT	2.000	CON	CT	OCO	ND	0.120
CAH	CAH	NAH	CI	2.000	CU2T	ND	NI	NA	0.050
CAH	CAH	NAH	H	2.000	NI2T	ND	NI	NA	0.070
CAH	CAH	NAX	CT	2.000	NOO	CT	ONO	ONO	0.120
CAH	CAH	SAH	H	2.000	OW	CT	CU2P	CU2P	0.500
CAH	NAH	NAH	CI	2.000	PT2	NB	NB	NT	1.000
CAH	NAH	NAH	H	2.000	PT2	NB	NT	NB	1.000
CAH	NAH	NAH	CT	2.000	PT2	NB	NT	NT	1.000
CCC	COC	COC	H	0.500	PT2	NT	NB	NB	1.000
CCO	CT	OCO	OC	0.120	PT2	NT	NT	NB	1.000

Bibliography

[1] Sessoli, R.; Gatteschi, D.; Caneschi, A.; Novak, M. A. *Nature (London)* **1993**, *365*, 141.

[2] Thomas, L.; Lionti, F.; Ballou, R.; Gatteschi, D.; Sessoli, R.; Barbara, B. *Nature (London)* **1996**, *383*, 145.

[3] Friedman, J. R.; Sarachik, M. P.; Tejada, J.; Ziolo, R. *Phys. Rev. Lett.* **1996**, *76*, 3830.

[4] Evangelisti, M.; Candini, A.; Ghirri, A.; Affronte, M.; Brechin, E. K.; McInnes, E. J. L. *Appl. Phys. Lett.* **2005**, 87.

[5] Karotsis, G.; Kennedy, S.; Teat, S. J.; Beavers, C. M.; Fowler, D. A.; Morales, J. J.; Evangelisti, M.; Dalgarno, S. J.; Brechin, E. K. *J. Am. Chem. Soc.* **2010**, *132*, 12983.

[6] Leuenberger, M. N.; Loss, D. *Nature* **2001**, *410*, 789.

[7] Wang, Y.; Li, W.; Zhou, S.; Kong, D.; Yang, H.; Wu, L. *Chem. Commun.* **2011**, *47*, 3541.

[8] Lin, P.-H.; Burchell, T. J.; Ungur, L.; Chibotaru, L. F.; Wernsdorfer, W.; Murugesu, M. *Angew. Chem. Int. Ed.* **2009**, *48*, 9489.

[9] Burton, V. J.; Deeth, R. J.; Kemp, C. M.; Gilbert, P. J. *J. Am. Chem. Soc.* **1995**, *117*, 8407.

[10] Burton, V. J.; Deeth, R. J. *J. Chem. Soc., Chem. Commun.* **1995**, 573.

[11] Comba, P.; Hambley, T. *Molecular modeling of inorganic compounds*; Wiley-VCH, Weinheim, 1995.

[12] Comba, P.; Hambley, T.; Martin, B. *Molecular modeling of inorganic compounds*; Wiley-VCH, Weinheim, 2009.

[13] Jahn, H. A.; Teller, E. *Proc. Roy. Soc. (London)* **1937**, *A161*, 220.

[14] Schrödinger, E. *Phys. Rev.* **1926**, *28*, 1049–1070.

[15] A. Szabo, N. O. *Modern Quantum Chemistry*; Mc Graw-Hill Publishing Company, 1982.

[16] Born, M.; Oppenheimer, J. R. *Ann. Physik* **1927**, *84*, 457.

[17] Born, M. *Nachr. Akad. Wiss. Göttingen Math. Phys. Kl.* **1951**, *6*, 1.

[18] Jensen, F. *Introduction to Computational Chemistry*; Wiley, New York, 1999.

[19] Pauli, W. *Z. Phys.* **1925**, *31*, 765.

[20] Slater, J. C. *Phys. Rev.* **1929**, *34*, 1293.

[21] Slater, J. C. *Phys. Rev.* **1930**, *36*, 57.

[22] Boys, S. F. *Proc. R. Soc. (London) A* **1950**, *200*, 542.

[23] Hehre, W. J.; Ditchfield, R.; Pople, J. A. *J. Chem. Phys.* **1972**, *56*, 2257.

[24] Schäfer, A.; Horn, H.; Ahlrichs, R. *J. Chem. Phys.* **1992**, *97*, 2571.

[25] Schäfer, A.; Huber, C.; Ahlrichs, R. *J. Chem. Phys.* **1994**, *100*, 5829.

[26] Neese, F. *ORCA, version 2.6 (Revision 04), an ab initio, density functional and semiempirical program package*; Max-Planck-Institut für Bioanorganische Chemie: Mülheim an der Ruhr, Germany, 2005.

[27] Frenking, G.; Antes, I.; Böhme, M.; Dapprioh, S.; Ehlers, A. W.; Jonas, V.; Nauhaus, A.; Otto, M.; Stegmann, R.; Veldkamp, A.; Vyboishchikov, S. F. *Rev. Comput. Chem.* **1996**, *8*, 63.

[28] Cundari, T. R.; Benson, M. T.; Lutz, M. L.; Sommerer, S. O. *Rev. Comput. Chem.* **1996**, *8*, 145.

[29] Hay, P. J.; Wadt, W. R. *J. Chem. Phys.* **1985**, *82*, 299.

[30] The LACV3P basis set is a triple-zeta contraction of the LACVP basis set developed and tested at Schrödinger, Inc.

[31] Neese, F. *Coord. Chem. Rev.* **2009**, *253*, 526.

[32] Koch, W.; Holthausen, M. C. *A Chemist's Guide to Density Functional Theory*; Wiley-VCH, Weinheim, 2000.

[33] Hohenberg, P.; Kohn, W. *Phys. Rev.* **1964**, *136*, B864.

[34] Fermi, E. *Rend. Accad. Naz. Lincei* **1927**, *6*, 602.

[35] Thomas, L. H. *Proc. Cambridge Phil. Soc.* **1927**, *23*, 542.

[36] Block, F. *Z. Physik* **1929**, *57*, 545.

[37] Dirac, P. A. M. *Proc. Cambridge Phil. Soc.* **1930**, *26*, 376.

[38] Kohn, W.; Sham, L. J. *Phys. Rev.* **1965**, *140*, A1133.

[39] Slater, J. C. *Phys. Rev.* **1951**, *81*, 385.

[40] Vosko, S. H.; Wilk, L.; Nusair, M. *Can. J. Phys.* **1980**, *58*, 1200.

[41] Perdew, J. P.; Wang, Y. *Phys. Rev. B* **1992**, *45*, 13244.

[42] Perdew, J. P.; Wang, Y. *Phys. Rev. B* **1986**, *33*, 8800.

[43] Becke, A. D. *Phys. Rev. A* **1988**, *38*, 3098.

[44] Lee, C.; Yang, W.; Parr, R. G. *Phys. Rev. B* **1988**, *37*, 785.

[45] Perdew, J. P. *Phys. Rev. B* **1986**, *33*, 8822.

[46] Perdew, J. P. *Phys. Rev. B* **1986**, *34*, 7406.

[47] Perdew, J. P.; Chevary, J. A.; Vosko, S. H.; Jackson, K. A.; Pederson, M. R.; Singh, D. J.; Fiolhais, C. *Phys. Rev. B* **1992**, *46*, 6671.

[48] Becke, A. D. *J. Chem. Phys.* **1992**, *98*, 1372.

[49] Becke, A. D. *J. Chem. Phys.* **1992**, *96*, 2155.

[50] Becke, A. D. *J. Chem. Phys.* **1992**, *97*, 9713.

[51] Becke, A. D. *J. Chem. Phys. B* **1993**, *98*, 5648.

[52] Adamo, C.; Barone, V. *Chem. Phys. Lett.* **1997**, *274*, 242.

[53] Reiher, M.; Salomon, O.; Hess, B. A. *Theor. Chem. Acc.* **2001**, *107*, 48.

[54] Salomon, O.; Reiher, M.; Hess, B. A. *J. Chem. Phys.* **2002**, *117*, 4729.

[55] Saunders, M.; Jarret, R. M. *J. Comp. Chem.* **1986**, *7*, 578.

[56] Bol, J. E.; Buning, C.; Comba, P.; Reedijk, J.; Ströhle, M. *J. Comput. Chem.* **1998**, *19*, 512.

[57] Comba, P.; Hilfenhaus, P.; Karlin, K. D. *Inorg. Chem.* **1997**, *36*, 2309.

[58] Comba, P.; Gloe, K.; Inoue, K.; Krüger, T.; Stephan, H.; Yoshizuka, K. *Inorg. Chem.* **1998**, *37*, 3310.

[59] Comba, P.; Gavrish, S. P.; Hay, R. W.; Hilfenhaus, P.; Lampeka, Y. D.; Lightfoot, P.; Peters, A. *Inorg. Chem.* **1999**, *38*, 1416.

[60] Comba, P.; Kerscher, M.; Merz, M.; Müller, V.; Pritzkow, H.; Remenyi, R.; Schiek, W.; Xiong, Y. *Chem. Eur. J.* **2002**, *8*, 5750.

[61] Born, K.; Comba, P.; Ferrari, R.; Lawrance, G. A.; Wadepohl, H. *Inorg. Chem.* **2007**, *46*, 458.

[62] Hill, T. *J. Chem. Phys.* **1948**, *16*, 399.

[63] Lennard-Jones, J. E. *Proc. R. Soc. London Ser. A* **1924**, *106*, 463.

[64] Rappé, A. K.; Casewit, C. J.; Colwell, K. S.; Goddard, W. A., III.; Skiff, W. M. *J. Am. Chem. Soc.* **1992**, *114*, 10024.

[65] Rappé, A. K.; Casewit, C. J.; Colwell, K. S. *J. Am. Chem. Soc.* **1992**, *114*, 10046.

[66] Rappé, A. K.; Colwell, K. S.; Casewit, C. J. *Inorg. Chem.* **1993**, *32*, 3438.

[67] Bleaney, B.; Bowers, K. D. *Proc. R. Soc. London A* **1952**, *214*, 451.

[68] *Magneto-structural correlations in exchange coupled systems*; Willett, R. D., Gatteschi, D., Kahn, O., Eds.; Reidel Publishing, Dordrecht, 1985.

[69] Gatteschi, D.; Guillou, O.; Zanchini, C.; Sessoli, R.; Kahn, O.; Verdaguer, M.; Pei, Y. *Inorg. Chem.* **1989**, *28*, 287.

[70] Yee, G. T.; Manriquez, J. M.; Dixon, D. A.; McLean, R. S.; Groski, D. M.; Flippen, R. B.; Narayan, K. S.; Epstein, A. J.; Miller, J. S. *Adv. Mater.* **1991**, *3*, 309.

[71] Weiss, P.; Foëx, G. *Le Magnétisme*; Armand Colin, Paris, 1926.

[72] Kahn, O. *Molecular Magnetism*; Wiley & Sons, Inc.: New York, 1993.

[73] Pascal, P.; Pacault, A.; Hoarau, J. *Comptes Rendus des Séances de L'Académie des Sciences* **1951**, *233*, 1078.

[74] van Vleck, J. H. *The Theory of Electric and Magnetic Susceptibility*; Oxford University Press: Oxford, 1932.

[75] Curie, P. *Ann. Chim. Phys.* **1895**, *5*, 289.

[76] *Molecular Nanomagnets*; Gatteschi, D., Sessoli, R., Villain, J., Eds.; Oxford University Press, Oxford, 2006.

[77] Rudra, I.; Wu, Q.; Voorhis, T. *J. Chem. Phys.* **2006**, *124*, 024103.

[78] Aizman, A.; Case, D. A. *J. Am. Chem. Soc.* **1982**, *104*, 3269.

[79] Noodleman, L. *J. Chem. Phys.* **1981**, *74*, 5737.

[80] Zhang, Y. Q.; Luo, C.-L. L.; Yu, Z. *New J. Chem.* **2005**, *29*, 1285.

[81] Ciofini, I.; Daul, C. A. *Coord. Chem. Rev.* **2003**, *238–239*, 187.

[82] Barclay, G. A.; Harris, C. M.; Hoskins, B. F.; Kokot, E. *Proc. Chem. Soc.* **1961**, 264.

[83] Jczowska-Trzebiatowska, B.; Jczierska, J.; Baranowski, J. *Chem. Phys. Lett.* **1977**, *52*, 590.

[84] Heisenberg, W. *Z. Phys.* **1926**, *38*, 411.

[85] Heisenberg, W. *Z. Phys.* **1928**, *49*, 619.

[86] Dirac, P. A. M. *Proc. R. Soc. London* **1929**, *A123*, 714.

[87] Neese, F. *J. Phys. Chem. Solids* **2004**, 781.

[88] Yamaguchi, K.; Takahara, Y.; Fueno, T. In *Applied Quantum Chemistry*; Smith, V., Ed.; V. Reidel, Dordrecht, 1986; p 155.

[89] Soda, T.; Kitagawa, Y.; Onishi, T.; Takano, Y.; Shigeta, Y.; Nagao, H.; Yoshika, Y.; Yamaguchi, K. *Chem. Phys. Lett.* **2000**, *319*, 223.

[90] Ruiz, E.; Alvarez, S.; Cano, J.; Polo, V. *J. Chem. Phys.* **2005**, *123*, 164110.

[91] Frisch, M. J. et al. *Gaussian 03 (Revision B.03)*; Gaussian Inc., Wallingford, CT, 2003.

[92] Schrödinger, *Jaguar 6.5*; Schrödinger LLC, New York, NY, 2005.

[93] Perdew, J. P.; Burke, K.; Wang, Y. *Phys. Rev. B* **1996**, *54*, 16533.

[94] Miehlich, B.; Savin, A.; Stoll, H.; Preuss, H. *Chem. Phys. Lett.* **1989**, *157*, 200.

[95] Perdew, J. P.; Burke, K.; Ernzerhof, M. *Phys. Rev. Lett.* **1996**, *77*, 3865.

[96] Binkley, J. S.; Pople, J. A.; Hehre, W. J. *J. Am. Chem. Soc.* **1980**, *102*, 939.

[97] Gordon, M. S.; Binkley, J. S.; Pople, J. A.; Pietro, W. J.; Hehre, W. J. *J. Am. Chem. Soc.* **1982**, *104*, 2797.

[98] Pietro, W. J.; Francl, M. M.; Hehre, W. J.; Defrees, D. J.; Pople, J. A.; Binkley, J. S. *J. Am. Chem. Soc.* **1982**, *104*, 5039.

[99] Dobbs, K. D.; Hehre, W. J. *J. Comput. Chem.* **1986**, *7*, 359.

[100] Dobbs, K. D.; Hehre, W. J. *J. Comput. Chem.* **1987**, *8*, 861.

[101] Dobbs, K. D.; Hehre, W. J. *J. Comput. Chem.* **1987**, *8*, 880.

[102] Dunning, T. H., Jr. *J. Chem. Phys.* **1979**, *53*, 2823.

[103] Dunning, T. H., Jr.; Hay, P. J. In *Modern Theoretical Chemistry*; Schaefer, H. F., III, Ed.; Plenum Press: New York, 1976; pp 1–28.

[104] Magnusson, E.; Schaefer, H. F., III *J. Chem. Phys.* **1985**, *83*, 5721.

[105] Ditchfield, R.; Hehre, W. J.; Pople, J. A. *J. Chem. Phys.* **1971**, *54*, 724.

[106] Hariharan, P. C.; Pople, J. A. *Mol. Phys.* **1974**, *27*, 209.

[107] Gordon, M. S. *Chem. Phys. Lett.* **1980**, *76*, 163.

[108] Hariharan, P. C.; Pople, J. A. *J. Chem. Phys.* **1973**, *82*, 213.

[109] Blaudeau, J.-P.; McGrath, M. P.; Curtiss, L. A.; Radom, L. *J. Chem. Phys.* **1997**, *107*, 5016.

[110] Francl, M. M.; Pietro, W. J.; Hehre, W. J.; Binkley, J. S.; DeFrees, D. J.; Pople, J. A.; Gordon, M. S. *J. Chem. Phys.* **1982**, *77*, 3654.

[111] Binning, R. C., Jr.; Curtiss, L. A. *J. Comput. Chem.* **1990**, *11*, 1206.

[112] Rassolov, V. A.; Pople, J. A.; Ratner, M. A.; Windus, T. L. *J. Chem. Phys.* **1998**, *109*, 1223.

[113] Rassolov, V. A.; Ratner, M. A.; Pople, J. A.; Redfern, P. C.; Curtiss, L. A. *J. Comput. Chem.* **2001**, *22*, 976.

[114] Frisch, M. J. et al. *Gaussian 09 (Revision A.02)*; Gaussian Inc., Wallingford, CT, 2009.

[115] Ruiz, E. *Struct. Bonding (Berlin)* **2004**, *113*, 71.

[116] Sinnecker, S.; Neese, F.; Noodleman, L.; Lubitz, W. *J. Am. Chem. Soc.* **2004**, *126*, 2613.

[117] Zhang, Y.-Q.; Luo, C.-L. *Eur. J. Inorg. Chem.* **2008**, 2199.

[118] Alborés, P.; Slep, L. D.; Weyhermüller, T.; Rentschler, E.; Baraldo, L. M. *Dalton. Trans.* **2006**, 948.

[119] Comba, P.; Helmle, S.; Wadepohl, H. Unpublished results.

[120] Atanasov, M.; Busche, C.; Comba, P.; Hallak, F. E.; Martin, B.; Rajaraman, G.; van Slageren, J.; Wadepohl, H. *Inorg. Chem.* **2008**, *47*, 8112.

[121] Wang, C.-F.; Zuo, J.-L.; Bartlett, B. M.; Song, Y.; Long, J. R.; You, X.-Z. *J. Am. Chem. Soc.* **2006**, *128*, 7162.

[122] Song, H. H.; Zhengn, L. M.; Liu, Y. J.; Xin, X. Q.; Jacobson, A. J.; Decurtins, S. *J. Chem. Soc., Dalton Trans.* **2001**, 3274.

[123] Felthouse, T. R.; Laskowski, E. D.; Hendrickson, D. N. *Inorg. Chem.* **1977**, *16*, 1077.

[124] Mathoniere, C.; Kahn, O.; Daran, J.; Hilbig, H.; Kohler, F. *Inorg. Chem.* **1993**, *32*, 4057.

[125] Sun, Y.; Melchior, M.; Summers, D. A.; Thompson, R. C.; Rettig, S. J.; Orvig, C. *Inorg. Chem.* **1998**, *37*, 3119.

[126] Haselhorst, G.; Wieghardt, K.; Keller, S.; Schrader, B. *Inorg. Chem.* **1993**, *32*, 520.

[127] Julve, M.; Lloret, F.; Faus, F.; Verdaguer, M.; Caneschi, A. *Inorg. Chem.* **1995**, *34*, 157.

[128] Birkelbach, F.; Winter, M.; Florke, U.; Haupt, H. J.; Butzlaff, C.; Lengen, M.; Bill, E.; Trautwein, A. X.; Wieghardt, K.; Chaudhuri, P. *Inorg. Chem.* **1994**, *33*, 3990.

[129] Rodríguez-Fortea, A.; Alemany, P.; Alvarez, S.; Ruiz, E. *Eur. J. Inorg. Chem.* **2004**, 143.

[130] Wieghardt, K.; Bossek, U.; Volckmar, K.; Swiridoff, W.; Weiss, J. *Inorg. Chem.* **1984**, *23*, 1387.

[131] Ceccato, A. S.; Neves, A.; d. Brito, M. A.; Drechsel, S. M.; Mangrich, A. S.; Werner, R.; Haase, W.; Bortoluzzi, A. *J. Chem. Soc.,Dalton Trans.* **2000**, *23*, 1567.

[132] Dean, N. S.; Bond, M. R.; O'Connor, C. J.; Carrano, C. J. *Inorg. Chem.* **1996**, *35*, 7643.

[133] Burojevic, S.; Shweky, I.; Bino, A.; Summers, D. A.; Thompson, R. C. *Inorg. Chim. Acta* **1996**, *251*, 75.

[134] Neves, A.; Wieghardt, K.; Nuber, B.; Weiss, J. *Inorg. Chim. Acta* **1988**, *150*, 183.

[135] Das, R.; Nanda, K. K.; Mukherjee, A. K.; Helliwell, M.; Nag, K. *J. Chem. Soc., Dalton Trans.* **1993**, 2241.

[136] Khan, M. I.; Chang, Y.-D.; Chen, Q.; Salta, J.; Lee, Y.-S.; O'Connor, C. J.; Zubieta, J. *Inorg. Chem.* **1994**, *33*, 6340.

[137] Plass, W. *Angew. Chem., Int. Ed. Engl.* **1996**, *35*, 627.

[138] Rodríguez-Fortea, A.; Alemany, P.; Alvarez, S.; Ruiz, E.; Scuiller, A.; Decroix, C.; Marvaud, V.; Vaissermann, J.; Verdaguer, M.; Rosenman, I.; Julve, M. *Inorg. Chem.* **2001**, *40*, 5868.

[139] Atanasov, M.; Comba, P.; Hausberg, S.; Martin, B. *Coord. Chem. Rev.* **2009**, *253*, 2296–2305.

[140] Atanasov, M.; Comba, P.; Daul, C. A. *J. Phys. Chem. A* **2006**, *110*, 13332.

[141] Atanasov, M.; Comba, P.; Daul, C. A. *Inorg. Chem.* **2008**, *47*, 2449.

[142] Atanasov, M.; Comba, P. In *Structure and Function*; Comba, P., Ed.; Springer Netherlands, 2010; pp 53–85.

[143] Bethe, H. *Ann. Phys.* **1929**, *3*, 133.

[144] van Vleck, J. H. *Phys. Rev.* **1932**, *41*, 208.

[145] Figgis, B. N.; Hitchman, M. A. *Ligand Field Theory and Its Applications*; Wiley-VCH, New York, 2000.

[146] Ballhausen, C. J.; Gray, H. B. *Inorg. Chem.* **1962**, *1*, 111.

[147] Hund, F. *Z. Phys.* **1925**, *33*, 345.

[148] Hund, F. *Z. Phys.* **1925**, *34*, 296.

[149] *Linienspektren und Periodisches System der Elemente*; Hund, F., Ed.; Springer, Berlin, 1927.

[150] Tanabe, Y.; Sugano, S. *J. Phys. Soc. Japan* **1954**, *9*, 753.

[151] Tanabe, Y.; Sugano, S. *J. Phys. Soc. Japan* **1954**, *9*, 766.

[152] Tanabe, Y.; Sugano, S. *J. Phys. Soc. Japan* **1954**, *11*, 864.

[153] Schäffer, C. E.; Jørgensen, C. K. *Mol. Phys.* **1965**, *9*, 401.

[154] Comba, P. *Inorg. Chem.* **1994**, *33*, 4577.

[155] Glerup, J.; Monsted, O.; Schäffer, C. E. *Inorg. Chem.* **1980**, *19*, 2855.

[156] Gerloch, M.; Harding, J. H.; Woolley, R. G. *Struct. Bonding (Berlin)* **1981**, *46*, 1.

[157] Vanquickenborne, L. G.; Coussens, B.; Postelmans, D.; Ceulemans, A.; Pierloot, K. *Inorg. Chem.* **1991**, *30*, 2978.

[158] Bernhardt, P. V.; Comba, P. *Inorg. Chem.* **1993**, *32*, 2798.

[159] Wolfsberg, M.; Helmholtz, L. *J. Chem. Phys.* **1952**, *20*, 837.

[160] Comba, P.; hambley, T. W.; Hitchman, M. A.; Stratemeier, H. *Inorg. Chem.* **1995**, *34*, 3903.

[161] Schäffer, C. E. *Structure and Bonding* **1968**, *5*, 68.

[162] Larsen, E.; Mar, G. N. L. *J. Chem. Educ.* **1974**, *51*, 633.

[163] Gerloch, M.; Woolley, R. G. *Prog. Inorg. Chem.* **1983**, *31*, 371.

[164] Gerloch, M. *Magnetism and Ligand Field Analysis*; Cambridge University Press, New York, 1983.

[165] Deeth, R. J.; Kemp, C. M.; Gilbert, P. J. *Inorg. Biochem.* **1991**, *43*, 222.

[166] Deeth, R. J.; Anastasi, A.; Diedrich, C.; Randell, K. *Coord. Chem. Rev.* **2009**, *253*, 795.

[167] Deeth, R. J. *Chem. Commun.* **2006**, 2551.

[168] Bentz, A.; Comba, P.; Deeth, R. J.; Kerscher, M.; Seibold, B.; Wadepohl, H. *Inorg. Chem.* **2008**, *47*, 9518.

[169] Deeth, R. J.; Foulis, D. L.; Williams-Hubbard, B. J. *Dalton. Trans.* **2003**, 3949.

[170] Diedrich, C.; Deeth, R. J. *Inorg. Chem.* **2008**, *47*, 2494.

[171] Deeth, R. J.; Fey, N.; Williams-Hubbard, B. J. *J. Comput. Chem.* **2005**, *26*, 123.

[172] Foulis, D. L.; Deeth, R. J. *Phys. Chem. Chem. Phys.* **2002**, *4*, 4292.

[173] *MOE Molecular Operating Environment*; Chemical Computing Group, Montreal, 2010.

[174] Woodley, S. M.; Battle, P. D.; Catlow, C. R. A.; Gale, J. D. *J. Phys. Chem. B* **2001**, *105*, 6824.

[175] Piquemal, J. P.; Williams-Hubbard, B.; Fey, N.; Deeth, R. J.; Gresh, N.; Giessner-Prettre, C. *J. Comput. Chem.* **2003**, *24*, 1963.

[176] Comba, P.; Hambley, T. W.; Ströhle, M. *Helv. Chim. Acta* **1995**, *78*, 2042.

[177] Comba, P.; Martin, B. *The Momec Homepage*, 2011. `http://momec.uni-hd.de/`.

[178] Halgren, T. A. *J. Comp. Chem.* **1996**, *17*, 490.

[179] Halgren, T. A. *J. Comp. Chem.* **1996**, *17*, 520.

[180] Halgren, T. A. *J. Comp. Chem.* **1996**, *17*, 553.

[181] Halgren, T. A.; Nachbar, R. B. *J. Comp. Chem.* **1996**, *17*, 587.

[182] Halgren, T. A. *J. Comp. Chem.* **1996**, *17*, 616.

[183] Halgren, T. A. *J. Comp. Chem.* **1999**, *20*, 720.

[184] Halgren, T. A. *J. Comp. Chem.* **1999**, *20*, 730.

[185] Comba, P.; Hambley, T. W.; Lauer, G.; Okon, N. *MOMEC97, a molecular modeling package for inorganic compounds*; Lauer & Okon Chemische Verfahrens- & Softwareentwicklung, 1997.

[186] *HyperChem(TM) 4.5*; Hypercube, Inc., 1115 NW 4th Street, Gainesville, Florida 32601, USA, 1995.

[187] Dalby, A.; Nourse, J. G.; Hounshell, W. D.; Gushurst, A. K. I.; Grier, D. L.; Leland, B. A.; Laufer, J. *J. Chem. Inf. Comput. Sci.* **1992**, *32*, 244.

[188] Deeth, R. J.; Gerloch, M. *Inorg. Chem.* **1984**, *23*, 3846.

[189] Deeth, R. J.; Hitchman, M. A. *Inorg. Chem.* **1986**, *25*, 1225.

[190] Norrby, P.-O.; Brandt, P. *Coord. Chem. Rev.* **2001**, *212*, 79.

[191] Kaitner, B.; Paulić, N.; Pavlović, G.; Sabolović, J. *Polyhedron* **1999**, *18*, 2301.

[192] Sabolović, J.; Tautermann, C. S.; Loerting, T.; Liedl, K. R. *Inorg. Chem.* **2003**, *42*, 2268.

[193] Norrby, P.-O.; Liljefors, T. *J. Comp. Chem.* **1998**, *19*, 1146.

[194] Jorgensen, W. L.; Maxwell, D. S.; Tirado-Rives, J. *J. Am. Chem. Soc.* **1996**, *118*, 11225.

[195] MacKerell, A. D., Jr. et al. *J. Phys. Chem. B* **1998**, *102*, 3586.

[196] Patel, S.; Brooks, C. L., III *J. Comp. Chem.* **2004**, *25*, 1.

[197] Rappé, A. K.; Goddard, W. A., III. *J. Phys. Chem.* **1991**, *95*, 3358.

[198] Maple, J. R.; Hwang, M.-J.; Stockfisch, T. P.; Dinur, U.; Waldman, M.; Eqig, C. S.; Hagler, A. T. *J. Comp. Chem.* **1994**, *15*, 162.

[199] Spendley, W.; Hext, G. R.; Himsworth, F. R. *Technometrics* **1962**, *4*, 441.

[200] Nelder, J. A.; Mead, R. *Comp. J.* **1965**, *7*, 308.

[201] Holland, J. *Adaption in Natural and Artificial Systems*; MIT Press, Cambridge, MA, 1975.

[202] Goldberg, D. E. *genetic Algorithms in Search, Research and Machine Learning*; Addison-Wesley, New York, 1989.

[203] Schmitt, L. M. *Theo. Comp. Sc.* **2001**, *259*, 1.

[204] Schmitt, L. M. *Theo. Comp. Sc.* **2004**, *310*, 181.

[205] Hæffner, F.; Brinck, T.; Haeberlein, M.; Moberg, C. *J. Mol. Struct. (Theochem)* **1997**, *397*, 39.

[206] Cornell, W. D.; Cieplak, P.; Bayly, C. I.; Gould, I. R.; Merz, K. M., Jr.; Ferguson, D. M.; Spellmeyer, D. C.; Fox, T.; Caldwell, J. W.; Kollman, P. A. *J. Am. Chem. Soc.* **1995**, *117*, 5179.

[207] Hunger, J.; Beyreuther, S.; Huttner, G.; Allinger, K.; Radelof, U.; Zsolnai, L. *Eur. J. Inorg. Chem* **1998**, 693.

[208] Hunger, J.; Huttner, G. *J. Comp. Chem.* **1999**, *20*, 455.

[209] Tafipolsky, M.; Schmid, R. *J. Phys. Chem. B* **2009**, *113*, 1341.

[210] Strassner, T.; Busold, M.; Radrich, H. *J. Mol. Model.* **2001**, *7*, 374.

[211] Strassner, T.; Busold, M.; Herrmann, W. A. *J. Comp. Chem.* **2002**, *23*, 282.

[212] Skopec, C. E.; Cukrowski, I.; Marques, H. M. *J. Mol. Struct.* **2006**, *783*, 21.

[213] Broyden, C. G. *J. Inst. Maths. Appl.* **1970**, *6*, 76.

[214] Fletcher, R. *Comp. J.* **1970**, *13*, 317.

[215] Goldfarb, D. *Math. Comp.* **1970**, *24*, 23.

[216] Shanno, D. F. *Math. Comp.* **1970**, *24*, 647.

[217] Polak, E. *Computational Methods in Optimization*; Academic Press, New York, 1971.

[218] Press, W. H.; Teukolsky, S. A.; Vetterling, W. T.; Flannery, B. P. *Numerical Recipes 3rd Edition: The Art of Scientific Computing*; Cambridge University Press, 2007.

[219] Maple, J. R.; Dinur, U.; Hagler, A. T. *Proc. Natl. Acad. Sci. USA* **1988**, *85*, 5350.

[220] Palmö, K.; Pietilä, L.-O.; Krimm, S. *J. Comp. Chem.* **1991**, *12*, 385.

[221] Leonard, J. M.; Asman, W. P. *J. Comp. Chem.* **1990**, *11*, 952.

[222] Seminario, J. M. *J. Quantum Chem.* **1996**, *30*, 1271.

[223] Dasgupta, S.; Goddard, W. A., III. *J. Chem. Phys.* **1989**, *90*, 7207.

[224] Dasgupta, S.; Yamasaki, T.; Goddard, W. A., III. *J. Chem. Phys.* **1996**, *104*, 2898.

[225] Dasgupta, S.; Brameld, K. A.; Fan, C.-F.; Goddard, W. A., III. *Spectrochimica Acta Part A* **1997**, *53*, 1347.

[226] Allen, F. H. *Acta Cryst.* **2002**, *B62*, 380.

[227] Martin, B. Ph.D. thesis, Universität Erlangen–Nürnberg, 2004.

[228] Chaudhuri, P.; Oder, K.; Wieghardt, K.; Weiss, J.; Reedijk, J.; Hinrichs, W.; Wood, J.; Ozarowski, A.; Stratemaier, H.; Reinen, D. *Inorg. Chem.* **1986**, *25*, 2951.

[229] Stephens, F. S. *J. Chem. Soc. A* **1969**, 2233.

[230] Hathaway, B. J.; Billing, D. E. *Coord. Chem. Rev.* **1970**, *5*, 143.

[231] Restivo, R. J.; Ferguson, G.; Hay, R. W.; Piplani, D. P. *J. Chem. Soc., Dalton Trans.* **1978**, 1131.

[232] Bang, E.; Monsted, O. *Acta Chem. Scand. A* **1982**, *36*, 353.

[233] Endicott, J. F.; Lilie, J.; Kuszaj, J. M.; Ramaswamy, B. S.; Schmonsees, W. G.; Simic, M. G.; Glick, M. D.; Rillema, D. P. *J. Am. Chem. Soc.* **1977**, *99*, 429.

[234] Kato, M.; Ito, T. *Bull. Chem. Soc. Jpn.* **1986**, *59*, 285.

[235] Barefeld, E. K.; Bianchi, A.; Billo, E. J.; Connolly, P. J.; Paoletti, P.; Summers, J. S.; Derveer, D. G. V. *Inorg. Chem.* **1986**, *25*, 4197.

[236] Curtis, N. F.; Gainsford, G. J.; Hambley, T. W.; Lawrance, G. A.; Morgan, K. R.; Siriwardena, A. *Chem. Commun.* **1987**, 295.

[237] Bernhardt, P. V.; Lawrance, G. A.; Hambley, T. W. *J. Chem. Soc., Dalton Trans.* **1989**, 1059.

[238] Antsyshkina, A. S.; Porai-Koshits, M. A.; Makhaev, V. D.; Borisov, A. P.; Kedrova, N. S.; Mal'tseva, N. N. *Koord. Khim. (Russ.)(Coord. Chem.)* **1992**, *18*, 474.

[239] Bernhardt, P. V.; Comba, P.; Hambley, T. W. *Inorg. Chem.* **1993**, *32*, 2804.

[240] Bakac, A.; Espenson, J. H.; Young, V. G., Junior *Inorg. Chem.* **1992**, *31*, 4959.

[241] Bernhardt, P. V.; Hambley, T.; Lawrance, G. A. *Chem. Commun.* **1989**, 553.

[242] Lai, T. F.; Poon, C. K. *Inorg. Chem.* **1976**, *15*, 1562.

[243] Beveridge, K.; Heyd, D.; Kirk, A. D. *Acta Crystallogr. Sect. C* **1993**, *49*, 1063.

[244] Goodson, P. A.; Glerup, J.; Hodgson, D. J.; Michelsen, K.; Rychlewska, U. *Inorg. Chem.* **1994**, *33*, 359.

[245] Mochizuki, K.; Kondo, T. *Inorg. Chem.* **1995**, *34*, 6241.

[246] Bernhardt, P. V.; Byriel, K. A.; Kennard, C. H. L.; Sharpe, P. C. *Inorg. Chem.* **1996**, *35*, 2045.

[247] Palmer, R. A.; Potter, B. S.; Tanriverdi, S.; Lisgarten, J. L.; Flint, C. D.; Gazi, D. M. *Acta Crystallogr. Sect. C* **1996**, *52*, 1177.

[248] Vrabel, V.; Lokaj, J.; Garaj, J. *Collect. Czech. Chem. Commun.* **1983**, *48*, 2893.

[249] Walsh, A.; Hathaway, B. J. *J. Chem. Soc., Dalton Trans.* **1984**, 15.

[250] Kamisawa, K.; Matsumoto, K.; Ooi, S.; Saito, R.; Kidani, Y. *Bull. Chem. Soc. Jpn.* **1981**, *54*, 1072.

[251] Hamalainen, R. *Suom. Kemistil. B* **1973**, *46*, 237.

[252] Bertini, I.; P-Dapporto,; Gatteschi, D.; Scozzafava, A. *J. Chem. Soc., Dalton Trans.* **1979**, 1409.

[253] Pajunen, A. *Suom. Kemistil. B* **1969**, *42*, 15.

[254] Pajunen, A. *Suom. Kemistil. B* **1969**, *42*, 261.

[255] Grenthe, I.; Paoletti, P.; Sandstrom, M.; Glikberg, S. *Inorg. Chem.* **1979**, *18*, 2687.

[256] Fortier, D. G.; McAuley, A. M. *J. Chem. Soc., Dalton Trans.* **1991**, 101.

[257] Lu, T. H.; Tahirov, T. H.; Bin, C. K.; Hsaio, C. D.; Liu, Y. L.; Lee, J. C.; Chung, C. S. *Acta Crystallogr. Sect. C.* **1993**, *49*, 1747.

[258] Cannas, M.; Cristini, A.; Marongiu, G. *Inorg. Chim. Acta* **1976**, *19*, 241.

Hiermit erkläre ich an Eides statt, dass ich die vorliegende Arbeit selbst verfasst habe und mich dabei keiner anderen als der von mir bezeichneten Quellen und Hilfen bedient habe.

Heidelberg im Mai 2011 　　　　　　　　　　　　＿＿＿＿＿＿＿＿＿＿＿＿＿＿＿＿＿＿＿

　　　　　　　　　　　　　　　　　　　　　　　(Sascha Hausberg)